National Library
of Canada

Bibliothèque nationale
du Canada

Canadian Theses Service

Service des thèses canadiennes

Ottawa, Canada
K1A 0N4

NOTICE

The quality of this microform is heavily dependent upon the quality of the original thesis submitted for microfilming. Every effort has been made to ensure the highest quality of reproduction possible.

If pages are missing, contact the university which granted the degree.

Some pages may have indistinct print especially if the original pages were typed with a poor typewriter ribbon or if the university sent us an inferior photocopy.

Reproduction in full or in part of this microform is governed by the Canadian Copyright Act, R.S.C. 1970, c. C-30, and subsequent amendments.

AVIS

La qualité de cette microforme dépend grandement de la qualité de la thèse soumise au microfilmage. Nous avons tout fait pour assurer une qualité supérieure de reproduction.

S'il manque des pages, veuillez communiquer avec l'université qui a conféré le grade.

La qualité d'impression de certaines pages peut laisser à désirer, surtout si les pages originales ont été dactylographiées à l'aide d'un ruban usé ou si l'université nous a fait parvenir une photocopie de qualité inférieure.

La reproduction, même partielle, de cette microforme est soumise à la Loi canadienne sur le droit d'auteur, SRC 1970, c. C-30, et ses amendements subséquents.

NL-339 (r. 88/04) c

Canada

National Library of Canada
Canadian Theses Service
Ottawa, Canada
K1A 0N4

Bibliothèque nationale du Canada
Service des thèses canadiennes

The author has granted an irrevocable non-exclusive licence allowing the National Library of Canada to reproduce, loan, distribute or sell copies of his/her thesis by any means and in any form or format, making this thesis available to interested persons.

The author retains ownership of the copyright in his/her thesis. Neither the thesis nor substantial extracts from it may be printed or otherwise reproduced without his/her permission.

L'auteur a accordé une licence irrévocable et non exclusive permettant à la Bibliothèque nationale du Canada de reproduire, prêter, distribuer ou vendre des copies de sa thèse de quelque manière et sous quelque forme que ce soit pour mettre des exemplaires de cette thèse à la disposition des personnes intéressées.

L'auteur conserve la propriété du droit d'auteur qui protège sa thèse. Ni la thèse ni des extraits substantiels de celle-ci ne doivent être imprimés ou autrement reproduits sans son autorisation.

ISBN 0-315-55442-8

Canada

THE UNIVERSITY OF ALBERTA

MANTLE PERIDOTITES: PETROLOGICAL AND EXPERIMENTAL INVESTIGATIONS

BY

DANTE CANIL ©

A THESIS SUBMITTED TO THE FACULTY OF GRADUATE
STUDIES AND RESEARCH IN PARTIAL FULFILMENT
OF THE REQUIREMENTS FOR THE DEGREE OF
DOCTOR OF PHILOSOPHY
DEPARTMENT OF GEOLOGY

EDMONTON, ALBERTA
FALL 1989

THE UNIVERSITY OF ALBERTA

RELEASE FORM

NAME OF AUTHOR: Dante Canil

TITLE OF THESIS: Mantle peridotites: petrological and experimental investigations

DEGREE: Doctor of Philosophy

YEAR THIS DEGREE GRANTED: Fall 1989

Permission is hereby granted to THE UNIVERSITY OF ALBERTA LIBRARY to reproduce single copies of this thesis and to lend or sell such copies for private, scholarly or scientific research purposes only.

The author reserves other publication rights, and neither the thesis nor extensive abstracts from it may be printed or otherwise reproduced without the author's written permission.

(Student's Signature)

1245 Surrey Rd
Windsor Ontario
N9H 1A8

(Student's Permanent address)

Date: Oct. 11, 1989

THE UNIVERSITY OF ALBERTA

FACULTY OF GRADUATE STUDIES AND RESEARCH

The undersigned certify that they have read, and recommend to the Faculty of Graduate Studies and Research for acceptance, a thesis entitled Mantle Peridotites: Petrological and Experimental Investigations submitted by Dante Canil in partial fulfilment of the requirements for the degree of Doctor of Philosophy.

....
K. Muehlenbachs - Supervisor

Reidar G. Trønnes
....
R.G. Tronnes

....
R.W. Luth

....
D. Schmitt

F. R. Boyd
....
F.R. Boyd - External Examiner

Date ......Oct 4, 85......

DEDICATED TO THE MEMORY OF CHRIS SCARFE,

AN ADVISOR AND FRIEND.

ABSTRACT

Petrographical and mineral chemical analyses of mantle xenoliths from Rayfield River, British Columbia indicate that the upper mantle beneath this area is composed dominantly of spinel lherzolite, and is heterogeneous on a cm to meter scale. A Miocene geotherm constructed for this area using the temperature of equilibration recorded by the xenoliths is similar to a geotherm derived from present day heat flow measurements.

Phlogopite has been recognized for the first time in mantle-derived xenoliths from the Canadian Cordillera. Petrographic and mineral chemical studies of phlogopite associated with fluid inclusions in mantle-derived xenoliths from Kostal Lake, British Columbia, indicate that fluids and/or melts fluxed the upper mantle beneath eastern British Columbia, possibly between 3.5 Ma and 400 years ago. The metasomatism caused oxidation of the mantle and may have been related to recent magmatism in this area.

Oxygen fugacities (f_{O2}'s) calculated for mantle-derived xenoliths from British Columbia range from about 0.5 to 1.5 log units below the fayalite - magnetite - quartz buffer at 15 kbar. These f_{O2}'s are more reducing than those reported for the upper mantle beneath the Massif Central and Japan, and fall within the range for fresh MORB glasses, and xenoliths from the southwestern United States and Mongolia. Significant variations

in f_{O2} between samples from different eruptive centers with varying ages are absent, indicating that the oxidation state of the mantle was unaffected by Late Cenozoic magmatism in this alkaline province.

Phase relations in simplified peridotite + CO_2 + H_2O systems investigated at 4 to 12 GPa demonstrate that uncontaminated, diamond-bearing kimberlites could be derived by partial melting of carbonated peridotite within a restricted depth interval of 150 to 250 km. This interval may represent the lithosphere/asthenosphere transition beneath stable cratons. If the f_{O2} recorded in samples from the upper 150 km of the mantle is maintained at depth, then magnesite is a potential host for carbon in the Earth to depths of at least 350 km.

Acknowledgements

It was a great privelege and honour for me to carry out my dissertation under the supervision of the late Dr. C.M. Scarfe. I thank Chris for introducing me to the "black art" of experimental petrology, and for advising me on many academic, logistic and personal aspects of this study. He and many other members of the high pressure lab, especially D. Sykes, made it fun and interesting to do experiments. I am also grateful to Dr. K. Muehlenbachs for supervising the final stage of my thesis. He and members of my commitee, especially Dr. R. Tronnes, are thanked for their advice and support when needed.

Drs. D. Virgo, R. Luth and P. Ulmer were very helpful in supervising my research at the Geophysical Laboratory. Numerous discussions with them and others at the Geophysical Lab helped shape my approach to scientific problems. My tenure there as a predoctoral fellow could not have been possible without the permission of Dr. C.T. Prewitt (Director).

Financial support for this thesis was provided through a NSERC postgraduate scholarship, a predoctoral fellowship from the Geophysical Laboratory, Carnegie Institution of Washington, and University of Alberta teaching assistantships.

Finally, I would like to thank my spouse Christine, for her confidence, patience and support, and for making me explain why people study rocks.

TABLE OF CONTENTS

1. THESIS INTRODUCTION....................................1

1.1 References...5

2. PETROLOGY OF ULTRAMAFIC XENOLITHS FROM RAYFIELD RIVER, SOUTH-CENTRAL BRITISH COLUMBIA....................6

2.1 Introduction.......................................6

2 2 Geological Setting.................................7

2.3 Analytical Methods.................................7

2.4 Host Lava..8

2.5 Ultramafic Xenoliths...............................8

  Petrography..9

  Mineral Chemistry...................................11

2.6 Discussion..13

  Cr bearing-diopside xenoliths.......................13

  Geothermometry......................................15

  Host Magma..17

2.7 Summary...18

2.8 References..31

3. ORIGIN OF PHLOGOPITE IN MANTLE XENOLITHS FROM KOSTAL LAKE, WELLS GRAY PARK, BRITISH COLUMBIA..........34

3.1 Introduction......................................34

3.2 Geological Setting................................35

3.3 Petrography.......................................36

  Type I Xenoliths....................................37

  Cumulate Xenoliths..................................38

3.4 Mineral Chemistry.................................39

Analytical Methods....................................39
Olivine...40
Orthopyroxene...41
Clinopyroxene...41
Phlogopite..42
Spinel..44
Rhonite...45
Glass...45
Fluid Inclusions......................................45
3.5 Discussion..46
Ultramafic Xenoliths..................................46
Origin of Phlogopite and Conditions During Metasomatism...................................48
Timing and Petrological Implications of Metasomatism.....................................53
3.6 Summary...55
3.7 References..72
4. OXIDATION STATE OF MANTLE XENOLITHS FROM BRITISH COLUMBIA......................................79
4.1 Introduction..79
4.2 Experimental Methods..................................82
4.3 Results...83
4.4 Discussion..86
Oxygen Fugacity of Spinel Lherzolites.................86
Errors in Ol-Opx-Sp Oxybarometers.....................87
Geological Implications...............................90

4.5 Summary....................................93

4.6 References.................................108

5. PHASE RELATIONS IN PERIDOTITE + CO_2 SYSTEMS TO 12 GPa: IMPLICATIONS FOR THE ORIGIN OF KIMBERLITE AND CARBONATE STABILITY IN THE UPPER MANTLE............113

5.1 Introduction................................113

5.2 Experimental Methods.......................116

Starting Compositions..........................116

High Pressure Experiments......................117

Analytical Methods.............................119

Equilibrium and Experimental Conditions.........120

Hydrogen Diffusion.............................122

5.3 Experimental Results.......................123

The Peridotite + CO2 Solidus...................124

The Peridotite + CO2 + H2O Solidus.............126

Clinopyroxene Compositions.....................126

5.4 Partial Melts Along the Peridotite + CO_2 Solidus and the Origin of Kimberlites..............127

5.5 Concerning Kimberlite and Melilitite...............130

5.6 The Storage of Carbon in the Earth's Upper Mantle.....................................131

5.7 Summary....................................132

5.8 References.................................148

6. THESIS SUMMARY AND CONCLUSIONS..................153

6.1 References.................................157

LIST OF TABLES

Table Page

2.1 Analysis of Rayfield River Host Hawaiite..........20

2.2 Analyses of Xenolith Minerals....................21

3.1 Compositions of Kostal Lake Lavas................56

3.2 Analyses of Xenolith Olivines....................57

3.3 Analyses of Xenolith Orthopyroxenes..............58

3.4 Analyses of Xenolith Clinopyroxenes..............59

3.5 Analyses of Xenolith Phlogopites.................60

3.6 Analyses of Xenolith Spinels.....................61

3.7 Analyses of Xenolith Rhonites and Glass..........62

3.8 Geothermometry of Kostal Lake Xenoliths..........63

3.9 Compositions of Xenolith-bearing Lavas...........64

4.1 Sample Locations in British Columbia.............95

4.2 Compositional Data for Spinels and Olivines......96

4.3 Compositional Data for Orthopyroxenes............99

4.4 Mossbauer Parameters for Spinels.................100

5.1 Starting Compositions for Peridotite + CO_2 + H_2O Experiments.....134

5.2 Experimental Run Conditions......................135

5.3 Analyses of Run Products.........................137

LIST OF FIGURES

Figure Page

2.1 Ultramafic Xenolith Occurrences in Canadian Cordillera....25

2.2 Frequency of Xenoliths from Rayfield River....26

2.3 Pyroxene Compositions - Rayfield River Xenoliths....27

2.4 Covariation in Spinel and Pyroxene Compositions....28

2.5 Temperatures of Equilibration for Rayfield River Xenoliths....29

2.6 Rayfield River Geotherm....30

3.1 Location of Xenolith-bearing Lavas in the Canadian Cordillera....65

3.2 Photomicrographs of Phlogopite in Ultramafic Xenoliths a) and b)....66

3.3 Photomicrographs of Phlogopite in Ultramafic Xenoliths a) and b)....67

3.4 Cumulate Texture in Wehrlite Xenolith....68

3.5 Mg#'s of Silicates in Xenoliths from Kostal Lake....69

3.6 Fe^{2+} - Fe^{3+} - Mg^{2+} Ternary for Xenolith Spinels....70

3.7 Energy Spectrum of Fluid Inclusion in Intercumulus Clinopyroxene....71

4.1 Mossbauer Spectra of Spinels a)....102

continued b)....................................103
continued c)....................................104
continued d)....................................105
4.2 Comparison of Fe^{3+}/total Fe Determined for Xenolith Spinels using Mossbauer Spectroscopy and Electron Microprobe..............106
4.3 Oxygen Fugacity of Mantle Xenoliths from British Columbia calculated at 15 kbar............107
5.1 Starting Compositions in the CaO - MgO - SiO2 Ternary....................................138
5.2 Thermal Gradient in 18M Assembly..................139
5.3 Cross Section of 18M Pressure Assembly............140
5.4 Back-scattered Electron Images of Run Products a)................................141
continued b)....................................142
5.5 Phase Relations for Peridotite CCMS2 a)...........143
Phase Relations for Peridotite CCMAS1 b)..........144
Phase Relations for Peridotite CCMSH2 c)..........145
5.6 Clinopyroxene Compositions from Experimental Runs................................146
5.7 Peridotite + CO_2 Partial Melts Projected in wt.% onto the C - M - S Plane 147

1. THESIS INTRODUCTION

Studies of mantle-derived xenoliths hosted in alkaline rocks are central to our understanding of the nature and evolution of the Earth's upper mantle, and its role in the generation of magma (Yoder, 1976). Because these "mantle samples" are the best evidence we have for the composition of the upper mantle, they impose major constraints on geophysical, geochemical and experimental investigations attempting to define the structure, physical properties, and petrology of this region in the Earth.

Upper mantle xenoliths are hosted in alkaline rocks throughout British Columbia and the Yukon. In Chapter 2, the petrological study of a xenolith suite from south-central British Columbia provides evidence for a heterogeneous upper mantle beneath the Cordillera, and demonstrates the overall uniformity of geothermal conditions during Late Cenozoic volcanism in this mountain belt. Mantle xenoliths from this locality are hosted in hawaiite, suggesting that such evolved compositions can be primary magmas derived from the mantle, and that magma generation has in some cases occurred at fairly shallow depths (30 to 40 km) in the Cordilleran upper mantle.

Mantle xenoliths may also record processes which have occurred in the upper mantle, such as metasomatism and the formation of hydrous phases. The importance of fluids in metasomatism and magmatism in the upper mantle has been emphasized in several petrological and experimental studies of mantle peridotites (Wyllie, 1979; Bailey, 1982). Metasomatic processes are envisaged to occur in the upper mantle above subduction zones (Tatsumi, 1989). Although there has been an extensive history of subduction throughout the Cordillera, surprisingly little petrologic evidence exists for a modally metasomatized mantle beneath this region.

In Chapter 3, the first occurrence of phlogopite in Cordilleran mantle-derived xenoliths is documented, and the perplexing absence of metasomatic phases in the sub-Cordilleran upper mantle is discussed. Evidence is presented for the infiltration of oxidized fluids or fluid-rich melt into the mantle lithosphere beneath eastern British Columbia. The overall petrologic significance of this metasomatism, is evaluated in the light of current proposals which suggest that mantle metasomatism is either a precursor to (Menzies and Murthy, 1980) or consequence of (Roden et al., 1984) magmatism in alkaline provinces worldwide.

The composition of metasomatic fluids or fluid-rich melts in the upper mantle is controlled by the activity or fugacity of oxygen. For this reason, the oxidation state of the upper mantle is an important variable governing the speciation of volatiles, and their role in magma genesis and mass transport in the mantle. The current oxidation state of the upper mantle may, furthermore, provide some record of core formation during the early stages of our planet's formation, or of its degassing history over time.

In recent years, there has been great debate concerning the oxidation state of the upper mantle. Arguments for both a reduced and oxidized state have been advanced. Some workers argue for a reduced oxidation state, while others propose a slightly oxidized state (Arculus, 1985). The possibility also exists for an upper mantle heterogeneous in its oxidation state (Haggerty and Tompkins, 1983), but limits on the degree of this lateral and vertical heterogeneity have yet to be defined.

In Chapter 4, the oxidation state of the upper mantle beneath the Canadian Cordillera is investigated using redox equilibria recorded by coexisting of olivine, orthopyroxene and spinel in mantle xenoliths from numerous localities throughout this region. Mossbauer spectroscopy is employed to precisely determine the Fe^{3+} content of spinels, a crucial parameter used in the calculation of oxygen fugacities recorded by the xenoliths. The results indicate that throughout the Cenozoic, the sub-Cordilleran upper mantle was oxidized, but not to the extent of mantle lithosphere above other subduction zones. The limited extent of lateral or vertical heterogeneity in oxidation state of the mantle beneath the Cordillera is also demonstrated.

The role of C-O-H volatiles in the genesis of magmas in the upper mantle has been a particularly enlightening area of research in experimental petrology over the last twenty years (Kushiro, 1969; Eggler, 1978; Wyllie, 1979). In view of these studies, it has long been appreciated that a significant

CO_2-component must be present in the mantle source regions of deep-seated, diamond-bearing kimberlites, in order to explain the Si-poor nature and explosive emplacment of these rocks. The origin of kimberlite and other volatile-rich, xenolith-bearing alkaline magmas deep in the Earth's peridotitic upper mantle is poorly understood, however, due to the lack of experimental information on peridotite + CO_2 + H_2O systems at pressures above 5 GPa, where diamonds are stable. Fortunately, the advent of multi-anvil presses for use in experimental geochemistry now makes this pressure - temperature region amenable to phase equilibrium experimentation.

In Chapter 5, phase relations in synthetic peridotite + CO_2 systems to 12 GPa are reported. The objectives of these experiments were to: 1) demonstrate the possible spectrum of magmas which can be derived from a peridotite + CO_2 source rock at very high pressures in the mantle, 2) provide constraints on the P - T regime for the generation of kimberlite and allied magmas in the mantle, and 3) comment on the stability of carbonates at depth in the mantle, and their potential for storing carbon in this region of the Earth. The results suggest a limited depth of 150 to 250 km for kimberlite generation in the upper mantle beneath stable cratons, and demonstrate that carbonates introduced into the mantle by subduction of altered oceanic lithosphere are potential reservoirs for carbon to depths of at least 350 km in the Earth.

1.1 REFERENCES

Arculus RJ (1985) Oxidation status of the mantle:past and present. Ann. Rev. Earth Planet. Sci. 13:75-96.

Bailey DK (1982) Mantle metasomatism - continuing chemical change within the Earth. Nature 296:525-530.

Eggler DH (1978) The effect of CO_2 on partial melting of peridotite in the system Na_2O - CaO - Al_2O_3 - MgO - SiO_2 - CO_2 to 35 kb, with an analysis of melting in a peridotite - H_2O - CO_2 system. Am. J. Sci. 278:305-343.

Haggerty SH, Tompkins LA (1983) Redox state of the Earth's upper mantle from kimberlitic ilmenites. Nature 303:295-300.

Kushiro I (1969) The system forsterite - diopside - silica with and without water at high pressure. Am. J. Sci. 267A:269-294.

Menzies M, Murthy VR (1980) Mantle metasomatism as a precursor to the genesis of alkaline magmas - isotopic evidence. Am. J. Sci. 280A:622-638.

Roden MF, Frey FA, Francis DM (1984) An example of consequent mantle metasomatism in peridotite inclusions from Nunivak Island, Alaska. J. Petrol. 25:546-577.

Tatsumi Y (1989) Migration of fluid phases and genesis of basalt magmas in subduction zones. J. Geophys. Res. 94:4697-4707.

Wyllie PJ (1979) Magmas and volatile components. Am. Miner. 64:469-500.

Yoder HS Jr. (1976) The Generation of Basaltic Magma. National Academy of Sciences, Washington DC, 265 p.

2. PETROLOGY OF ULTRAMAFIC XENOLITHS FROM RAYFIELD RIVER, SOUTH-CENTRAL BRITISH COLUMBIA

2.1 INTRODUCTION

The study of mantle xenoliths hosted in alkali basalts and kimberlites worldwide is central to our understanding of the mineralogy and chemistry of the upper mantle. Several recent studies have described ultramafic xenoliths hosted in Late Cenozoic alkaline volcanics in British Columbia (Littlejohn and Greenwood, 1974; Nicholls et al., 1982; Scarfe et al., 1982; Fujii and Scarfe, 1982; Ross, 1983; Brearley and Scarfe, 1984; Brearley et al., 1984) that show evidence for a heterogeneous and possibly metasomatized upper mantle beneath this region.

This paper documents a new occurrence of ultramafic xenoliths near Rayfield River, south-central British Columbia. In this paper, I describe the mineralogy and mineral chemistry of xenoliths derived from the upper mantle and show additional evidence for a heterogeneous upper mantle beneath British Columbia. These data are used to estimate the temperatures of equilibration of the xenoliths and to construct a geotherm for the upper mantle beneath Rayfield River.

2.2 GEOLOGICAL SETTING

The Rayfield River locality ($51^{\circ}20'$N, $121^{\circ}7'$W) is one of a growing list of xenolith occurrences in the Cordillera, all of which occur along a northwest-trending belt (Fig. 2.1). This belt parallels a thinning of the lithosphere beneath southern British Columbia (Nicholls _et al_., 1982). Xenoliths at Rayfield River are hosted in a massive flow. The flow may represent a distal portion of the Chilcotin Group plateau lavas to the west, which erupted between 6 - 10 Ma ago (Bevier, 1983).

2.3 ANALYTICAL METHODS

Electron microprobe analyses of the mineralogy of the xenoliths and host lava were performed at the Department of Geology, University of Alberta, using an ARL SEMQ microprobe fitted with an ORTEC energy dispersive spectrometer. Routine analyses of standards and samples used a rastered beam (10 um^2) with an operating voltage of 15 kV, probe current of 4 nA, and 240 s counting times. Data were processed with full ZAF corrections using EDATA2 (Smith and Gold, 1979). The limit of detection using EDA is 500 ppm and accuracies for major and minor elements are comparable to WDA (Smith, 1976; Fujii and Scarfe, 1982).

Analysis of the whole rock host lava was done using WDA on a glass bead fused in air at 1300°C for two hours. To avoid volatilization of alkalies, a point beam was moved continuously over the sample throughout the 400 s counting time. Ferrous iron in the host lava was determined by wet chemistry.

2.4 HOST LAVA

The host lava contains up to 5% microphenocrysts of olivine (Fo_{68}) set in a groundmass of plagioclase (An_{44}), titanaugite and titanomagnetite, with rare apatite and glass. Xenocrysts of olivine and pyroxene that show reactions with the host lava may be derived from disaggregation of the xenoliths. The composition of the host lava (Table 2.1), which is the average of three analyses, is close in composition to a separate XRF determination for the same rock sample (Smith, 1986). The lava is a hawaiite according to the classifications of MacDonald and Katsura (1964), Irvine and Baragar (1971), and Le Bas et al. (1986).

2.5 ULTRAMAFIC XENOLITHS

One hundred xenoliths were collected and examined in hand specimen. The xenoliths are subrounded and range in size from 1 - 10 cm. The xenolith suite consists of ultramafic rocks, with subordinate crustal rocks of granitoid composition (Fig. 2.2). The ultramafic xenoliths can be subdivided into two major groups: 1) green Cr diopside-bearing xenoliths and, 2) black Al augite-bearing xenoliths. Only the former group are described in this paper.

The Cr diopside-bearing xenoliths are dominated by spinel lherzolite, with lesser amounts of dunite, websterite, harzburgite and olivine websterite (Fig. 2.2). Centimeter-scale Cr diopside-rich bands occur in two spinel lherzolite xenoliths. Two other xenoliths contain dark websterite veins which cross-cut lherzolite or dunite. Similar features have been observed in other mantle xenoliths (e.g. Irving, 1980; Scarfe _et al_., 1982; Brearley _et al_., 1984) and are thought to be strong evidence for a heterogeneous upper mantle beneath British Columbia.

Petrography

Seventeen representative samples of the Cr diopside-bearing suite were chosen for petrographic examination. All of the xenoliths have protogranular textures (Mercier and Nicolas, 1975). Olivines range in size from 1 - 5 mm and occasionally show undulatory extinction. Orthopyroxenes range from 1 - 4 mm and rarely show exsolution lamellae, 10 - 20 um thick, parallel to (010). Clinopyroxenes are clear to pale green and usually occur as granules less than 1 mm in size. Exsolution lamellae up to 40 um in width are occasionally present. Both pale green (Al-rich) and dark brown (Al-poor) spinels occur as interstitial grains less than 0.5 mm in size. These two different types of spinel do not coexist in any of the xenoliths examined.

Websterite inclusion RR108 contains pale green Al-rich spinel with coronas of plagioclase, suggesting re-equilibration in the plagioclase stability field. The petrological implications of this texture will be discussed later.

Clinopyroxenes commonly contain small vermicular pockets of glass along their grain boundaries. The glass blebs are less than 50 um in long dimension. It is unclear whether they are the result of natural partial melting in the upper mantle (e.g. Maaloe and Printzlau, 1979), simple heating by the host magma during transport, or decompression during ascent of the xenoliths (Brearley et al., 1984).

Reaction with the host magma is evident in some samples, particularly where pyroxene occurs at the contact between the xenolith and host magma. The reaction is represented by a spongy-textured zone of elongated pyroxene, granular magnetite, hopper-shaped olivine and basaltic glass along the contact between orthopyroxene and the host hawaiite. Similar features have been noted in ultramafic xenoliths by Kuo and Kirkpatrick (1985). Brearley and Scarfe (1986) attribute these textures to the instability of pyroxene in alkali basalt magmas at low pressure.

Mineral Chemistry

Microprobe analyses of minerals from seventeen Cr diopside-bearing xenoliths representative of the Rayfield River suite are given in Table 2.2.

Olivine

Olivine ranges in composition from Fo_{89} to Fo_{92} and NiO contents (0.3 - 0.5 wt.%) do not correlate with Fo content. CaO was not detected in any of the olivines analyzed.

Orthopyroxene

Orthopyroxenes in most of the xenoliths vary in composition from $En_{92}Wo_{1}Fs_{7}$ to $En_{88}Wo_{2}Fs_{10}$. Al_2O_3 and Cr_2O_3 range from 3.3 - 5.0 and 0.2 - 0.5 wt.%, respectively. Pyroxenes in websterite bands usually have slightly higher Al_2O_3 contents when compared to lherzolite or harzburgite pyroxenes (Table 2.2). Three discrete websterite xenoliths (RR61, RR91, RR108) have orthopyroxenes with up to 19 mole % of the Fs component (Fig. 2.3). These Fe-rich compositions contain more Al_2O_3 (upto 7.0 wt.%) and less Cr_2O_3 (< 0.2 wt.%) than orthopyroxenes from the other xenoliths (Table 2.2).

Clinopyroxene

Clinopyroxenes range in composition from $En_{52}Wo_{43}Fs_5$ to $En_{48}Wo_{49}Fs_3$, and contain up to 7.0 wt.% Al_2O_3 and 1.4 wt.% Cr_2O_3. When plotted in the pyroxene quadrilateral, they lie within the diopside compositional field, and are referred to as Cr diopsides (Fig. 2.3). Black, Fe-rich clinopyroxenes from the same discrete websterite xenoliths noted above (Fig. 2.3), have higher Al_2O_3 (up to 9 wt.%), and lower Cr_2O_3 (< 0.2 wt.%) when compared to normal Cr diopsides. These compositions appear to be compositionally intermediate between Al augites ($Al_2O_3 > 10$ wt.%, $Cr_2O_3 < 0.2$ wt.%) and Cr diopsides. Similar clinopyroxenes have been described at Summit Lake (Brearley et al., 1984) and they may represent a chemical continuum between the green and black clinopyroxenes. Alumina contents of pyroxenes show a negative correlation with $Cr/Cr+Al+Fe^{3+}$ in coexisting spinels (Fig. 2.4).

Spinel

Spinels in all but the Fe-rich websterites are low in TiO_2 (< 0.15 wt.%). They also show a negative correlation between $Mg/Mg+Fe^{2+}$ (0.79 - 0.89) and $Cr/Cr+Al+Fe^{3+}$ (0.05 - 0.26). All of the Fe-rich websterites contain pale green, Al-rich spinels ($Cr/Cr+Al+Fe^{3+} < 0.05$). These spinels usually have lower $Mg/Mg+Fe^{2+}$ (0.69 - 0.83) than spinels from the other Cr diopside-bearing xenoliths.

Plagioclase

Plagioclase replacing spinel in websterite RR108 is An_{53} in composition (Table 2.2). Based on stoichiometry, the small amount of iron in the analysis is assumed to be Fe^{3+} replacing Al^{3+} (Deer et al., 1966).

2.6 DISCUSSION

Cr diopside-bearing xenoliths

The Cr diopside-bearing xenoliths are similar in their major and minor element mineral compositions to xenoliths of this type described elsewhere (e.g. Kuno and Aoki, 1970; Wilshire and Shervais, 1975; Frey and Prinz, 1978). The refractory composition of olivine strongly suggests that most of the xenoliths have undergone one or more previous partial melting events. This is also borne out by the presence of protogranular textures in the xenoliths, which are thought to record a recrystallization process during partial melting (Mercier and Nicolas, 1975).

The range in $Cr/Cr+Al+Fe^{3+}$ in mantle spinels is pressure dependent (Haggerty, 1979); hence, it is a measure of the depth interval sampled by the host hawaiite. The limited range in this ratio for Rayfield River spinels (0.01 - 0.26) when compared to other xenolith localities (e.g. Summit Lake - $Cr/Cr+Al+Fe^{3+}$= 0.01 - 0.50), suggests that the depth interval sampled by the host hawaiite was rather small.

Websterite veins that cross-cut the lherzolite xenoliths most likely represent melts frozen in the upper mantle (e.g. Irving, 1980). They have since re-equilibrated with their host lherzolite as indicated by the similar compositions for minerals in both the websterite veins and host lherzolite (Table 2.2). Reaction halos between the websterite veins and their host lherzolite were not detected petrographically or by microprobe; therefore, they may have been obliterated by partial re-melting of the original veinlet/host composite (e.g. Frey and Prinz, 1978).

The Fe-rich websterite xenoliths contain black clinopyroxenes similar in appearance to those described by Wilshire and Shervais (1975) and Frey and Prinz (1978). However, the clinopyroxenes analyzed here are better described as Cr-poor diopsides, rather than Al-augites (Fig. 2.3). When compared to the Group II clinopyroxenes of Frey and Prinz (1978), clinopyroxenes from the Fe-rich websterites contain less FeO and TiO_2. Orthopyroxenes and spinels from these same websterites are also similar to Group II compositions, but are less Fe-rich.

The Fe-rich mineral chemistry of the websterite xenoliths, suggests that they may have crystallized from basaltic melt at high pressures in the mantle. A similar origin has been inferred for "metacumulates" of this type in xenolith suites elsewhere (Frey and Prinz, 1978; Ross, 1983; Brearley et al., 1984; Esperanca and Garfunkel, 1986). The coronas of plagioclase (An_{53}) replacing Al-rich spinel in websterite inclusion RR108, suggest that it resided for a limited time in the lower crust, causing re-equilibration of the xenolith in the plagioclase stability field (< 30 km depth).

Geothermometry

The uniform composition and lack of significant zoning in any of the mineral phases suggest that the xenoliths are well equilibrated. For this reason, the temperature of equilibration of the xenoliths can be calculated using element partition geothermometers.

To estimate the temperature of equilibration of the xenoliths, I used the Wells (1977) two-pyroxene geothermometer. This particular thermometer was chosen to facilitate comparison with other work of this nature in British Columbia. Temperature estimates using the Wells (1977) geothermometer are accurate to ±70°C. Errors in the microprobe analyses introduce uncertainties of $\pm10^{o}C$. The results of the calculations are shown in Figure 2.5. Most of the temperatures for the xenoliths range from 860 - 980^{o}C. These temperatures of equilibration are well below solidus temperatures for both anhydrous mantle peridotite (Takahashi and Kushiro, 1983) and alkali basalt (Arculus, 1975). This confirms that the xenoliths are accidental fragments derived from the upper mantle, and are not cognate with their host magma, as has been inferred for ultramafic xenoliths from some other localities (e.g. Sen and Presnall, 1986).

Due to the lack of a suitable geobarometer for spinel lherzolite, the pressure of equilibration of the xenoliths cannot be accurately determined. However, published phase equilibria for spinel lherzolite bracket their pressure of equilibration between 7 - 16 kbar at 900^{o}C (Herzberg, 1978). This corresponds to a depth of equilibration between 23 - 53 km at the temperatures estimated from the geothermometry.

Figure 2.6a shows a geotherm constructed for the upper mantle beneath Rayfield River using the temperature and depth estimates calculated above. Two extreme geotherms (dashed lines) are drawn through the lower and upper depth limits estimated for the xenoliths. An average of these two extreme geotherms (solid line), lies very close to the geotherm calculated for this region using heat flow measurements (Davis and Lewis, 1984), and gives a depth of equilibration for the Rayfield River xenoliths of between 30 - 40 km (Figure 2.6a). This is consistent with the inferred 30 - 35 km depth to the Moho in the Rayfield River area (Nicholls et al., 1982). Alternatively, if we assume the xenoliths equilibrated on the average Cordilleran geotherm of Ranalli (1980), their depth of equilibration would be 35 - 45 km (Fig. 2.6b). This inferred depth of equilibration is less than that estimated for other xenolith suites from southern British Columbia (e.g. Fujii and Scarfe 1981, 1982; Brearley et al., 1984).

Host magma

Most mantle xenolith-bearing lavas from British Columbia range in composition from nephelinite to alkali basalt. Because the host lava for the Rayfield River xenoliths is a more evolved composition (hawaiite), it is unique to this region. The occurrence of mantle xenoliths hosted in the Rayfield River hawaiite implies that magmas of similar evolved composition can be derived from the upper mantle. Takahashi (1980) and Takahashi and Kushiro (1983) have shown that a similar but slightly more primitive composition than the Rayfield River hawaiite (KRB - see Table 2.1) is saturated with olivine, orthopyroxene, and clinopyroxene at pressures between 13 - 15 kbar. This experimental evidence suggests that the Rayfield River hawaiite may have been generated by melting at similar pressures in the upper mantle beneath British Columbia. Generation of the host hawaiite at shallow depths (40 - 45 km) would allow it to sample only the uppermost lid of the mantle upon ascent to the surface. Such an origin is in accord with the shallow depth of equilibration derived from the xenolith geothermometry, and the limited depth interval implied by the small range in $Cr/Cr+Al+Fe^{3+}$ in xenolith spinels.

2.7 SUMMARY

Ultramafic xenoliths hosted in a hawaiite flow near Rayfield River are dominantly spinel lherzolite, implying that the upper mantle beneath this region is composed largely of this rock type. Local regions of dunite, websterite, harzburgite, and olivine websterite also exist. Mineralogically banded xenoliths are further evidence for this local heterogeneity. The refractory mineral compositions, protogranular textures, and inferred temperatures and depths of equilibration of the xenoliths (860 - 980°C, 30 - 40 km), require that they be fragments of the upper mantle, which have undergone one or more episodes of partial melting. Three Fe-rich websterite xenoliths, one of which contains plagioclase, are most likely high pressure cumulates which crystallized from magmas in transit through the uppermost mantle.

A geotherm constucted for the upper mantle beneath

Rayfield River is similar to one calculated for this area using heat flow measurements. The depth of equilibration of the Rayfield River xenoliths is somewhat less than that inferred for other xenolith suites from southern British Columbia. The hawaiite hosting the Rayfield River xenoliths may have been generated at considerably lower pressures than the more primitive, alkali basalt to nephelinitic lavas hosting mantle xenoliths elsewhere in British Columbia.

Table 2.1. Whole Rock Analysis and CIPW Norm Of Rayfield River Host Hawaiite and Alkali Basalt KRB*

Oxide (wt.%)			CIPW Norm (wt.%)		
	HOST HAWAIITE	KRB		HOST HAWAIITE	KRB
SiO_2	47.99	47.47			
Al_2O_3	15.67	17.15	Or	7.33	9.98
Fe_2O_3	3.20	2.26	Ab	30.88	24.82
FeO	8.29	7.22	An	21.72	25.33
MnO	0.17	0.15	Ne	1.01	3.38
MgO	7.30	8.76	Di-wo	6.11	4.26
CaO	8.21	8.03	Di-en	3.84	2.90
Na_2O	3.87	3.67	Di-fs	1.89	1.02
K_2O	1.24	1.69	Ol	15.48	18.38
TiO_2	2.41	2.43	Mt	4.64	3.28
P_2O_5	0.67	0.66	Il	4.58	4.62
			Ap	1.58	1.53
Total	99.02	99.49			
$Mg/Mg+Fe^{2+}$	73.0	79.0			

Notes: * Data for alkali basalt KRB are from Takahashi (1980).

Table 2.2 Representative Analyses of Xenolith Minerals

Olivines

	RR31 OLV 1-1	RR224 OLV 2-1	RR182B OLV 1-1
SiO_2	40.32	40.43	40.59
TiO_2	n.d.	n.d.	n.d.
Al_2O_3	n.d.	n.d.	n.d.
Cr_2O_3	n.d.	n.d.	n.d.
Fe_2O_3	n.a.	n.a.	n.a.
FeO	8.47	9.76	9.77
MnO	0.09	0.17	0.17
MgO	49.49	48.38	49.45
CaO	n.d.	n.d.	n.d.
Na_2O	n.d.	n.d.	n.d.
K_2O	n.d.	n.d.	n.d.
NiO	0.45	0.50	0.49
Total	98.82	99.24	100.47
O	4.000	4.000	4.000
Si	0.998	0.999	0.993
Al	n.d.	n.d.	n.d.
Ti	n.d.	n.d.	n.d.
Cr	n.d.	n.d.	n.d.
Fe3+	n.a.	n.a.	n.a.
Fe2+	0.175	0.202	0.200
Mn	0.002	0.002	0.003
Mg	1.826	1.792	1.802
Ca	n.d.	n.d.	n.d.
Na	n.d.	n.d.	n.d.
K	n.d.	n.d.	n.d.
Ni	0.008	0.010	0.010
Sum	3.009	3.005	3.008
Mg#	91.2	89.8	90.0
Ca	0.0	0.0	0.0
Mg	91.2	89.8	90.0
Fe	8.8	10.2	10.0
	Dun	Sp-L	Sp-L

Notes: n.d.= not detected n.a.= not analyzed. All Fe in silicates (except PL 1-1) as FeO. Fe_2O_3 in spinel and plagioclase by stoichiometry. Cr#= Cr/Cr+Al+Fe^{3+} Mg#=Mg/Mg+Fe^{2+} rock type — Sp-L= spinel lherzolite, Dun= dunite, Web= Fe-rich websterite, Web-b= websterite vein

Table 2.2 continued...

Orthopyroxenes

	RR224 OPX 1-1	RR222 OPX 2-1	RR84 OPX 3-1	RR175B OPX 2-1	RR91 OPX 1-1	RR108 OPX 2-1
SiO_2	55.45	55.41	54.71	55.42	52.69	52.46
TiO_2	n.d.	n.d.	n.d.	n.d.	n.d.	n.d.
Al_2O_3	3.86	4.10	5.04	3.37	5.39	7.16
Cr_2O_3	0.46	0.31	0.21	0.33	0.20	n.d.
Fe_2O_3	n.a.	n.a.	n.a.	n.a.	n.a.	n.a.
FeO	6.23	6.62	6.57	6.14	11.79	8.48
MnO	0.10	0.19	0.13	n.d.	0.22	0.22
MgO	33.26	33.43	33.46	34.16	28.79	30.73
CaO	0.73	0.57	0.55	0.49	0.61	0.71
Na_2O	n.d.	n.d.	n.d.	n.d.	n.d.	n.d.
K_2O	n.d.	n.d.	n.d.	n.d.	n.d.	n.d.
NiO	0.12	0.09	0.14	0.10	n.d.	n.d.
Total	100.21	100.72	100.81	100.01	99.69	99.76
O	6.000	6.000	6.000	6.000	6.000	6.000
Si	1.910	1.904	1.878	1.913	1.871	1.835
Al	0.157	0.166	0.204	0.137	0.225	0.295
Ti	n.d.	n.d.	n.d.	n.d.	n.d.	n.d.
Cr	0.013	0.008	0.006	0.009	0.006	n.d.
Fe3+	n.a.	n.a.	n.a.	n.a.	n.a.	n.a.
Fe2+	0.180	0.190	0.189	0.177	0.350	0.248
Mn	0.003	0.006	0.004	n.d.	0.007	0.007
Mg	1.708	1.712	1.712	1.757	1.524	1.602
Ca	0.027	0.021	0.020	0.018	0.023	0.027
Na	n.d.	n.d.	n.d.	n.d.	n.d.	n.d.
K	n.d.	n.d.	n.d.	n.d.	n.d.	n.d.
Ni	0.003	0.002	0.004	0.003	n.d.	n.d.
Sum	4.001	4.009	4.017	4.014	4.006	4.014
Mg#	90.5	90.0	90.1	90.8	81.3	86.6
Ca	1.4	1.1	1.1	0.9	1.2	1.4
Mg	89.2	89.0	89.1	90.0	80.3	85.4
Fe	9.4	9.9	9.8	9.1	18.5	13.2
	Sp-L	Sp-L	Web-b	Sp-L	Web	Web

Table 2.2 continued...

Clinopyroxenes

	RR210A	RR39	RR84	RR91	RR108	RR61
	CPX 2-1	CPX 2-1	CPX 4-1	CPX 2-1	CPX 3-1	CPX 3-1
SiO_2	52.14	51.92	52.22	50.80	51.18	50.29
TiO_2	0.45	0.23	0.27	0.39	0.15	0.24
Al_2O_3	5.89	6.10	7.35	6.87	8.79	8.05
Cr_2O_3	0.73	1.07	0.55	0.35	0.18	0.54
Fe_2O_3	n.a.	n.a.	n.a.	n.a.	n.a.	n.a.
FeO	2.68	2.52	2.75	5.10	3.54	5.51
MnO	n.d.	n.d.	n.d.	0.10	n.d.	0.07
MgO	15.63	15.37	15.15	14.08	14.66	13.92
CaO	20.97	20.43	20.41	21.37	21.05	20.80
Na_2O	1.31	1.77	1.55	0.90	1.30	1.02
K_2O	n.d.	n.d.	n.d.	n.d.	n.d.	n.d.
NiO	n.d.	0.09	0.09	n.d.	n.d.	n.d.
Total	99.80	99.50	100.33	99.96	100.85	100.44
O	6.000	6.000	6.000	6.000	6.000	6.000
Si	1.890	1.889	1.878	1.860	1.838	1.834
Al	0.252	0.262	0.312	0.297	0.372	0.346
Ti	0.012	0.006	0.007	0.011	0.004	0.007
Cr	0.021	0.031	0.016	0.010	0.005	0.015
Fe3+	n.a.	n.a.	n.a.	n.a.	n.a.	n.a.
Fe2+	0.081	0.077	0.083	0.156	0.106	0.168
Mn	n.d.	n.d.	n.d.	0.003	n.d.	0.002
Mg	0.845	0.833	0.812	0.768	0.785	0.757
Ca	0.815	0.796	0.787	0.838	0.810	0.813
Na	0.092	0.125	0.108	0.064	0.091	0.072
K	n.d.	n.d.	n.d.	n.d.	n.d.	n.d.
Ni	n.d.	0.003	0.002	n.d.	n.d.	n.d.
Sum	4.008	4.022	4.005	4.007	4.011	4.014
Mg#	91.2	91.6	90.8	83.1	88.1	81.8
Ca	46.8	46.7	46.8	47.5	47.6	46.8
Mg	48.5	48.8	48.3	43.6	46.1	43.5
Fe	4.7	4.5	4.9	8.9	6.3	9.7
	Sp-L	Sp-L	Web-b	Web	Web	Web

Table 2.2 continued...

Spinels Plagioclase

	RR182B SPN 1-1	RR39 SPN 1-1	RR84 SPN 1-1	RR108 SPN 3-1	RR61 SPN 3-1	RR108 PL 1-1
SiO_2	n.d.	0.24	n.d.	0.25	n.d.	55.47
TiO_2	n.d.	n.d.	n.d.	n.d.	0.32	n.d.
Al_2O_3	54.71	56.06	59.88	65.45	55.19	27.89
Cr_2O_3	11.11	11.22	5.28	1.20	3.50	n.d.
Fe_2O_3	4.90	3.02	5.09	3.36	9.84	0.41
FeO	5.88	6.48	5.63	8.47	13.93	n.a.
MnO	0.13	0.20	0.11	0.15	0.23	n.d.
MgO	22.24	21.94	22.87	21.85	17.38	n.d.
CaO	n.d.	n.d.	n.d.	0.08	n.d.	10.97
Na_2O	n.d.	n.d.	n.d.	n.d.	n.d.	5.14
K_2O	n.d.	n.d.	n.d.	n.d.	n.d.	0.24
NiO	0.38	0.44	0.51	0.51	0.55	n.d.
Total	99.35	99.60	99.37	101.32	100.94	100.12
O	4.000	4.000	4.000	4.000	4.000	8.000
Si	n.d.	0.006	n.d.	0.006	n.d.	2.504
Al	1.671	1.704	1.793	1.908	1.714	1.487
Ti	n.d.	n.d.	n.d.	n.d.	0.006	n.d.
Cr	0.228	0.229	0.106	0.023	0.073	n.d.
Fe3+	0.096	0.059	0.097	0.062	0.195	0.014
Fe2+	0.127	0.140	0.120	0.175	0.307	n.a.
Mn	0.003	0.004	0.002	0.003	0.005	n.d.
Mg	0.859	0.844	0.866	0.806	0.683	n.d.
Ca	n.d.	n.d.	n.d.	0.002	n.d.	0.532
Na	n.d.	n.d.	n.d.	n.d.	n.d.	0.449
K	n.d.	n.d.	n.d.	n.d.	n.d.	0.014
Ni	0.008	0.009	0.010	0.011	0.009	n.d.
Sum	2.992	2.995	2.996	2.997	2.992	5.000
Mg#	87.1	85.8	87.9	82.1	69.0	An= 53
Cr#	0.11	0.12	0.05	0.01	0.04	Ab= 45
						Or= 2
	Sp-L	Sp-L	Web-b	Web	Web	Web

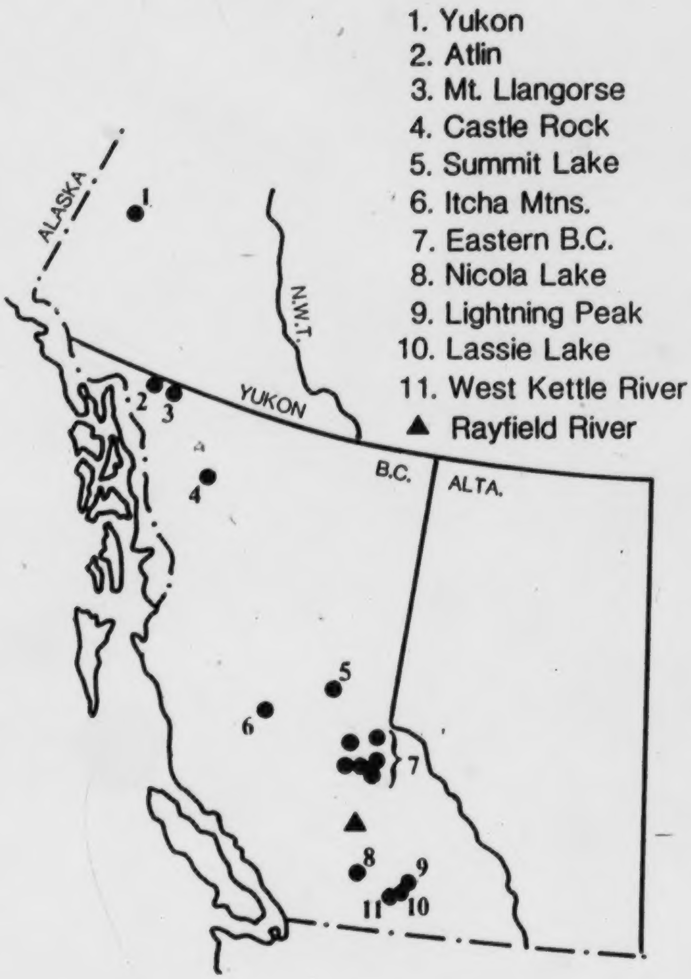
1. Yukon
2. Atlin
3. Mt. Llangorse
4. Castle Rock
5. Summit Lake
6. Itcha Mtns.
7. Eastern B.C.
8. Nicola Lake
9. Lightning Peak
10. Lassie Lake
11. West Kettle River
▲ Rayfield River
ALASKA
N.W.T.
YUKON
B.C.
ALTA.
1
2
3
4
5
6
7
8
9
10
11

Figure 2.1. Ultramafic xenolith occurrences in the Canadian Cordillera adapted from: (1) Sinclair et al., 1978; (2) and (6) Nicholls et al., 1982; (3) Higgins and Allen, 1985; (4) and (8) Littlejohn and Greenwood, 1974; (5) Brearley et al., 1984; (7) Fiesinger and Nicholls, 1977; Fujii and Scarfe, 1981 (9) Brearley and Scarfe, 1984; (10) Ross, 1983; (11) Fujii and Scarfe, 1982.

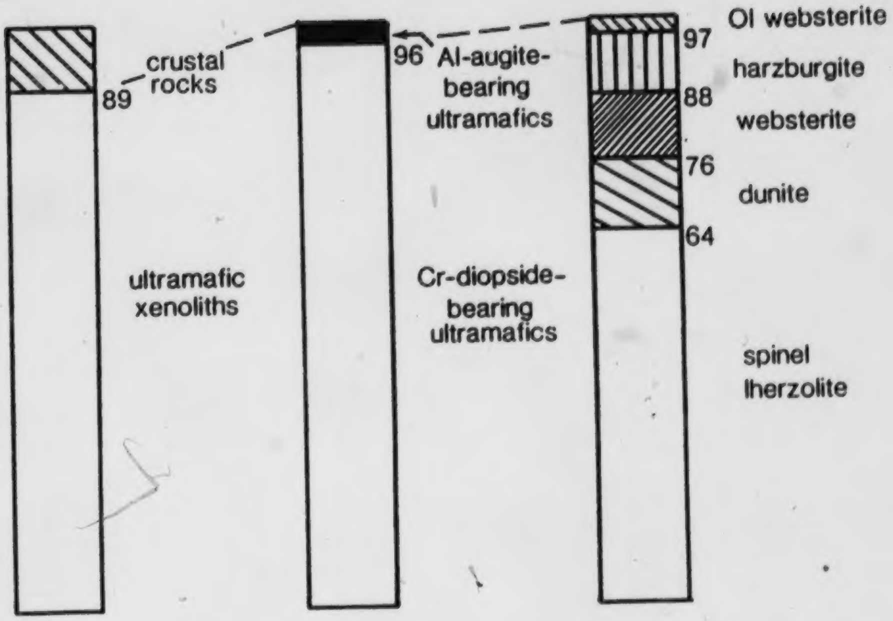

Figure 2.2. Frequency distribution of xenoliths from Rayfield River.

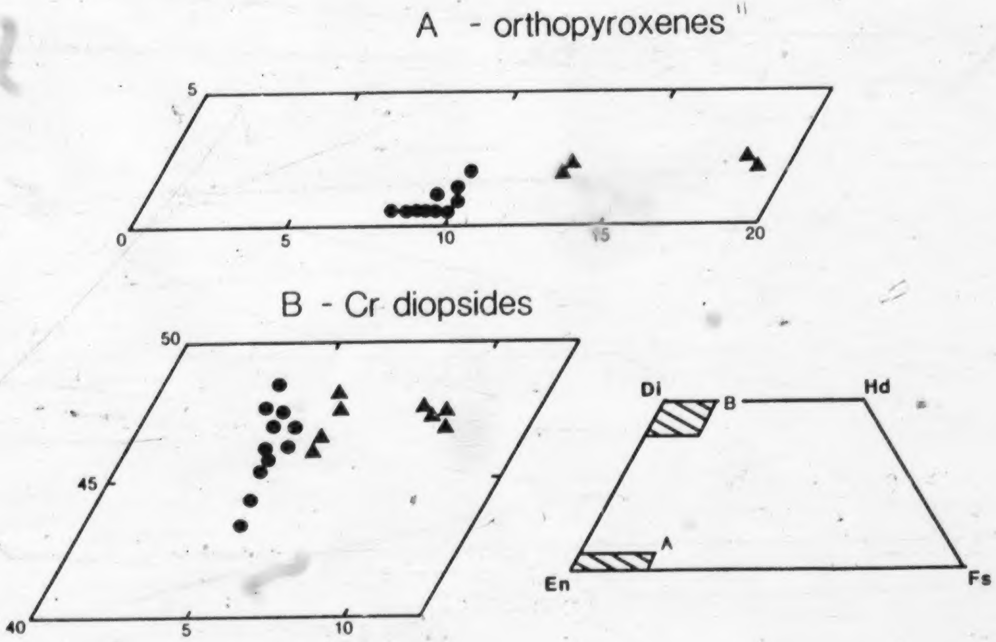

Figure 2.3. Compositional variation of pyroxenes in ultramafic xenoliths at Rayfield River. Circles - spinel lherzolite, dunite, harzburgite, and olivine websterite xenoliths. Triangles - discrete Fe-rich websterite xenoliths.

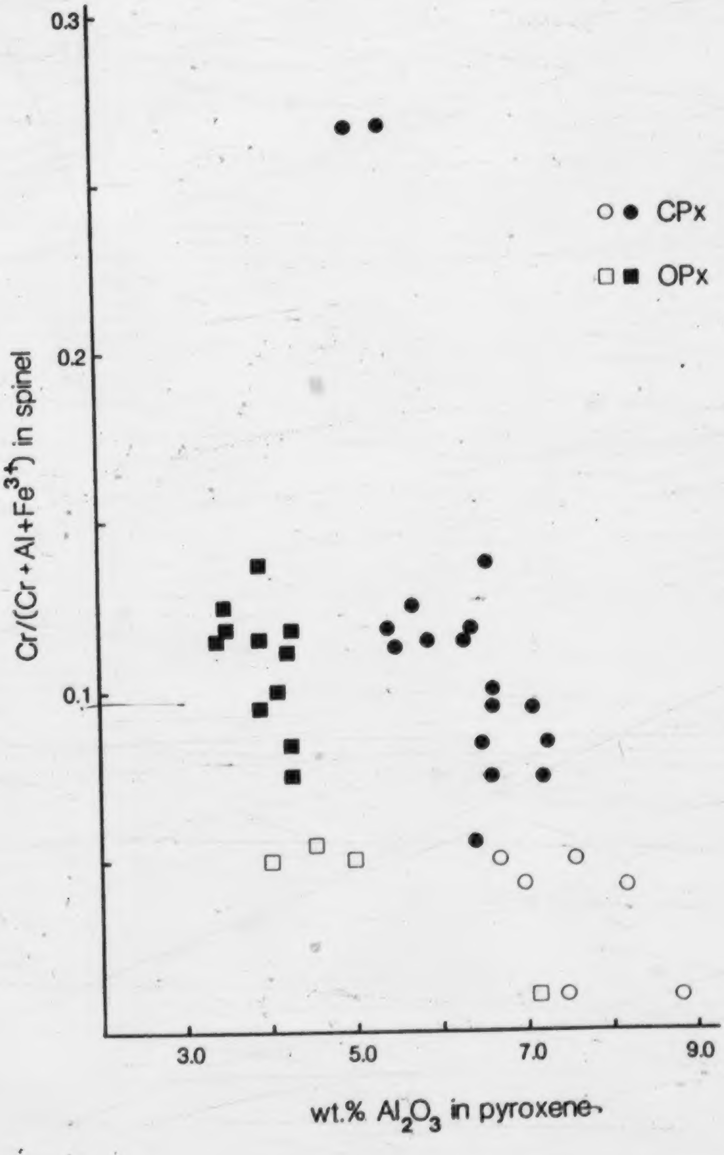

Figure 2.4. Covariation of Cr/Cr+Al+Fe^{3+} in spinels with wt.% Al_2O_3 in pyroxenes. Solid symbols - spinel lherzolite, dunite, harzburgite, and olivine websterites xenoliths. Open symbols - Fe-rich websterite xenoliths.

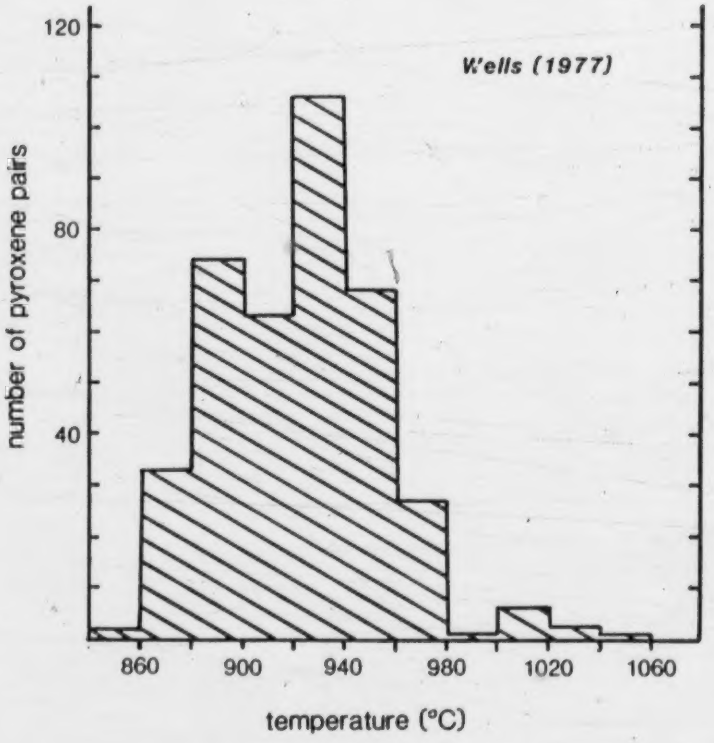

Figure 2.5. Range in calculated temperatures of equilibration for clinopyroxene - orthopyroxene pairs in Rayfield River ultramafic xenoliths.

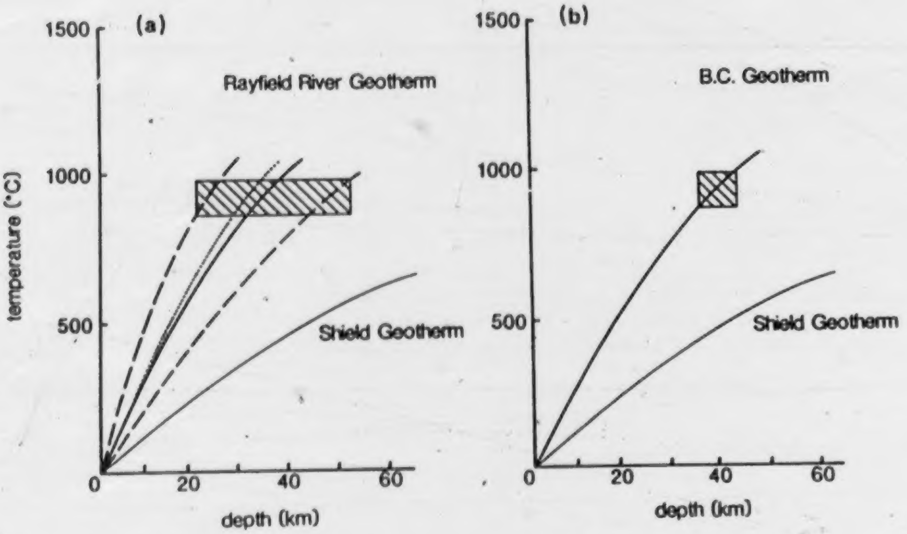

Figure 2.6. a) Geotherm constructed for the upper mantle beneath Rayfield River using the calculated temperatures of equilibration for the xenoliths and phase equilibrium constraints for spinel lherzolite. Dashed lines are the extreme errors in the geotherm. Dotted line is a geotherm based on heat flow measurements for south-central British Columbia (adapted from Davis and Lewis, 1984). b) Depth estimates for the Rayfield River xenoliths using the average Cordilleran geotherm adapted from Ranalli (1980). Also shown for comparison is the average shield geotherm adapted from Clark and Ringwood (1964).

2.8 REFERENCES

Arculus RJ (1975) Melting behaviour of two basanites in the range 10 to 35 kbar and the effect of TiO_2 on the olivine-diopside reactions at high pressures. Carnegie Inst. Washington Yb. 74:512-515.

Bevier ML (1983) Regional stratigraphy and age of Chilcotin Group basalts, south-central British Columbia. Can. J. Earth Sci. 20:515-524.

Brearley M, Scarfe CM (1984) Amphibole in a spinel lherzolite xenolith: evidence for volatiles and partial melting in the upper mantle beneath southern British Columbia. Can. J. Earth Sci. 21:1067-1072.

Brearley M, Scarfe CM, Fujii T (1984) The petrology of ultramafic xenoliths from Summit Lake, near Prince George, British Columbia. Contrib. Mineral. Petrol. 88:53-63.

Brearley M, Scarfe CM (1986) Dissolution rates of upper mantle minerals in an alkali basalt melt at high pressure: an experimental study and implications for ultramafic xenolith survival. J. Petrol. 27:1157-1182.

Clark SP Jr., Ringwood AE (1964) Density distribution and composition of the upper mantle. Rev. Geophys. 2:35-88.

Davis EE, Lewis TJ (1984) Heat flow in a back-arc environment: Intermontane and Omenica Crystalline belts, southern Canadian Cordillera. Can. J. Earth Sci. 21:715-726.

Deer WA, Howie RA, Zussman J (1966) An introduction to the rock-forming minerals. Longman Group Limited, London. 528 p.

Esperanca S, Garfunkel Z (1986) Ultramafic xenoliths from the Mt. Carmel area (Karem Maharal Volcano), Israel. Lithos 19:43-51.

Fiesinger DW, Nicholls J (1977) Petrography and petrology of Quaternary volcanic rocks, Quesnel Lake region, east-central British Columbia. In: Volcanic regimes in Canada. Edited by W.R.A. Baragar, L.C. Coleman, and J.M. Hall. Geol. Assoc. Can. Spec. Pap. 16:25-38.

Frey FA, Prinz M (1978) Ultramafic inclusions from San Carlos, Arizona: petrologic and geochemical data bearing on their petrogenesis. Earth Planet. Sci. Lett. 38:129-176.

Fujii T, Scarfe CM (1981) Petrology of ultramafic nodules from Boss Mountain, central British Columbia. Geol. Assoc. Can./Min. Assoc. Can. Prog. Abs. 6:A-20.

Fujii T, Scarfe CM (1982) Petrology of ultramafic nodules from West Kettle River, near Kelowna, southern British Columbia. Contrib. Mineral. Petrol. 80:297-306.

Haggerty SE (1979) Spinels in high pressure regimes. In: The mantle sample: inclusions in kimberlites and other volcanics. Edited by F.R. Boyd and H.O.A. Meyer. American Geophysical Union, Washington, D.C., pp. 183-196.

Herzberg CT (1978) Pyroxene geothermometry and geobarometry: experimental and thermodynamic evaluation of some subsolidus phase relations involving pyroxenes in the system $CaO-MgO-Al_2O_3-SiO_2$. Geochim. Cosmochim. Acta 41:945-957.

Higgins MD, Allen JM (1985) A new locality for primary xenolith-bearing nephelinites in northwestern British Columbia. Can. J. Earth Sci. 22:1556-1559.

Irvine TN, Baragar WRA (1971) A guide to the chemical classification of the common volcanic rocks. Can. J. Earth Sci. 8:523-548.

Irving AJ (1980) Petrology and geochemistry of composite ultramafic xenoliths in alkalic basalts and implications for magmatic processes within the mantle. Am. J. Sci. 280A:389-426.

Kuo LC, Kirkpatrick RJ (1985) Dissolution of mafic minerals and its implications for the ascent velocities of peridotite-bearing basaltic magmas. J. Geol. 93:691-700.

Le Bas MJ, Le Maitre RW, Streckeisen A, Zanettin AB (1986) A chemical classification of volcanic rocks based on the total alkali-silica diagram. J. Petrol. 27:745-750.

Kuno H, Aoki K (1970) Chemistry of ultramafic nodules and their bearing on the origin of basaltic magmas. Phys. Earth Planet. Int. 3:273-301.

Littlejohn AL, Greenwood HJ (1974) Lherzolite nodules in basalts from British Columbia, Canada. Can. J. Earth Sci. 11:1288-1308.

Maaloe S, Printzlau I (1979) Natural partial melting of spinel lherzolite. J. Petrol. 20:727-741.

MacDonald GA, Katsura, T (1964) Chemical composition of Hawaiian lavas. J. Petrol. 5:82-133.

Mercier JC, Nicolas A (1975) Textures and fabrics of upper mantle peridotites as illustrated by xenoliths from basalts. J. Petrol. 16:454-487.

Nicholls J, Stout MZ, Fiesinger DW (1982) Petrologic variations in Quaternary volcanic rocks, British Columbia, and the nature of the underlying mantle. Contrib. Mineral. Petrol. 79:201-218.

Ranalli G (1980) Rheological properties of the upper mantle in Canada from olivine microrheology. Can. J. Earth Sci. 17:1499-1505.

Ross JV (1983) The nature and rheology of the Cordilleran upper mantle of British Columbia: inferences from peridotite xenoliths. Tectonophys. 100:321-357.

Scarfe CM, Fujii T, Brearley M (1982) Heterogeneities in the upper mantle beneath south and central British Columbia. EOS, Trans. Amer. Geophys. Union 63:463.

Sen G, Presnall DC (1986) Petrogenesis of dunite xenoliths from Koolau Volcano, Oahu, Hawaii: implications for Hawaiian volcanism. J. Petrol. 27:197-219.

Sinclair PD, Tempelman-Kluit DJ, Medaris LG Jr. (1978) Lherzolite nodules from a Pleistocene cinder cone in central Yukon. Can. J. Earth Sci. 15:220-226.

Smith AD (1986) Isotopic and geochemical studies of Terrane I, south-central British Columbia. Unpublished Ph.D. Thesis, Univ. Alberta, Edmonton, 195 p.

Smith DGW (1976) Quantitative energy dispersive microanalysis. In: Short course in microbeam techniques. Edited by: D.G.W. Smith. Min. Assoc. Can. Short Course Handbook, 1, pp. 63-106.

Smith DGW, Gold CM (1979) EDATA2: a FORTRAN IV computer program for processing wavelength- and/or energy-dispersive electron microprobe analyses. Microbeam Anal.Soc.Proc.14th Ann.Conf. (San Antonio: Newbury D.E. ed), pp. 272-278.

Takahashi E (1980) Melting relations of an alkali-olivine basalt to 30 kbar, and their bearing on the origin of alkali basalt magmas. Carnegie Inst. Washington Yb. 79:271-276.

Takahashi E, Kushiro I (1983) Melting of a dry peridotite at high pressures and basalt magma genesis. Am. Miner. 68:859-879.

Wells PRA (1977) Pyroxene thermometry in simple and complex systems. Contrib. Mineral. Petrol. 68:129-139.

Wilshire HG, Shervais JW (1975) Al augite and Cr diopside ultramafic xenoliths in basaltic rocks from western United States. In: Physics and Chemistry of the Earth. Edited by: L.H. Ahrens, F. Press, S.K. Runcorn, and H.C. Urey. Vol.9. Pergammon Press, Oxford, pp. 257-272.

3. ORIGIN OF PHLOGOPITE IN MANTLE XENOLITHS FROM KOSTAL LAKE, WELLS GRAY PARK, BRITISH COLUMBIA

3.1 INTRODUCTION

The discovery of phlogopite in mantle xenoliths by Dawson and Powell (1969) confirmed that a discrete K-bearing phase existed in the upper mantle, and that it may be responsible for the presence of potassium in many magmas erupted on the Earth's surface. Since then, numerous other studies of phlogopite hosted in upper mantle xenoliths have demonstrated the capacity of this phase to retain K, Rb, Ba, H_2O and other incompatible elements in the source region of mantle derived magmas (Aoki, 1975; Boettcher and O'Neil, 1980; Delaney et al., 1980). Phlogopite may influence the trace element and isotope systematics of melts generated in the upper mantle (Bailey, 1982; Menzies, 1983). In addition, experimental studies have shown that the presence of phlogopite in mantle assemblages influences the melting behaviour of mantle peridotite (Wyllie, 1979; Wendlandt and Eggler, 1980; Olafsson and Eggler, 1983).

Previous investigations of Cordilleran ultramafic xenoliths have revealed an overall paucity of hydrous phases in the upper mantle beneath this region (e.g. Fujii and Scarfe, 1982; Ross, 1983; Brearley et al., 1984; Canil et al., 1987; Francis, 1987). Only a few occurences of amphibole and apatite have been described (Brearley and Scarfe, 1984; Higgins and Allen, 1986; Metcalfe et al., 1986). The general absence of hydrous minerals in the extensive number of xenoliths and localities studied (Fig. 3.1) is especially puzzling when considering the evidence for metasomatism manifest in the geochemical signatures of alkaline lavas derived from the Cordilleran upper mantle (e.g. Smith, 1986; Metcalfe et al., 1986; Eiche et al. 1987).

In this paper, the first major occurrence of phlogopite in ultramafic xenoliths from the Canadian Cordillera is documented. Using petrographic and mineralogical data, the paragenesis of phlogopite in lherzolite, dunite and cumulate wehrlite xenoliths hosted in lavas and ejecta of a Quaternary alkaline volcano in eastern British Columbia is described. Because of the unique origin of the phlogopites, the implications for metasomatism and alkaline magmatism in the Cordilleran upper mantle are discussed.

3.2 GEOLOGICAL SETTING

The Wells Gray Park area is situated within the Quesnel-Shuswap Highlands of eastern British Columbia and is underlain by Hadrynian and possibly younger metamorphic rocks of the Kaza Group and Shuswap Complex (Hickson and Souther, 1984). Volcanism in the region began about 3.5 Ma ago and continued into the Quaternary with the eruption of post-glacial cinder cones and blocky lava flows (Hickson and Souther, 1984).

The Kostal Lake volcanic center ($52^{o}10'$N $119^{o}57'$W) is one of four isolated, post-glacial eruptive centers located in Wells Gray Provincial Park (Hickson and Souther, 1984; Metcalfe, 1987). The center is comprised of two cinder cones; one well preserved and a second less-well preserved to the north (Metcalfe, 1987). Both centers are of central type, and are estimated to have an age of less than 7550 B.P. (Metcalfe, 1987). Most of the xenoliths in this study were collected from ejecta surrounding the rim of the southern cone and from a lava tube in a breached portion of this cone. All eruptive products from both vents are basanitoid in composition (Table 3.1).

3.3 PETROGRAPHY

Fifty ultramafic xenoliths were collected and divided into two groups based on their hand sample features. The first group is termed Type I xenoliths (Menzies, 1983) and contains dominantly olivine with subordinate orthopyroxene, apple green clinopyroxene, and spinel. The Type I xenoliths are subrounded and consist of lherzolites (47%), harzburgites (24%), dunites (24%), olivine websterites (3%), and olivine clinopyroxenites (2%), ranging in size from 2 to 8 cm. These samples show granular textures, and sometimes have a sheared appearance.

The second group has cumulate textures, and is comprised entirely of wehrlites. The cumulate xenoliths range in size from 2 to 10 cm and are subrounded. The cumulus texture is defined by large 2 to 4 mm grains of olivine or olivine aggregates enclosed in poikilitic, dark greenish black clinopyroxene.

In the field many xenoliths were weathered or altered due to hydrothermal activity during eruption. Thus, the sampling of xenoliths was biased towards large and fresh samples. However, an unbiased estimate of the xenolith population proximal to the cinder cone is 40% Type I and 60% cumulates.

Polished sections for petrographic examination and microprobe analysis were made for 18 Type I xenoliths and 12 cumulate-textured xenoliths.

Type I Xenoliths

All Type I xenoliths from Kostal Lake have either coarse equant or coarse tabular textures when classified according to Harte (1977). Olivines range in size from 1 to 3 mm, and may be strained or kink-banded, especially in harzburgite xenoliths. Olivines at the contacts between the host lava and xenoliths show a simple dissolution reaction defined by a 50 to 100 um wide zone of euhedral olivine and brown glass. Orthopyroxenes range in size from 1 to 4 mm, and at the contact with the host lava show a complex dissolution reaction defined by a 100 to 300 um wide zone of subhedral olivine, elongate clinopyroxene, opagues and brown glass. Similar features have been noted in many other spinel lherzolite xenoliths (e.g. Kuo and Kirkpatrick, 1985) and in high pressure dissolution experiments on orthopyroxene in basalt melt (Brearley and Scarfe, 1986). Clinopyroxene is usually pale green, less than 1 mm in size, and may show evidence of melting at grain boundaries as vermicular pockets of glass. Clinopyroxenes in phlogopite-bearing xenoliths contain many fluid inclusions, whereas clinopyroxenes in anhydrous xenoliths are relatively devoid of fluid inclusions. Spinels usually occur as small granules less than 2 mm in size and can be blood red, dark brown or pale green in colour.

Seven of the 18 Type I xenoliths examined in thin section contain phlogopite. In most cases, phlogopite comprises less than 1% of the mode. Phlogopites in the Type I xenoliths are dark reddish brown, pleochroic, unzoned, and may occur as 0.5 to 1.5 mm sub-euhedral grains along grain boundaries in dunite and lherzolite xenoliths (Fig. 3.2a). In addition, phlogopite also occurs as subhedral grains hosted in primary 10 to 100 um diameter fluid inclusions in clinopyroxene. The fluid inclusions hosting phlogopite show preferred orientations in their long dimension, possibly reflecting crystallographic control by the host clinopyroxene (Fig. 3.2b,3.3a). None of the phlogopites show reaction relationships with other coexisting phases.

Cumulate Xenoliths

The wehrlite xenoliths all show meso- and/or adcumulate texture (Irvine, 1982) defined by large ($\leq$ 2 cm), optically continuous, pale green clinopyroxene oikocrysts enclosing 3.5 mm diameter, subhedral single grains of olivine or 1 to 5 mm sized polycrystalline aggregates of olivine (Fig. 3.4). The polycrystalline aggregates contain inclusions of dark brown, granular spinel, and are texturally (but not compositionally) identical to other discrete dunite xenoliths from Kostal Lake. Intercumulus clinopyroxene often contains lamellae of orthopyroxene, 5 to 50 um thick, exsolved along (100). In rare cases, intercumulus clinopyroxene has been melted, resulting in the formation of pockets of clear glass which contain small grains of euhedral clinopyroxene, pale green spinel, and euhedral prisms of reddish brown rhonite. Clinopyroxenes usually show fritted margins adjacent to olivines, possibly due to infiltration of the host magma along grain boundaries.

Six of the 12 cumulate xenoliths studied in thin section contain phlogopite. Phlogopite in the wehrlites comprises less than 1% of the mode, and can occur as either subhedral grains contained in 10 to 100 um diameter fluid inclusions, or as thin plates associated with pale green spinel oriented parallel to orthopyroxene lamellae exsolved from intercumulus clinopyroxene (Fig. 3.3b).

3.4 MINERAL CHEMISTRY

Analytical Methods

Mineral compositions for 18 of 30 xenoliths examined in thin section were determined using wavelength dispersive analysis (WDA) on an ARL SEMQ microprobe at the University of Alberta, and on a MAC three channel microprobe at the Geophysical Laboratory. Routine analysis for all elements by WDA employed an operating voltage of 15 kV and a probe current of 10 to 12 nA. Data for the ARL probe were reduced with ZAF corrections using MAGIC IV (Colby, 1972). Raw data for the MAC probe were reduced using the Bence and Albee (1968) method, with the correction factors of Albee and Ray (1970). Core and rim compositions were analyzed for most minerals. Energy Dispersive Analysis (EDA) was used for qualitative analysis of fluid inclusions. EDA spectra of the fluid inclusions were reproduced using EDATA2 (Smith and Gold, 1979).

Olivine

Olivines in the Type I xenoliths range in composition from Fo_{84} to Fo_{92} (Fig. 3.5, Table 3.2). The bimodal distribution in olivine compositions might suggest that some of the more Fe-rich compositions are representative of Type II xenoliths, or re-equilibrated cumulates (Fig. 3.5). The NiO content of olivine ranges from 0.15 to 0.40 wt.% and shows no correlation with Fo content. There is also no correlation between the Fo content of xenolith olivines and the presence or absence of phlogopite. The CaO contents of all Type I olivines are less than 0.09 wt.%.

Olivines in the wehrlite cumulates range from Fo_{80} to

$Fo_{84.5}$ and contain less than 0.3 wt.% NiO (Table 3.2). On average, CaO contents of wehrlite olivines are higher than in Type I olivines (0.07 to 0.29 wt.%).

Orthopyroxene

Orthopyroxenes in the Type I xenoliths are $En_{88}Wo_2Fs_{10}$ to $En_{83}Wo_3Fs_{14}$ in composition and range in Al_2O_3 and Cr_2O_3 content from 1.21 to 3.60 and 0.36 to 0.75 wt.%, respectively (Table 3.3). Most Type I xenoliths contain orthopyroxenes which show slight increases in Al_2O_3 and Cr_2O_3 towards their rim, possibly due to thermal perturbation in the mantle prior to their entrainment in the host magma (e.g. Witt and Seck, 1987).

Clinopyroxene

Clinopyroxenes in Type I xenoliths from Kostal Lake plot mainly within the diopside field of Morimoto (1988) in terms of their major quadrilateral components (Table 3.4). They contain high amounts of Cr_2O_3 (0.69 to 2.7 wt.%) and are referred to as chrome diopsides (Wilshire and Shervais, 1975). The Al_2O_3 content of the chrome diopsides ranges from 2.78 to 5.80 wt.%. Unlike the orthopyroxenes described above, most chrome diopsides from Kostal Lake show little if any zoning in Al_2O_3 or Cr_2O_3 (Table 3.4). Chrome diopsides hosting inclusions of phlogopite (see Fig. 3.2b,3.3a) show no observable differences in composition when compared to chrome diopsides in which phlogopite is absent.

Intercumulus clinopyroxenes in the wehrlite xenoliths are augite in composition (using nomenclature of Morimoto, 1988), and contain more Al_2O_3 (up to 8.17 wt.%), TiO_2 (> 0.88 wt.%) and less Cr_2O_3 (0.53 to 1.00 wt.%) than the Type I clinopyroxenes (Table 3.4). Wehrlite clinopyroxenes also contain a greater proportion of Al^{IV} (Table 3.4). In many wehrlites, intercumulus clinopyroxene has exsolved lamellae of orthopyroxene with compositions close to those of the Type I orthopyroxenes, but with greater amounts of Fs component (Table 3.3). Where intercumulus clinopyroxene has melted to form large patches of glass, decreases in Na_2O ,CaO, Al_2O_3, Cr_2O_3 and FeO, and increases in MgO and TiO_2 are observed adjacent to the melted region (Table 3.4).

Phlogopite

Phlogopites in Type I xenoliths have ($Mg/Mg+Fe^{2+}x100$) (Mg#'s) similar to those of coexisting olivines, orthopyroxenes and clinopyroxenes (Fig. 3.5). The partition coeffecients for Fe and Mg between phlogopites and coexisting clinopyroxene and olivine ($K_D = [Fe/Mg]_{phl} / [Fe/Mg]_{ol,cpx}$) range from 0.99 to 1.37 in both the Type I and wehrlite cumulate xenoliths. These K_D's are similar to those observed for other phlogopite-bearing mantle peridotites (0.96 to 1.52 - Wilkinson, 1975; Francis, 1976; Girod et al., 1981; Nicholls et al., 1981), and for phlogopites coexisting with clinopyroxene and olivine in high pressure melting experiments on ultramafic bulk compositions (1.00 to 1.60 - Lloyd et al., 1985). This observation suggests that phlogopites in the Kostal Lake xenoliths have equilibrated with their coexisting phases. The remarkably constant Fe/Mg ratios across phlogopite grains from the Kostal Lake xenoliths also strongly implies they have attained chemical equilibrium. Unfortunately, the influence of temperature, pressure, oxygen fugacity and bulk composition on the mineral chemistry of Ti-bearing phlgopites prevents a rigorous comparison of the Kostal Lake K_D's with K_D's extracted from experimental data. Experimental investigations in which phlogopite, olivine and/or clinopyroxene are equilibrated at high pressure show a wide range of K_D's (0.65 to 3.00) that appear uncorrelated with either pressure, temperature, oxygen fugacity, H_2O activity or bulk composition (c.f. Lloyd et al., 1985; Esperanca and Holloway, 1986, 1987). This may be due to the complex solid solutions permissable in Ti-bearing micas.

Type I phlogopites from Kostal Lake are enriched in TiO_2 (3.49 to 6.13 wt.% - Table 3.5) with values approaching those found in kimberlite-hosted mantle xenoliths (e.g. Delaney et al., 1980; Boyd et al., 1982). On TiO_2 vs. Mg# plots, Type I phlogopites from Kostal Lake fall within the field for lherzolite phlogopites hosted in alkaline rocks (Bachinski and

Simpson, 1984). Fluorine and chlorine contents measured for a few Type I phlogopites (Table 3.5) are lower than those of many kimberlite-hosted xenoliths (Smith et al., 1981). Type I phlogopites have Na/Na+K (0.09 to 0.19) typical of many other spinel lherzolite-hosted phlogopites (Arai, 1986) but contain much less X_{Si} (X_{Si}=Si/Si+Al on tetrahedral sites - Table 3.5) than phlogopites from other spinel lherzolites (e.g. Arai, 1984).

Phlogopites in wehrlite xenoliths tend to have higher TiO_2 (6 to 7 wt.%) and, like their coexisting olivines and clinopyroxenes, lower Mg#'s when compared to the Type I phlogopites. Again, the similarity in Mg# between wehrlite phlogopites and their coexisting silicates suggests they have attained equilibrium (Fig. 3.5).

Spinel

Spinels from the phlogopite-bearing xenoliths from Kostal Lake are typically more Fe-rich than other spinels from lherzolite xenoliths from British Columbia (Fig. 3.6). Some spinels are anomalously rich in TiO_2 (up to 1.21 wt.%) and Cr_2O_3 (up to 42.00 wt%) when compared to spinels from other xenoliths in British Columbia (Table 3.6). Spinels in phlogopite-bearing xenoliths, especially those directly associated with phlogopite (Fig. 3.3b), usually contain more Fe^{3+} when compared to anhydrous xenoliths from Kostal Lake and elsewhere in the Canadian Cordillera (Fig. 3.6, Table 5.5). Spinels from all xenoliths are zoned in Mg#, with higher Mg#'s toward their grain rims (Table 3.6). This zoning is due to cation interdiffusion during heating of the xenoliths in the upper mantle prior to entrainment in their host magma (Ozawa, 1983).

Rhonite

Analyses of rhonite hosted in patches of glass contained in intercumulus clinopyroxene are given in Table 3.7. The compositions are comparable to rhonites with similar parageneses from other ultramafic xenoliths (e.g. Gamble and Kyle, 1987).

Glass

Analyses of glasses produced by melting of intercumulus clinopyroxene are presented in Table 3.7. The glasses are peraluminous and are heterogeneous in SiO_2 and alkalies. Similar siliceous and peraluminous glasses were noted by Frey & Green (1974) in ultramafic xenoliths from Australia.

Fluid Inclusions

Fluid inclusions hosted by interculmulus clinopyroxene in wehrlite xenolith KLC18 (which contains inclusions of phlogopite) were found by back scattered electron (BSE) imaging during routine electron microprobe analysis. The inclusions existed just beneath the surface of their host grain. Upon bombardment with electrons the fluid inclusions burst, and a qualitative estimate of their compositions was determined by Energy Dispersive Analysis (EDA). Examination of the analyzed inclusions afterwards showed a thin bubble of fluid expelled beneath the carbon coating of the polished thin section, thus indicating that the fluid inclusion did indeed burst during analysis. The EDA spectra of these inclusions show significant concentrations of Na, P, K and Cl, and minor S (Fig. 3.7). The exact speciation of these elements in the fluid, or whether they are the components of minerals (e.g. apatite, phlogopite) crystallized within the fluid inclusions, could not be determined by EDA, BSE or petrographic examination.

3.5 DISCUSSION

Ultramafic Xenoliths

Type I xenoliths from Kostal Lake are similar in their major and minor element mineral chemistry to numerous other Type I xenoliths from British Columbia and elsewhere (e.g. Wilshire and Shervais, 1975; Frey and Prinz, 1978; Fujii and Scarfe, 1982). The Fe-rich character of some of the xenoliths when compared to other xenoliths from British Columbia may be a source characteristic, or may be due to metasomatism, as will be discussed later.

The temperatures of equilibration of the Type I xenoliths, estimated from two-pyroxene and olivine-spinel geothermometry, range from 900 to 1100°C (Table 3.8). These temperatures of equilibration suggest the Type I xenoliths have equilibrated in the upper mantle at depths between 40 and 50 km, if typical Cordilleran geotherms are assumed (23°C/km - e.g. Fujii and Scarfe, 1982; Brearley et al., 1984; Canil et al., 1987).

The presence of orthopyroxene lamellae in intercumulus clinopyroxene of both phlogopite-bearing and "dry" wehrlite xenoliths indicates that these xenoliths have experienced a higher temperature history prior to their incorporation in the host magma. Two-pyroxene temperatures calculated for the intercumulus clinopyroxenes and their coexisting orthopyroxene lamellae indicate that the wehrlites cumulates initially crystallized at temperatures above about 1080°C, but re-equilibrated on cooling (Table 3.8).

Wehrlite xenoliths from Kostal Lake most likely represent cumulates of magmas precursory to the post-glacial alkaline lavas in which they are entrained. Volcanism in the Wells Gray area began about 3.5 Ma ago, and predates the eruption of basanitoid lavas at Kostal Lake by at least 3.0 Ma (Hickson and Souther, 1984; Metcalfe, 1987). These precursory magmas may have arrested at the uppermost mantle due to density constraints (e.g. Stolper and Walker, 1980) and fractionated olivine and clinopyroxene. Subsequent alkaline magmas traversing this part of the lithosphere below eastern British Columbia may have disrupted these earlier olivine/clinopyroxene cumulates and transported them to the surface as the Kostal Lake wehrlite xenoliths. The crystallization sequence present in the wehrlite cumulates is identical to that observed in melting experiments on some tholeiitic and alkalic basalts at pressures of 10 to 12 kbar (e.g. Arculus, 1975; Bender et al., 1978; Takahashi, 1980; Fisk et al., 1988). These pressures correspond to depths of about 30 to 36 km, the estimated depth of uppermost mantle beneath the Shuswap Metamorphic Complex (Cook, 1986), which underlies volcanics of the Wells Gray region.

Origin of Phlogopite and Conditions During Metasomatism

Numerous petrological studies of mantle xenoliths have described possible reactions or mechanisms for phlogopite formation in the upper mantle (e.g. Lloyd and Bailey, 1975; Erlank et al., 1987). All phlogopite-forming reactions investigated experimentally (e.g. Yoder and Kushiro, 1969; Modreski and Boettcher, 1973) have indicated that the reaction of alkalic melts of varying degrees of silica saturation with olivine in the upper mantle can form phlogopite. These types of reactions are consistent with textural information recorded in some phlogopite-bearing xenoliths (e.g. Lloyd and Bailey, 1975). However, the fact that phlogopites and coexisting olivines in the Kostal Lake xenoliths do not show any reaction relationships, and are in chemical equilibrium (Fig. 3.5, see also previous discussion) suggests that none of these reactions are probably responsible for the formation of phlogopite in either the wehrlite or Type I xenoliths.

Francis (1976) and Delaney _et al._ (1980) have described "secondary" phlogopites in a variety of xenolith parageneses involving the breakdown of amphibole, in association with secondary clinopyroxene and spinel. Aoki (1975) also outlined breakdown reactions involving amphibole or garnet as possible precursor phases to mantle phlogopites. There is, however, no evidence for amphibole breakdown in any of the Kostal Lake xenoliths.

The association of phlogopites with orthopyroxene lamellae exsolved from intercumulus clinopyroxene in the wehrlite cumulates may indicate that phlogopite formed as a breakdown product of orthopyroxene or spinel. It was noted above, however, that phlogopite in the wehrlite xenoliths can occur as inclusions in intercumulus clinopyroxenes which _have not_ exsolved orthopyroxene. Therefore, phlogopites crystallizing along the orthopyroxene lamellae are not necessarily the reaction products of exsolved orthopyroxene.

The phlogopites themselves, along with orthopyroxene and spinel, may have exsolved from host intercumulus clinopyroxene in the wehrlite cumulates. If this were the case, however, then the higher water activities of the magma which crystallized these "wet" intercumulus clinopyroxenes should be reflected in the clinopyroxene compositions. Hydrous magmas undergoing crystallization would have silica activities which are higher than those for anhydrous magmas (Kushiro, 1975) and precipitate clinopyroxenes with greater Al^{IV} and lower Wo contents (Irvine, 1974; Campbell and Borley, 1974; Wass, 1979). However, clinopyroxenes in both the "dry" and phlogopite-bearing wehrlites contain similar amounts of Al^{IV} and Wo component (Table 3.4), and have exsolved orthopyroxene. For this reason, the precipitation of phlogopite cannot be due to the exsolution process.

Two petrographic observations in the Kostal Lake xenoliths shed light on the possible origin of phlogopite in the upper mantle beneath this region. Firstly, because the phlogopites are crystallographically controlled (see Fig. 3.2,3.3) crystallization after formation of their host pyroxenes is suggested. Secondly, the common association of crystallographically controlled fluid inclusions with the phlogopites (Fig. 3.3a,b) implies that a fluid phase was involved, and it infiltrated along planes of weakness in xenolith minerals. Inferences can be made regarding the composition of the metasomatic agents responsible for the formation of phlogopite by examining the mineral and fluid inclusion chemistry in the xenoliths. EDA analysis of fluid inclusions indicates that the fluid or melt from which they formed contained considerable Na, K, Cl, P, and S. The

H_2O/CO_2 ratios of the fluids are unknown; however, the crystallization of phlogopite within some of the inclusions suggests considerable amounts of H_2O were present.

The TiO_2 contents of the phlogopites in these inclusions are problematic in that they suggest high Ti concentrations in fluids at upper mantle temperatures and pressures, which are not observed experimentally (e.g. Schneider and Eggler, 1986). Thus, it is probable that the metasomatic fluid which crystallized phlogopite exsolved from silicate melt. The existence of such a melt, however, remains unconstrained by either the minerals or fluid inclusions in the xenoliths; glass was not identified in any of the inclusions examined. A "Fe-Ti enriched" melt, possibly basanitic in composition, has been inferred as a metasomatizing agent in other lherzolite xenoliths (e.g. Menzies, 1983; Hawkesworth et al., 1984; Kempton, 1987). The Fe-rich nature of other Cordilleran xenoliths has been attributed to reaction with Fe-rich melt in the mantle (Francis, 1987). This could explain the more Fe-rich character of some Kostal Lake xenoliths, when compared to other Cordilleran xenolith populations (Fig. 3.5). However, phlogopites occur in both Fe-rich and Fe-poor xenoliths from Kostal Lake (Fig. 3.5), thereby invalidating any relationship between Fe-enrichment and formation of phlogopite in the upper mantle beneath this area.

Spinels are a particularly useful indicator of the oxygen fugacity (f_{O2}) recorded in spinel lherzolite xenoliths (e.g. O'Neill and Wall, 1987; Wood and Virgo, 1987; Mattioli and Wood, 1988). Most spinels from phlogopite-bearing xenoliths from Kostal Lake are notably high in Fe^{3+} (Fig. 3.6). The high Fe^{3+} concentrations of some spinels, particularly those texturally associated with phlogopites (Fig. 3.3b), implies increased f_{O2} attendant upon metasomatism of the upper mantle beneath Kostal Lake. The f_{O2} calculated for two xenoliths from Kostal Lake using the thermobarometric method of O'Neill and Wall (1988) and Fe^{3+} contents of spinels determined by Mossbauer spectroscopy, plot at the oxidized end (near the FMQ (fayalite-magnetite-quartz) buffer at 15 kbar) of all anhydrous spinel lherzolite xenoliths from British Columbia (Canil et al., in prep.). Thus, the higher f_{O2} recorded by spinels from these metasomatized xenoliths may be attributed to the influx of oxidized fluids (containing H_2O) that were responsible for the formation of phlogopite.

All the above compositional information recorded in the mineralogy of the Kostal Lake xenoliths suggests that metasomatism of the upper mantle beneath this region involved a H_2O-bearing fluid/melt phase rich in incompatible elements, with H_2O, K and Ti being partitioned into phlogopite. The ingress of metasomatic fluids resulted in oxidation of the upper mantle beneath this region. The oxidation state of the fluid/melt involved in metasomatism was at least as high as FMQ, possibly higher. The composition of a coexisting silicate melt phase, if it were responsible for the modal metasomatism, is difficult to discern. Nonetheless, the Fe-rich nature of some

Kostal Lake xenoliths is probably not attributed to infiltration of "Fe-Ti enriched" melt attendant upon metasomatism and formation of phlogopite.

Timing and Petrological Implications of Metasomatism

There has been considerable debate as to whether metasomatism in the upper mantle, either by fluids or melts, is a necessary "precursor" or "consequence" of alkaline magmatism. Most of this discussion is centered on radiogenic isotope studies of alkaline lavas and their entrained spinel lherzolite xenoliths (e.g. Menzies and Murthy, 1980; Roden et al., 1984). Textural relationships in xenoliths showing metasomatic enrichment have also been useful in providing constraints on the temporal as well as spatial relationships between metasomatic agents and their host upper mantle wall rocks (Francis, 1976; Irving, 1980; Erlank et al., 1987).

The textural relationships preserved in xenoliths from the Kostal Lake suite can provide some constraints on the timing of metasomatism in the upper mantle beneath this region. The fact that phlogopites have crystallized from ingressing fluid/melt in presumed accumulates (i.e. wehrlites) of magmas precursory to the post-glacial alkaline phase of volcanism in the Wells Gray area, suggests that the metasomatic event responsible for the formation of phlogopite occurred after the initial phase of volcanism in the region. Volcanism in the Wells Gray region began 3.5 Ma ago (Hickson and Souther, 1984). If the wehrlite cumulates formed as a result of this early stage of magmatism, then metasomatism of the upper mantle beneath Kostal Lake must have taken place after 3.5 Ma, and prior to about 400 B.P. (the minimum age of post-glacial lavas in which the wehrlites are entrained - Metcalfe, 1987).

The scarcity of phlogopite in numerous Cordilleran xenoliths exclusive of the Kostal Lake suite attests to its probable localized occurrence in the upper mantle beneath the Canadian Cordillera. Thus, if a K-rich component occurs only locally in the upper mantle beneath the Canadian Cordillera, and if the lateral extent of partial melting beneath this region is limited to small "batch"-type processes (e.g. Eiche et al., 1987), then the eruption of K-rich lavas should be random and of limited extent within this alkaline province. Indeed, a survey of the geochemistry of primary Cenozoic alkaline lavas from the Canadian Cordillera reveals that most of these lavas have sodic chemical characteristics (Table 3.9). This would suggest that if any volatile-bearing phase played a major role in the genesis of alkaline magmas in this region, amphibole, rather than phlogopite, would be a more likely candidate (e.g. Brearley and Scarfe, 1984). Nonetheless, the occurrence of phlogopite in the upper mantle beneath eastern British Columbia is significant in that this phase can be considered a potential reservoir for alkalies, incompatible elements and volatiles in the source regions of more K-rich alkaline lavas erupted at some volcanic centers within the Canadian Cordillera (Table 3.9).

3.6 SUMMARY

Phlogopite occurs in both wehrlite cumulate and Type I xenoliths hosted in basanitoid flows and ejecta of the Kostal Lake volcanic center, Wells Gray Park, British Columbia. The phlogopites are enriched in Ti and Cr, and have attained chemical equilibrium with their coexisting phases.

The common association of crystallographically controlled fluid inclusions (which contain phlogopite) with phlogopite-bearing xenoliths, supports the contention that a fluid phase infiltrated the upper mantle beneath Kostal Lake, and precipitated phlogopite. Qualitative analysis of fluid inclusions preserved in the xenoliths indicates that the fluid phase contained Na, K, Cl, P, S and H_2O. The higher Fe^{3+} content of spinels from phlogopite-bearing xenoliths, compared with anhydrous xenoliths from Kostal Lake and elsewhere in the Canadian Cordillera, suggests that metasomatism resulted in oxidation of the upper mantle beneath this region. Metasomatism by fluids/melts most likely occurred after the initial phase of volcanism (3.5 Ma) in the Wells Gray area, and prior to the eruption of post-glacial, xenolith-bearing lavas and ejecta at Kostal Lake (about 400 B.P.).

Table 3.1 Representative Compositions of Kostal Lake Lavas*

	(wt.%)		CIPW Norm (wt.%)		
SiO_2	44.40	44.17	Q	-	-
TiO_2	2.62	2.50	Co	-	-
Al_2O_3	13.14	12.72	Or	8.9	9.2
Fe_2O_3	4.12	4.00	Ab	12.8	10.9
FeO	8.56	8.69	An	14.7	12.1
MnO	0.18	0.16	Ne	10.1	12.5
MgO	10.68	11.43	Wo	12.0	12.5
CaO	9.49	9.21	En	8.4	8.7
Na_2O	3.72	4.01	Fs	2.6	2.7
K_2O	1.51	1.55	Fo	12.8	13.9
P_2O_5	0.55	0.56	Fa	4.4	4.7
Total	98.97	99.00	Mt	6.0	5.8
			Il	5.0	4.8
			Ap	1.2	1.2

Notes: * Adapted from Metcalfe (1987). Fe_2O_3 calculated by the method of Irvine and Baragar (1971).

Table 3.2 Representative Analyses of Xenolith Olivines

	KLBR1	KL3	KL28	KLC18	KL29	KLC18
	OLV 2-2	OLV 2-1	OLV 1-1	OLV 2-1	OLV 1-1	OLV 3-1
SiO_2	40.60	40.05	41.00	39.85	38.84	39.64
TiO_2	n.d.	n.d.	0.00	n.d.	n.d.	n.d.
FeO	13.39	14.81	9.21	17.79	16.09	18.79
MnO	0.18	0.05	0.16	0.23	0.17	0.20
MgO	47.06	45.52	50.15	43.06	44.05	42.49
CaO	n.d.	0.05	0.09	0.16	0.07	0.11
NiO	0.35	0.19	0.34	0.32	0.23	0.30
Total	101.58	100.67	100.98	101.41	99.46	101.53
O	3.995	3.997	4.000	4.000	3.985	3.998
Si	0.995	0.997	0.992	1.000	0.985	0.998
Ti	-	-	0.001	-	-	-
Fe^{2+}	0.265	0.302	0.171	0.373	0.310	0.391
Mn	0.004	0.001	0.003	0.005	0.004	0.004
Mg	1.720	1.689	1.809	1.611	1.664	1.594
Ca	-	0.001	0.002	0.004	0.002	0.003
Ni	0.007	0.004	0.007	0.006	0.005	0.006
Mg#	86.2	84.6	90.7	81.2	83.0	80.1
Rock Type	LHZ	LHZ	DUN	WER	WER	WER

Notes: n.d.=not detected Mg#=(Mg/Mg+Fe^{2+})x100 Rock Type: LHZ=lherzolite, WER=wehrlite, DUN=dunite

Table 3.3 Representative Analyses of Xenolith Orthopyroxenes

	KLBR1	KLBR1	KLBR7	KLBR7	KL3	KL3	KLC18*
	OPX 1-1	OPX 1-2	OPX 6-1	OPX 6-2	OPX 1-1	OPX 1-2	OPX 1-1
SiO_2	55.29	54.57	56.12	55.36	56.15	56.17	54.15
TiO_2	0.13	0.25	0.05	0.06	0.06	0.18	0.20
Al_2O_3	3.60	4.54	1.39	2.17	1.86	2.02	4.11
Cr_2O_3	0.36	0.66	0.44	0.58	0.38	0.41	0.44
FeO	8.49	8.72	6.41	6.54	8.99	9.10	9.98
MnO	0.15	0.23	0.14	0.11	0.18	0.19	0.13
MgO	31.10	30.89	33.03	32.69	30.79	30.50	30.78
CaO	1.05	0.92	0.88	0.91	0.59	0.74	1.15
Na_2O	n.d.	n.d.	0.18	0.20	0.15	0.16	n.d.
K_2O	n.d.	n.d.	n.d.	n.d.	n.d.	n.d.	n.d.
NiO	n.d.	0.23	0.11	0.10	0.07	0.07	n.d.
Total	100.17	101.01	98.75	98.72	99.22	99.54	100.96
O	6.012	6.001	6.004	6.001	6.004	6.028	5.978
Si	1.930	1.893	1.966	1.954	1.984	1.981	1.882
Al	0.148	0.186	0.057	0.089	0.077	0.084	0.168
Ti	0.003	0.007	0.001	0.002	0.002	0.005	0.006
Cr	0.010	0.018	0.012	0.016	0.011	0.011	0.012
Fe^{2+}	0.248	0.253	0.188	0.190	0.266	0.268	0.247
Mn	0.004	0.007	0.004	0.003	0.005	0.006	0.004
Mg	1.618	1.597	1.724	1.696	1.621	1.604	1.595
Ca	0.039	0.034	0.033	0.034	0.022	0.028	0.043
Na	-	-	0.012	0.014	0.010	0.011	
K	-	-	-	-	-	-	-
Ni	-	0.006	0.003	0.003	0.002	0.002	-
Mg#	86.7	86.3	90.2	89.9	85.9	85.7	84.6
Ca	2.1	1.8	1.7	1.8	1.2	1.5	2.2
Mg	84.9	84.8	88.7	88.3	84.9	84.4	82.
Fe	13.0	13.4	9.7	9.9	13.9	14.1	15.0
Rock Type	LHZ	LHZ	LHZ	LHZ	LHZ	LHZ	WER

Notes: Grain rims are labelled with -2 (e.g. OPX 1-2). Grain cores are labelled with -1 (e.g. OPX 1-1). * Orthopyroxene lamellae exsolved from intercumulus clinopyroxene. See Table 3.2 for Rock Type abbreviations.

Table 3.4 Representative Analyses of Xenolith Clinopyroxenes

	KLBR1 CPX 1-1	KLBR1 CPX 1-2	KL28 CPX 1-1	KL9 CPX 2-1	KLC18 CPX 1-1	KL29 CPX 3-1	KL29[a] CPX 3-2
SiO_2	52.70	52.47	52.24	53.65	51.00	49.21	50.00
TiO_2	0.50	0.56	0.84	0.23	0.88	1.34	1.77
Al_2O_3	5.38	5.80	2.78	3.52	6.76	8.17	6.19
Cr_2O_3	0.69	0.95	2.08	1.35	0.53	1.00	0.54
FeO	4.49	4.44	2.56	3.07	5.57	5.03	4.24
MnO	n.d.	0.07	0.07	0.08	n.d.	0.10	0.06
MgO	16.10	15.87	17.30	16.04	16.04	14.76	17.20
CaO	19.65	19.98	21.36	20.95	18.95	19.13	18.73
Na_2O	0.73	0.71	0.64	1.37	0.72	1.21	0.66
K_2O	n.d.	n.d.	n.d.	n.d.	n.d.	n.d.	n.d.
NiO	n.d.	n.d.	0.08	n.d.	n.d.	0.05	0.03
Total	100.24	100.95	99.95	100.26	100.45	100.00	99.42
O	6.026	6.024	5.991	6.000	5.977	6.000	6.990
Si	1.913	1.896	1.901	1.939	1.849	1.793	1.824
Al	0.230	0.247	0.119	0.150	0.289	0.351	0.266
Ti	0.014	0.015	0.023	0.006	0.024	0.037	0.049
Cr	0.020	0.027	0.060	0.039	0.015	0.029	0.016
Fe^{2+}	0.136	0.134	0.078	0.076	0.169	0.107	0.109
Mn	-	0.002	0.002	0.002	-	0.003	0.002
Mg	0.871	0.855	0.938	0.864	0.867	0.802	0.935
Ca	0.764	0.774	0.833	0.811	0.736	0.747	0.732
Na	0.051	0.050	0.045	0.096	0.051	0.086	0.047
K	-	-	-	-	-	-	-
Ni	-	-	0.002	-	-	0.001	0.001
Mg#	86.5	86.4	92.3	90.3	83.7	83.9	87.9
Ca	43.1	43.9	45.0	45.9	41.5	43.9	40.7
Mg	49.2	48.5	50.7	48.9	48.9	47.1	42.1
Fe	7.7	7.6	4.2	5.2	9.5	9.0	7.2
AlVI/AlIV	1.67	1.37	0.20	1.45	0.92	0.70	0.51
Rock Type	LHZ	LHZ	DUN	LHZ	WER	WER	WER

Notes: [a]Clinopyroxene adjacent to patches of melt. See Table 3.2 for Rock Type abbreviations.

Table 3.5 Representative Analyses of Xenolith Phlogopites

	KLBR1 PHL 1-1	KLBR1 PHL 2-1	KL28 PHL 1-1	KL28 PHL 3-1	KLC18 PHL 3-1	KLC18 PHL 2-1
SiO_2	37.08	37.81	37.77	38.18	36.94	36.74
TiO_2	5.20	3.49	6.13	6.06	6.12	7.07
Al_2O_3	15.98	16.26	15.56	14.74	15.94	15.62
Cr_2O_3	1.26	0.82	2.24	2.07	0.53	0.55
FeO	6.35	5.11	4.09	4.18	6.44	7.14
MnO	n.d.	n.d.	n.d.	n.d.	n.d.	n.d.
MgO	18.86	20.23	20.26	20.25	18.03	17.05
CaO	n.d.	n.d.	n.d.	n.d.	n.d.	0.16
Na_2O	0.70	0.46	1.13	1.20	0.49	0.49
K_2O	9.65	10.05	8.50	8.12	9.62	9.41
NiO	n.d.	n.d.	0.17	0.25	0.12	n.d.
F	0.19	0.20	n.a.	n.a.	0.10	n.a.
Cl	0.07	0.05	n.a.	n.a.	0.20	n.a.
Total	95.34	94.48	95.85	95.05	94.53	94.19
O	22.000	22.000	22.000	22.000	22.000	22.000
Si	5.368	5.478	5.353	5.448	5.385	5.373
Al	2.728	2.777	2.600	2.478	2.739	2.695
Ti	0.567	0.380	0.652	0.648	0.671	0.775
Cr	0.143	0.017	0.249	0.234	0.061	0.066
Fe^{2+}	0.770	0.621	0.483	0.498	0.786	0.874
Mn	-	-	-	-	-	-
Mg	4.070	4.367	4.278	4.304	3.922	3.718
Ca	-	-	-	-	-	-
Na	0.198	0.127	0.312	0.333	0.138	0.143
K	1.782	1.859	1.536	1.477	1.788	1.754
Ni	-	-	-	-	-	-
Sum	15.626	15.626	15.463	15.420	15.490	15.398
Na/Na+K	0.10	0.06	0.17	0.18	0.07	0.08
Mg#	84.1	87.6	89.8	89.6	83.3	81.0
X_{Si}	0.671	0.685	0.674	0.681	0.673	0.672
Rock Type	LHZ	LHZ	DUN	DUN	WER	WER

Notes: n.a.=not analyzed, X_{Si}=Si/Si+Al on tetrahedral sites. See Table 3.2 for Rock Type abbreviations. Cations based on 22 oxygens, with all Fe assumed to be Fe^{2+}, and without considering F and Cl anions.

Table 3.6 Representative Analyses of Xenolith Spinels

	KLBR1	KL3A	KLC18*	KL3	KL28	KL28	KLC1
	SPN 1-1	SPN 3-1	SPN 3-1	SPN 2-1	SPN 6-1	SPN 6-2	SPN 1-1
SiO_2	-	0.08	0.48	0.08	0.09	0.13	0.09
TiO_2	0.46	0.19	2.25	1.21	1.20	1.15	0.01
Al_2O_3	46.00	49.30	31.25	23.82	22.58	22.15	53.39
Cr_2O_3	16.57	18.39	20.82	38.88	41.97	41.35	15.06
Fe_2O_3	5.68	2.87	14.74	6.84	5.73	6.70	2.18
FeO	13.11	9.98	13.64	16.76	13.35	12.80	8.16
MnO	0.26	0.14	0.23	0.25	0.21	0.20	0.12
MgO	16.79	19.55	16.78	13.18	15.12	15.31	20.96
NiO	0.34	0.30	n.d.	0.10	0.20	0.26	0.32
Total	99.20	100.80	100.10	101.12	100.55	100.05	100.29
O	3.941	3.971	3.839	3.922	3.935	3.923	3.979
Si	-	0.002	0.014	0.002	0.003	0.004	0.002
Al	1.500	1.544	1.072	0.852	0.805	0.793	1.641
Ti	0.010	0.004	0.048	0.028	0.027	0.026	0.000
Cr	0.363	0.386	0.479	0.932	1.004	0.993	0.311
Fe3+	0.118	0.057	0.323	0.156	0.130	0.153	0.043
Fe2+	0.303	0.222	0.332	0.425	0.338	0.325	0.178
Mn	0.006	0.003	0.003	0.006	0.005	0.005	0.003
Mg	0.692	0.774	0.728	0.596	0.682	0.693	0.815
Ni	0.008	0.006	0.000	0.002	0.005	0.006	0.007
Mg#	69.5	77.7	68.7	58.4	66.9	68.1	82.1
Cr#	0.20	0.20	0.31	0.52	0.56	0.56	0.16
Rock Type	LHZ	LHZ	WER	LHZ	DUN	DUN	LHZ

Notes: * Spinel adjacent to phlogopite (same grain as in Fig. 3.3b). Note high Fe^{3+}. Mg# = (Mg/(Mg+Fe^{2+})) x 100 Cr# = Cr/(Cr+Al) See Table 3.2 for abbreviations for rock types. Grain cores denoted as -1 (i.e. SPN 1-1). Grain rims denoted as -2 (i.e. SPN 1-2).

Table 3.7 Analyses of Xenolith Rhonites and Glasses*

	KL29 RHN 3-1	KL29 RHN 2-1		KL29 GLASS 1	KL29 GLASS 2
SiO_2	26.11	25.76		58.47	63.68
TiO_2	14.48	14.90		1.13	1.09
Al_2O_3	16.69	16.50		22.44	24.82
Cr_2O_3	0.07	0.05		0.05	n.d.
FeO	11.87	12.13		2.37	2.25
MnO	0.08	0.08		0.02	0.04
MgO	17.46	17.51		0.42	0.34
CaO	11.08	10.97		0.99	0.87
Na_2O	1.25	1.24		6.71	2.96
K_2O	0.01	0.03		5.93	4.19
NiO	0.04	0.05		n.d.	n.d.
Total	99.14	99.22		98.53	100.24
O	20.000	20.000			
Si	3.419	3.379	Q	-	26.92
Al	2.575	2.550	Co	3.23	13.81
Ti	2.575	1.469	Or	35.63	24.74
Cr	0.006	0.005	Ab	43.75	24.99
Fe^{2+}	1.299	1.330	Ne	7.54	-
Mn	0.008	0.008	En	-	0.85
Mg	3.407	3.423	Fs	-	2.33
Ca	1.554	1.541	Fo	0.74	-
Na	0.317	0.315	Fa	1.95	-
K	0.002	0.005	Il	2.18	2.07
Ni	0.004	0.005			
Mg#	72.4	72.0		35.6	32.3
Rock Type	WER	WER		WER	WER

Notes: *Glasses are patches of melted intercumulus clinopyroxene. See Table 3.2 for Rock Type abbreviations.

Table 3.8 Geothermometry of Kostal Lake Xenoliths

Sample	Rock Type	Temperature of Equilibration (°C)	
		Olivine-Spinel*	Two Pyroxene**
Type I			
KL37	LHZ	1047	968
KL15	LHZ	-	972
KLC1	LHZ	1088	1002
KL3A	LHZ	1127	1003
KLBR1	LHZ	1019	1051
KLBR7	LHZ	984	1020
KL3	LHZ	1092	-
KL39	DUN	1102	-
KL28	DUN	1030	-
Cumulate			
KL36	WER	1017	-
KLBR2	WER	-	1094
KLC18	WER	-	1086

Notes: The Fabries (1979)* and Wells (1977)** geothermometers were used to facilitate comparison with similar work in British Columbia. Errors for these thermometers are ± 50°C and ± 70°C, respectively. See Table 3.2 for Rock Type abbreviations.

Table 3.9 Compositional Data for Xenolith-Bearing Lavas***

Eruptive Center	Location	K/Na	$Mg/(Mg+Fe^{2+})$	Type@
Itcha Mtns.	central B.C.	0.39	0.60	Sodic
Kettle River	southern B.C.	0.39	0.67	Sodic
Summit Lake	eastern B.C.	0.96	0.74	Potassic
Atlin	northern B.C.	0.40	0.67	Sodic
Rayfield Riv.	southern B.C.	0.32	0.61	Sodic
Mt. Ihangorse	northern B.C.	0.37	0.70	Sodic
Lassie Lake	southern B.C.	0.38	0.65	Sodic
Boss Mtn.	central B.C.	0.77	0.62	Potassic
Alligator L.	Yukon	0.45	0.70	Potassic
Kostal Lake	eastern B.C.	0.40	0.69	Sodic

Notes: *** Data sources for all localities in caption to Fig. 2.1, except for Alligator Lake (adapated from Eiche *et al.*, 1987). @ Classified according to Irvine and Baragar (1971). B.C. = British Columbia.

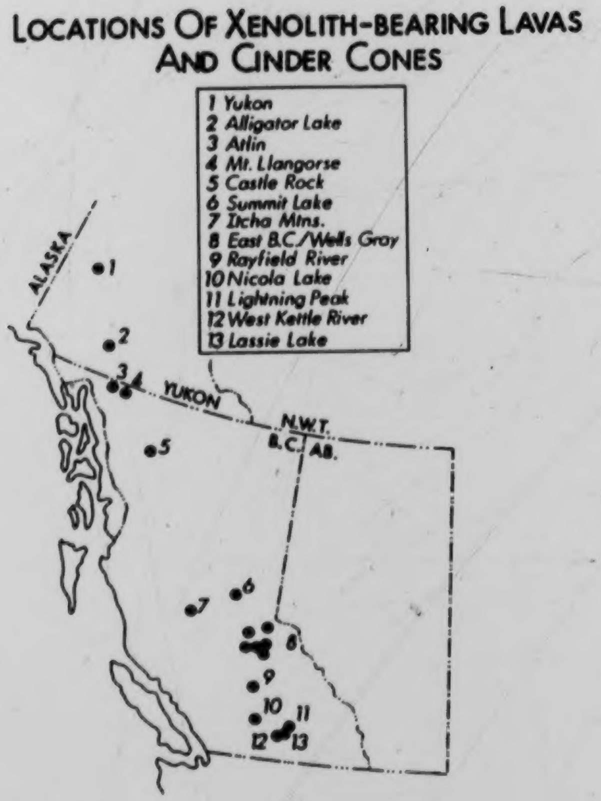
LOCATIONS OF XENOLITH-BEARING LAVAS AND CINDER CONES
1 Yukon
2 Alligator Lake
3 Atlin
4 Mt. Llangorse
5 Castle Rock
6 Summit Lake
7 Itcha Mtns.
8 East B.C./Wells Gray
9 Rayfield River
10 Nicola Lake
11 Lightning Peak
12 West Kettle River
13 Lassie Lake
ALASKA
YUKON
N.W.T.
B.C.
AB.
1
2
3
4
5
6
7
8
9
10
11
12
13

Figure 3.1. Location of xenolith-bearing lavas in the Canadian Cordillera. Location for Alligator Lake adapted from Francis (1987). The Kostal Lake volcanic center is one of the easternmost centers labelled as East B.C./ Wells Gray.

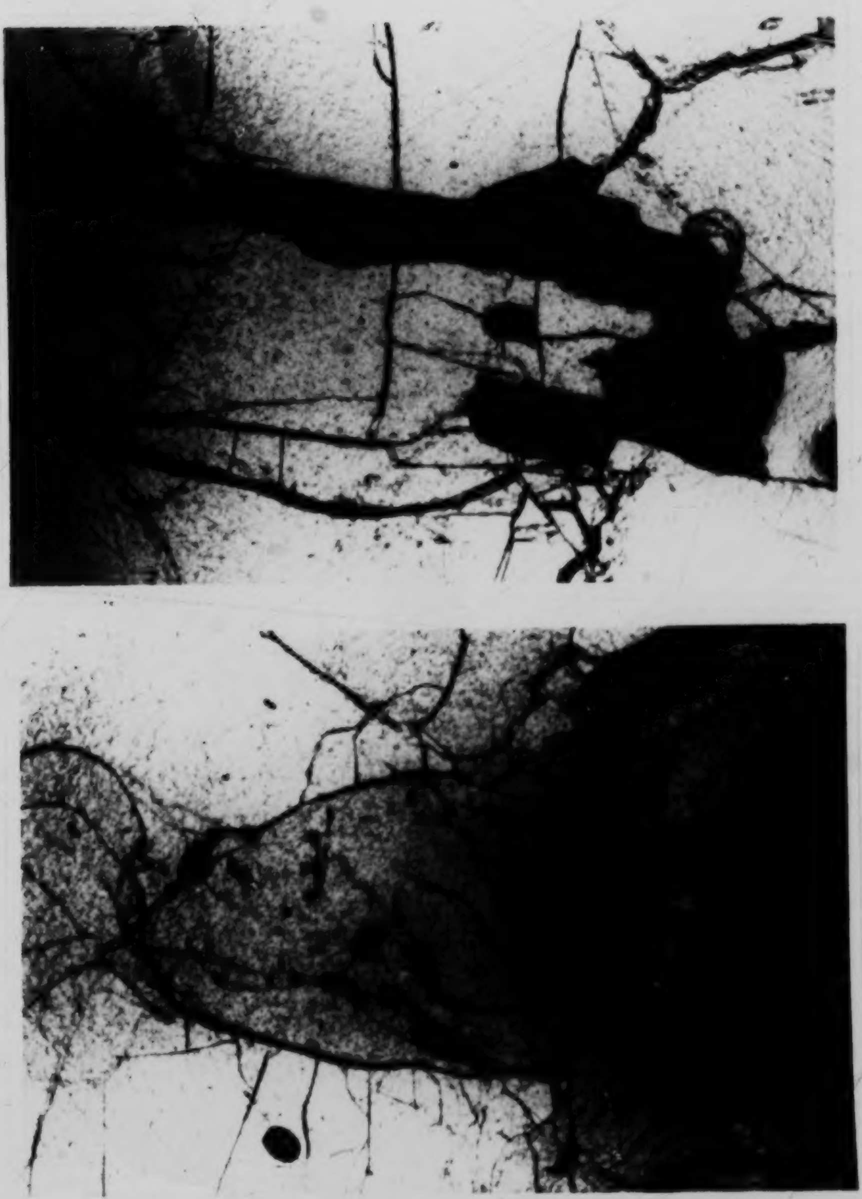

Figure 3.2. All photomicrographs taken in plane polarized light, except (d) which is in cross polarized light. (a) Interstitial phlogopite (ph) in dunite xenolith KL28. Note lack of reaction relation with coexisting olivine (ol). Width of base of photo is 2.5 mm. (b) Phlogopites (ph) and fluid inclusions (fl) oriented crytstallographically in clinopyroxene (cp) from lherzolite xenolith KLBR1. Scale bar is 500 um.

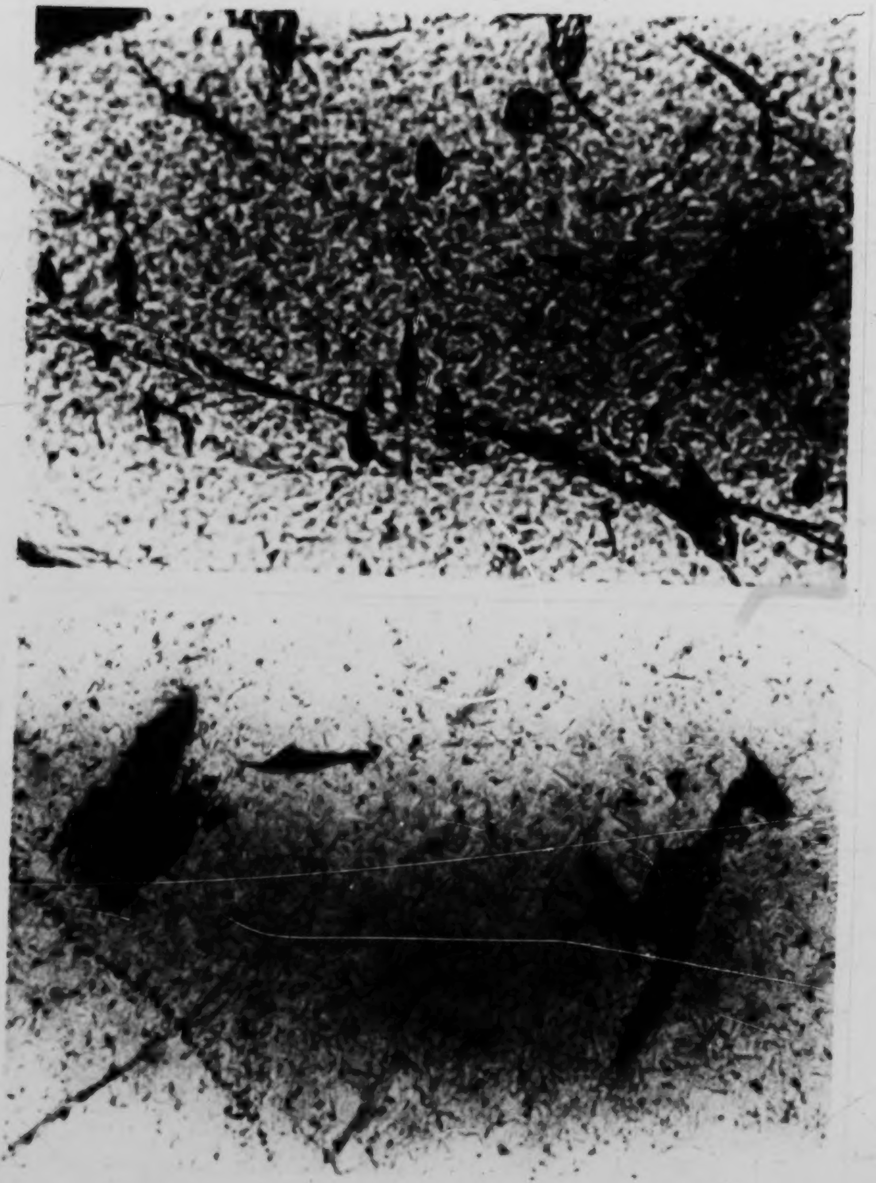

Figure. 3.3 (a) Enlarged area of photo (3.2b). Arrow points to phlogopite crystallized within fluid inclusion in left hand area of photo. Scale bar is 100 um. (b) Phlogopites (ph) oriented along the (100) plane of intercumulus clinopyroxene (cp) in wehrlite xenolith KLC18. Also note spinel (sp) associated with phlogopite flakes, and orthopyroxene (op) lamallae. Scale bar is 50 um.

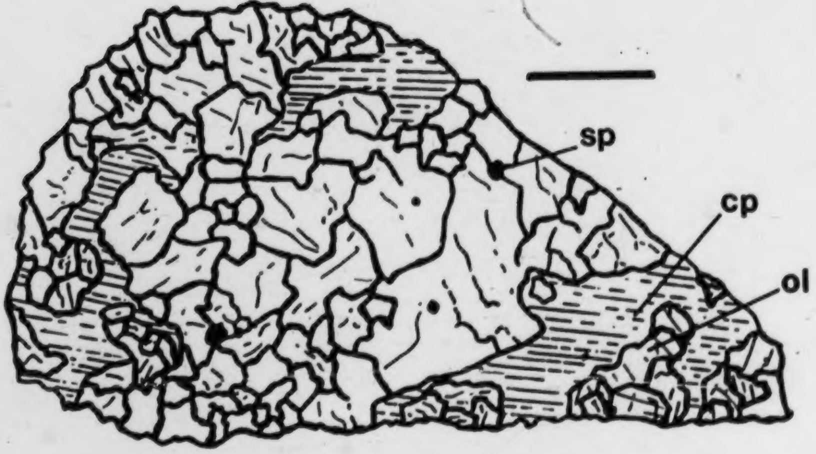

Figure 3.4. Sketch of wehrlite xenolith KL29 showing cumulate texture. Note sub-euhedral olivine (ol) and metamorphic texture of dunite fragment (containing spinel (sp)) enclosed by poikilitic intercumulus clinopyroxene (cp). Scale bar is 4 mm.

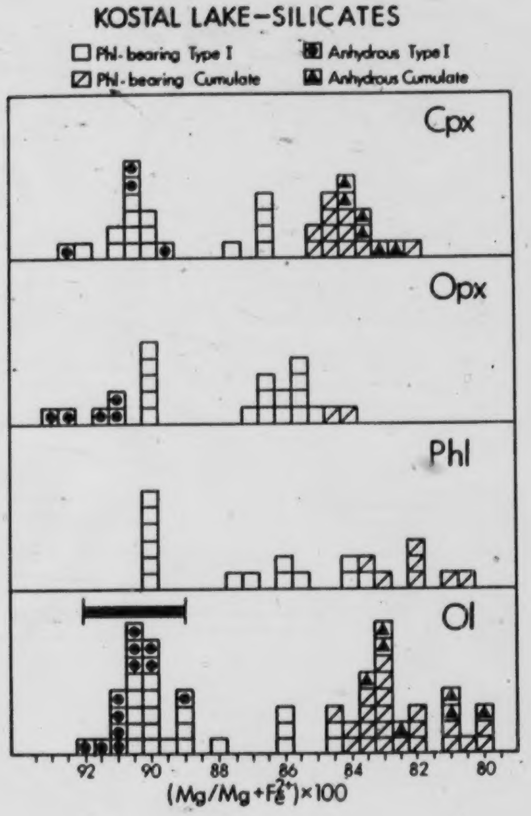

Figure 3.5. Mg/Mg+Fe^{2+} of silicates from both Type I and cumulate wehrlite xenoliths from Kostal Lake. Thick bar in olivine histogram represents the range of olivine compositions for spinel lherzolite xenoliths from the Canadian Cordillera. Note similar Mg/Mg+Fe^{2+} for phlogopites and coexisting silicates.

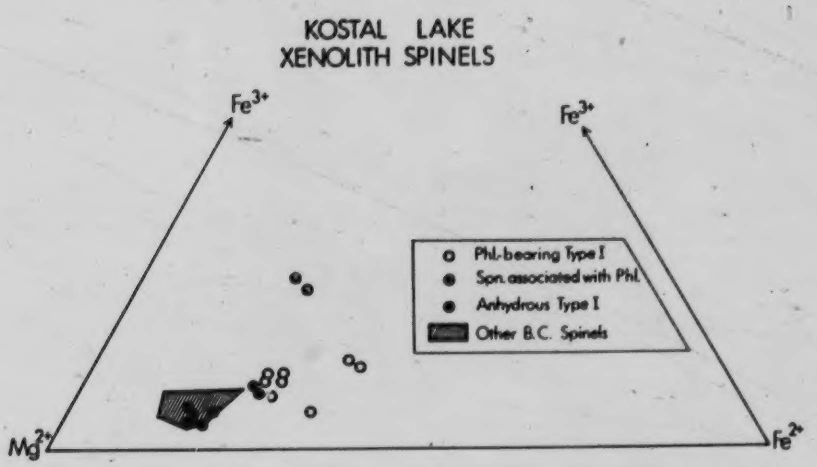

Figure 3.6. Fe^{2+} - Fe^{3+} - Mg^{2+} ternary (based on 3 cation stoichiometry) for spinels in xenoliths from Kostal Lake and other localities in the Canadian Cordillera. Note the Fe-rich character of spinels from Kostal Lake, and high concentrations of Fe^{3+} in spinels from xenoliths containing phlogopite. Also note anomalously high Fe^{3+} content of spinel spatially associated with phlogopite (same spinel as in Fig. 3.3b).

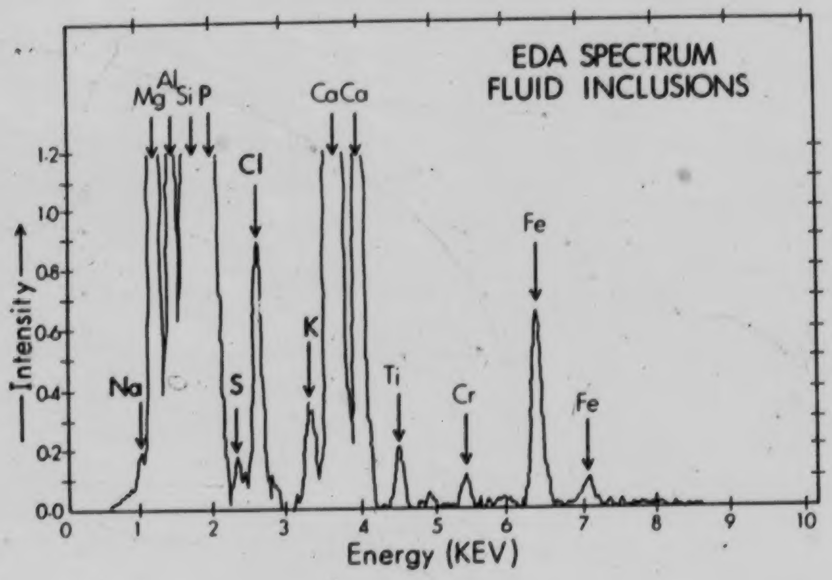

Figure 3.7. Energy spectrum of fluid inclusion hosted in intercumulus clinopyroxene from wehrlite xenolith KLC18: Note peaks for Na, K, Cl, P and S. K alpha and K beta lines for Mg, Al, Si, Ca, Ti, Cr, and Fe are interpreted as background excitation from intercumulus clinopyroxene.

3.7 REFERENCES

Albee AL, Ray L (1970) Correction factors for electron probe microanalysis of silicates, oxides, carbonates, phophates and sulfates. Anal. Chem. 42:1408-14.

Aoki K (1975) Origin of phlogopite- and potassic richterite-bearing peridotite xenoliths from South Africa. Contrib. Mineral. Petrol. 53:145-56.

Arai S (1984) Pressure-temperature dependent compositional variation of phlogopitic micas in upper mantle peridotites. Contrib. Mineral. Petrol. 87:260-64.

Arai S (1986) K/Na variation in phlogopite and amphibole of upper mantle peridotites due to fractionation of the metasomatizing fluids. J. Geol. 94:436-44.

Arculus RJ (1975) Melting behaviour of two basanites in the range 10 to 35 kbar and the effect of TiO_2 on the olivine diopside reactions at high pressures. Carnegie Inst. Washington Ybook. 74:512-515.

Bachinski S, Simpson EL (1984) Ti-phlogopites of the Shaw's Cove minette: a comparison with micas of other lamprophyres, potassic rocks, kimberlites and mantle xenoliths. Am. Miner. 96:41-56.

Bailey DK (1982) Mantle metasomatism - continuing chemical change in the Earth. Nature 296:525-30.

Bence AE, Albee AL (1968) Empirical correction factors for the electron microanalysis of silicates and oxides. J. Geol. 76:382-403.

Bender JF, Hodges FN, Bence AE (1978) Petrogenesis of basalts from the project FAMOUS area: experimental study from 0 to 15 kbars. Earth Planet. Sci. Lett. 41:277-302.

Boettcher AL, O'Neil JR (1980) Stable isotope, chemical and petrographic studies of high pressure amphiboles and micas: evidence for mantle metasomatism in the source regions of alkali basalts and kimberlites. Am. J. Sci. 280A:594-622.

Boyd FR, Jones RA, Nixon PH (1982) Mantle metasomatism: the Kimberley dunites. Carnegie Inst. Washington Ybook. 82:330-36.

Bevier ML (1983) Implications of chemical and isotopic compositions for the petrogenesis of the Chilcotin Group basalts, British Columbia. J. Petrol. 24:207-226.

Brearley M, Scarfe CM (1984) Amphibole in a spinel lherzolite xenolith: evidence for volatiles and partial melting in the upper mantle beneath southern British Columbia. Can. J. Earth. Sci. 21:1067-72.

Brearley M, Scarfe CM, Fujii T (1984) Petrology of ultramafic xenoliths from Summit Lake, near Prince George, British Columbia. Contrib. Mineral. Petrol. 88:53-63.

Brearley M, Scarfe CM (1986) Dissolution rates of upper mantle minerals in an alkali basalt melt at high pressure: an experimental study and implications for ultramafic xenolith survival. J. Petrol. 27:1157-82.

Campbell IH, Borley GD (1974) The geochemistry of pyroxenes from the lower layered series of the Jimberlana Intrusion, Western Australia. Contrib. Mineral. Petrol. 47:281-297.

Canil D, Brearley M, Scarfe CM (1987) Petrology of ultramafic xenoliths from Rayfield River, south-central British Columbia. Can. J. Earth. Sci. 24:1679-87.

Canil D, Virgo D, Scarfe CM Oxidation state of mantle xenoliths from British Columbia, Canada. (submitted Contrib. Mineral. Petrol.).

Colby JW (1972) Tutorial Notes. Proceedgs. 7th Nat. Conf. Electron Probe Anal.

Cook FA (1986) Seismic reflection geometry of the Columbia River Fault Zone and east margin of Shuswap Metamorphic Complex in the Canadian Cordillera. Tectonics 5:669-85.

Dawson JB, Powell DG (1969) Mica in the upper mantle. Contrib. Mineral. Petrol. 22:233-38.

Delaney JS, Smith JV, Carswell DA, Dawson JB (1980) Chemistry of micas from kimberlites and xenoliths. II Primary-secondary textured micas from peridotite xenoliths. Geochim. Cosmochim. Acta. 44:857-72.

Eiche G, Francis DM, Ludden JN (1987) Primary alkaline magmas associated with the Quaternary Alligator Lake volcanic complex, Yukon Territory, Canada. Contrib. Mineral. Petrol. 95:191-201.

Erlank AJ, Waters FG, Hawkesworth CJ, Haggerty SE, Altsopp HL, Rickard RS, Menzies MA (1987) Evidence for mantle metasomatism in peridotite nodules from the Kimberley Pipes, South Africa. In: Menzies, M.A. and Hawkesworth, C.J. (eds.) Mantle Metasomatism. New York:Academic Press, 221-309.

Esperanca S, Holloway JR (1986) The origin of the high-K latites from Camp Creek, Arizona: constraints from experiments with variable f_{O2} and a_{H2O}. Contrib. Mineral. Petrol. 93:504-512.

Esperanca S, Holloway JR (1987) On the origin of mica-lamprophyres: experimental evidence from a mafic minette. Contrib. Mineral. Petrol. 95:207-216.

Fabries J (1979) Spinel-olivine geothermometry in peridotites from ultramafic complexes. Contrib. Mineral. Petrol. 69:329-36.

Fisk MR, Upton BGJ, Ford CE (1988) Geochemical and experimental study of the genesis of magmas of Reunion Island, Indian Ocean. J. Geophys. Res. 93:4933-4950.

Francis DM (1976) The origin of amphibole in lherzolite xenoliths from Nunivak Island, Alaska. J. Petrol. 17:357-78.

Francis DM (1987) Mantle-melt interaction recorded in spinel lherzolite xenoliths from the Alligator Lake volcanic complex, Yukon, Canada. J.Petrol. 28:569-99.

Frey FA, Green DH (1974) The mineralogy, geochemistry and origin of lherzolite inclusions in Victorian basanites. Geochim. Cosmochim. Acta. 38:1023-61.

Frey FA, Prinz M (1978) Ultramafic inclusions from San Carlos, Arizona: petrologic and geochemical data bearing on their petrogenesis. Earth. Planet. Sci. Lett. 38:129-76.

Fujii T, Scarfe CM (1982) Petrology of ultramafic nodules from West Kettle River, near Kelowna, British Columbia. Contrib. Mineral. Petrol. 80:297-306.

Gamble JA, Kyle PR (1987) The origins of glass and amphibole in spinel wehrlite xenoliths from Foster Crater, McMurdo Volcanic Group, Antarctica. J. Petrol. 28:755-81.

Girod M, Dautria JM, deGiovanni R (1981) A first insight into the constitution of the upper mantle under the Hoggar area (southern Algeria): the lherzolite xenoliths in the alkali basalts. Contrib. Mineral. Petrol. 77:66-73.

Harte B (1977) Rock nomenclature with particular relation to deformation and recrystallization textures in olivine-bearing xenoliths. J. Geol. 85:279-88.

Hawkesworth CJ, Rogers NW, Van Calsteren PWC, Menzies MA (1984) Mantle enrichment processes. Nature 311:331-35.

Hickson CJ, Souther JG (1984) Late Cenozoic volcanic rocks of the Clearwater-Wells Gray Area, British Columbia. Can. J. Earth. Sci. 21:267-77.

Higgins MD, Allen JM (1985) A new locality for primary xenolith-bearing nephelinites in northwestern British Columbia. Can. J. Earth Sci. 22:1556-59.

Irvine TN (1974) Petrology of the Duke Island ultramafic complex, southeastern Alaska. Geol. Soc. Amer. Mem. 138,240p.

Irvine TN (1982) Terminology for layered intrusions. J. Petrol. 23,127-62.

Irvine TN, Baragar WRA (1971) A guide to the chemical classification of the common volcanic rocks. Can. J. Earth Sci. 8:523-48.

Irving AJ (1980) Petrology and geochemistry of composite ultramafic xenoliths in alkalic basalts and implications for magmatic processes within the mantle. Am. J. Sci. 280A:389-426.

Kempton PA (1987) Mineralogic and geochemical evidence for differing styles of metasomatism in spinel lherzolite xenoliths: enriched mantle source regions of basalts? In: Menzies, M.A. and Hawkesworth, C.J. Mantle Metasomatism. New York: Academic Press,45-89.

Kushiro I (1975) On the nature of silicate melt and its significance in magma genesis: regularities in the shift of the liquidus boundaries involving olivine, pyroxene and silica minerals. Am. J. Sci. 275:411-431.

Kuo LC, Kirkpatrick RJ (1985) Dissolution of mafic minerals and its implications for the ascent velocities of peridotite-bearing basaltic magmas. J. Geol. 93:691-706.

Lloyd FE, Bailey DK (1975) Light element metasomatism of the continental mantle: the evidence and the consequences. Phys. Chem. Earth. 9:389-416.

Lloyd FE, Arima M, Edgar AD (1985) Partial melting of a phlogopite-clinopyroxenite nodule from south-west Uganda: an experimental study bearing on the origin of highly potassic continental rift volcanics. Contrib. Mineral. Petrol. 91:321-329.

Mattioli GS, Wood BJ (1988) Magnetite activities across the $MgAl_2O_4$ - Fe_3O_4 spinel join, with application to thermobarometric estimates of upper mantle oxygen fugacity. Contrib. Mineral. Petrol. 98:148-62.

Menzies MA (1983) Mantle ultramafic xenoliths in alkaline magmas: evidence for mantle heterogeneity modified by magamtic activity. In: Hawkesworth, C.J., and Norry, M.J. (eds.) Continental Basalts and Mantle Xenoliths. United Kingdom: Shiva Publishing Limited, 92-110.

Menzies MA, Murthy VK (1980) Mantle metasomatism as a precursor to the genesis of alkaline magmas - isotopic evidence. Am. J. Sci. 280A:622-38.

Metcalfe PM (1987) Petrogenesis of alkaline lavas from Wells Gray Provincial Park and constraints on the subCordilleran upper mantle. Unpubl. Ph.D. Dissertation. University of Alberta. 395 pp.

Metcalfe PM, Smith AD, Scarfe CM (1986) Apatite control on Sm and Nd in Quaternary basalts of Wells Gray Provincial Park, British Columbia. Geol. Assoc. Can./Min. Assoc. Can. Abs. Prog. 11:101.

Modreski PM, Boettcher AL (1973) Phase relationships of phlogopite in the system K_2O-MgO-CaO-Al_2O_3 -SiO_2-H_2O to 35 kbar: a better model for micas in the interior of the Earth. Am. J. Sci. 273:385-414.

Morimoto N (1988) Nomenclature of pyroxenes. Am.Miner. 73:1123-1133.

Nicholls IA, Ferguson J, Jones H, Marks GP, Mutter JC (1981) Ultramafic blocks from the ocean floor southwest of Australia. Earth Planet. Sci. Lett. 56:362-374.

Olafsson M, Eggler DH (1983) Phase relations of amphibole-, amphibole-phlogopite, and amphibole-carbonate peridotite: petrologic constraints on the asthenosphere. Earth Planet. Sci. Lett. 64:305-315.

O'Neill HStC, Wall VJ (1987) The olivine-orthopyroxene-spinel oxygen geobarometer, the nickel precipitation curve, and the oxygen fugacity of the Earth's upper mantle. J. Petrol. 28:1169-93.

Ozawa K (1983) Evaluation of olivine-spinel geothermometry as an ndicator of thermal history for peridotites. Contrib. Mineral. Petrol. 82:52-65.

Roden MF, Frey FA, Francis DM (1984) An example of consequent mantle metasomatism in peridotite inclusions from Nunivak Island, Alaska. J. Petrol. 25:546-77.

Ross JV (1983) The nature and rheology of the Cordilleran upper mantle of British Columbia: inferences from peridotite xenoliths. Tectonophys. 100:321-57.

Schneider DE, Eggler DH (1986) Fluids in equilibrium with peridotite minerals: implications for mantle metasomatism. Geochim. Cosmochim. Acta 50:711-24.

Smith DGW, Gold C (1979) EDATA2: a FORTRAN IV computer program for processing wavelength and/or energy dispersive electron microprobe analyses. In: Newbury, D.E. (ed.) Microbeam. Anal. Soc. Proc. 14th Ann. Conf.,273-8.

Smith JV, Delaney JS, Hervig RL, Dawson JB (1981) Storage of F and Cl in the upper mantle: geochemical implications. Lithos 14:133-49.

Smith AD (1986) Isotopic and geochemical studies of Terrane I, south-central British Columbia. Unpubl. Ph.D. Dissertation. University of Alberta, 195pp.

Stolper EM, Walker D (1980) Melt density and the average composition of basalt. Contrib. Mineral. Petrol. 74:7-13.

Takahashi E (1980) Melting relations of an alkali-olivine basalt to 30 kbar, and their bearing on the origin of alkali basalt magmas. Carnegie. Inst. Washington Ybook. 79:271-276.

Wass SY (1979) Multiple origins of clinopyroxenes in alkali basaltic rocks. Lithos 12:115-33.

Wells PRA (1977) Pyroxene thermometry in simple and complex systems. Contrib. Mineral. Petrol. 62:129-39.

Wendlandt RF, Eggler DH (1980) The origin of potassic magmas 2: Stability of phlogopite in natural spinel lherzolite and in the system $KAlSiO_4$-MgO-SiO_2-H_2O-CO_2. Am. J. Sci. 280:421-58.

Wilkinson JFG (1975) Ultramafic inclusions and high pressure megacrysts from a nephelinite sill, Nandewar Mountains, northeastern New South Wales and their bearing on the origin of certain ultramafic inclusions in alkaline volcanic rocks. Contrib. Mineral. Petrol. 51:235-62.

Wilshire HG, Shervais JW (1975) Al-augite and Cr-diopside ultramafic xenoliths in basaltic rocks from the western United States. Phys. Chem. Earth 9:257-72.

Witt G, Seck HA (1987) Temperature history of sheared mantle xenoliths from the West Eifel, West Germany: evidence for mantle diapirism beneath the Rhenish Massif. J. Petrol. 28:475-95.

Wood BJ, Virgo D (1987) Oxidation state of the upper mantle: ferric-ferrous ratios in coexisting minerals from spinel lherzolites. Geol. Soc. Am. Abs. Prog. 19:896.

Wyllie PJ (1979) Magmas and volatile components. Am. Miner. 64:469-500.

Yoder HS, Kushiro I (1969) Melting of a hydrous phase: phlogopite. Am. J. Sci. 267A:558-82.

4. OXIDATION STATE OF MANTLE XENOLITHS FROM FROM BRITISH COLUMBIA

4.1 INTRODUCTION

Information regarding the oxidation state of the upper mantle is important in understanding the oxygen fugacity (f_{O2}) attending magma generation in the source regions of mantle-derived melts. Moreover, the present oxidation state of the upper mantle may in some way reflect that of the Earth's earlier primitive mantle, and is, therefore, central to models for the evolution of the Earth's core and atmosphere (Arculus, 1985).

Estimates for the oxidation state of the Earth's upper mantle have been the subject of much recent controversy in igneous petrology. Much of this controversy stems from the different methods used to determine the oxidation state of the samples studied. Studies applying the intrinsic oxygen fugacity (IOF) technique to lherzolite xenoliths and olivine megacrysts hosted in alkaline basalts, and to ilmenite megacrysts found in kimberlites, indicate that upper mantle f_{O2}'s range from below the iron-wustite buffer (IW) to at or near FMQ (Arculus et al., 1984; Ulmer et al., 1987). Virgo et al. (1988) have shown, however, that much of the range in f_{O2}'s for different mantle-derived ilmenites obtained using the IOF technique may be due to chemical and physical modification of samples during an IOF experiment, resulting from the presence of carbon in the natural samples. Virgo et al. (1988) demonstrate quite clearly that carbon-free samples are not altered during the course of an IOF experiment, and give f_{O2}'s near FMQ. Nonetheless, phase equilibrium analysis of peridotite-C-O-H systems (Woermann and Rosenhauer, 1985), the oxidation state of oceanic basaltic glasses (Christie et al., 1986) and some "high confidence" IOF data (Ulmer et al., 1987) indicate a heterogeneous upper mantle with respect to its oxidation state.

Recently, thermobarometric methods have been calibrated to estimate the oxidation state recorded by spinels in lherzolite xenoliths (Mattioli and Wood, 1986, 1988; O'Neill and Wall, 1987). These methods give f_{O2}'s at or near FMQ for spinel lherzolite xenoliths from worldwide localities, consistent with thermobarometric calculations (Eggler, 1983) and IOF measurements (Virgo et al., 1988) for ilmenite megacrysts in kimberlites. Unfortunately, f_{O2} estimates for spinel lherzolite xenoliths using the thermobarometric method rely upon the estimation of the magnetite component (X_{Fe3O4}) in upper mantle spinels by electron microprobe analysis. Because spinels in upper mantle peridotites commonly contain less than 10 mol% X_{Fe3O4}, estimation of this component is difficult by microprobe methods. Errors in a typical microprobe analysis have a large effect on the calculation of ferric iron, and thus X_{Fe3O4}, in spinels (Finger, 1972; Virgo et al., 1988). This shortcoming was explored in previous studies which showed that errors in Fe^{3+} determinations for spinels must be small for precise estimates of f_{O2} in the spinel lherzolite facies of the upper mantle (O'Neill and Wall, 1987; Mattioli and Wood, 1988; Wood and Virgo, 1989). Thus, the minimization of these errors is necessary in order to delineate any "fine structure" in f_{O2} recorded by different lherzolite xenoliths within a given alkaline province. This "fine structure" may be relevant, for example, in recognizing variations in the f_{O2} of xenoliths from a given geographical region, or from the same eruptive center, and would provide limits on both the magnitude and scale of vertical and lateral heterogeneity in the oxidation state of the upper mantle.

In this study, ^{57}Fe Mossbauer spectroscopy is used to determine the Fe^{3+}/total Fe ratio of spinels from mantle xenoliths hosted in alkaline lavas from British Columbia, Canada. Comparison of this value with those determined by electron microprobe analysis reveals the error in the resultant calculated f_{O2} of the spinel to be on the order of 1 to 2 log f_{O2} units. These data are then used to compare and contrast the oxidation state of spinel lherzolite xenoliths from different eruptive centers with varying ages within both this alkaline province and worldwide. The results of this study reveal systematic trends in the oxidation state of the spinels, which can correlate with the evidence for metasomatism recorded in some xenoliths.

4.2 EXPERIMENTAL METHODS

Spinels free of inclusions, glass and alteration were hand-picked from 17 mantle xenoliths from six different alkaline eruptive centers in British Columbia (Table 4.1). All of these xenoliths are spinel lherzolites, except for sample KR37, which is a spinel harzburgite. Detailed mineralogical studies of mantle xenoliths from these localities have been presented elsewhere (Table 4.1). Compositions of the spinels, and their coexisting olivines, orthopyroxenes and clinopyroxenes were determined at the Geophysical Laboratory by wavelength dispersive analysis (WDA) on a MAC 3-channel microprobe. Operating conditions for the MAC probe were 15 kV operating voltage, 30 nA probe current, and counting times of 30 s on peaks. Data from the MAC probe were reduced using the Bence and Albee (1968) method with the correction factors of Albee and Ray (1970). Microprobe analyses of selected samples were also carried out at the University of Alberta using WDA on an ARL SEMQ microprobe. Operating conditions were 15 kV operating voltage, 12 nA probe current and counting times of 100 s on peaks. Data from the ARL probe were reduced with full ZAF corrections using EDATA2 (Smith and Gold, 1979). At least three grains of each mineral, and two points on each grain, were analyzed.

Resonant absorption spectra were obtained at 298 and 77 K on powdered samples mixed with plastic transoptic powder and pressed into thin discs. Absorber thicknesses ranged from 1.5 to 5.0 mg Fe/cm^2. Mirror image Mossbauer spectra were collected over 512 channels using a 25mC ^{57}Co in Pd source. Spectra were allowed to accumulate at least 1x10^6 counts per channel. Mirror image resonance envelopes were deconvoluted separately with a least squares routine (MOSSFITA) using Lorentzian line shapes and with width and area constraints on the component peaks of the single ferric absorption doublet, and on two ferrous absorption doublets. Hyperfine parameters given in Table 4.3 are the average values for the left- and right-hand side fits. Fits to the spectra were evaluated using MISFIT, MISFIT and X^2 parameters.

4.3 RESULTS

Mossbauer spectra obtained at both 77 and 298 K were fit with one Fe^{3+} doublet and two Fe^{2+} doublets, with different quadrupole splittings (QS), but nearly identical isomer shifts (IS) (Fig. 4.1ab, Table 4.4). Attempts to fit either the 77 or 298 K spectra with only one Fe^{2+} doublet resulted in poor fits with large residuals and anomalously large line widths (~ 1.0 mm/s FWHH - Fig. 4.1d). Large line widths could be attributed to next-nearest neighbour interactions on tetrahedral sites in the spinel structure (Osborne et al., 1981,1984); however, the slight skew in the high velocity peak of the resonance envelope at 77 K (see arrow in Fig. 4.1c) and the broad line width for the high velocity peak in all 298 K spectra (Fig. 4.1d) suggest the presence of a second Fe^{2+} doublet. The validity of this fit is also discussed in Wood and Virgo (1989).

The differences in Fe^{3+}/total Fe determined for the spinels by electron microprobe and Mossbauer spectroscopy are as high as 45% relative, and do not show any systematic trend (Table 4.2, Fig. 4.2). In most cases, the assumptions of stoichiometry used in calculating Fe^{3+} from microprobe analyses result in overestimation of Fe^{3+}/total Fe ratios (Fig. 4.2).

Most previous Mossbauer studies of natural and synthetic spinels were performed at 298 K. The principal aim of this study was to obtain accurate Fe^{3+}/total Fe ratios for mantle spinels. Therefore, most of the Mossbauer measurements in this study were obtained at 77 K as opposed to 298 K, due to increased resolution of the Fe^{3+} doublet in these spinels at lower temperatures (Fig. 4.1); however, a limited number of measurements at 298 K permit comparison of Mossbauer spectra for upper mantle spinels with other natural and synthetic spinel solid solutions.

Isomer shifts for the single Fe^{3+} doublet at 298 K in the xenolith spinel spectra range from 0.27 to 0.32 mm/s (Table 4.4), consistent with tetrahedrally coordinated Fe^{3+} (Marshall and Dollase, 1984, p. 930). No evidence was found in either the 298 K or 77 K spectra for octahedrally coordinated Fe^{3+}. Quadrupole splittings for the Fe^{3+} doublet at 298 K range from

0.73 to 0.77 mm/s (Table 4.4), and show little change with decreasing temperature, as expected for Fe^{3+} (Bancroft, 1973). Isomer shifts for the single Fe^{3+} doublet increase with decreasing temperature to values ranging from 0.41 to 0.45 mm/s at 77 K. Line widths for this doublet also broaden at lower temperatures (Table 4.4).

Isomer shifts for both the "inner" and "outer" Fe^{2+} doublets at 298 K (Fe^{2+}[I] and Fe^{2+}[II], respectively, in Table 4.4) have values ranging from 0.90 to 0.94 mm/s, and indicate that Fe^{2+} is tetrahedrally coordinated in these spinels. The presence of two Fe^{2+} doublets suggest that some degree of ordering of Fe^{2+} on two different "types" of tetrahedral sites may occur in mantle spinels. Attempts to fit the Fe^{2+} doublets with different isomer shifts, for example, by switching the line position of one of the inner Fe^{2+} peaks with the outer, resulted in larger residuals, anomalously low isomer shifts, and a generally poorer fit. Line widths and isomer shifts for both Fe^{2+} doublets increase with decreasing temperature (Table 4.4).

Osborne _et al._, (1981) studied spinels with similar bulk chemistry to those presented here, but did not fit two Fe^{2+} doublets to their 298K Mossbauer spectra. Spinels presented in this study, however, were quenched from higher temperature and pressure environments than those measured by Osborne _et al._, (1981), who studied mainly spinels from low pressure, slow cooling ultramafic intrusions, suggesting that the pressure and/or temperature histories of spinels may be a major factor affecting their cation distributions.

4.4 DISCUSSION

Oxygen Fugacity of Spinel Lherzolites

The oxidation state of spinel lherzolites is buffered by the heterogeneous equilibrium (O'Neill et al., 1982):

$$\underset{Ol}{6Fe_2SiO_4} + O_2 = \underset{Sp}{2Fe_3O_4} + \underset{Opx}{3Fe_2Si_2O_6} \quad [4.1]$$

Mattioli and Wood (1986, 1988) and O'Neill and Wall (1987) using thermochemical data and activity-composition relations for olivine, orthopyroxene and spinel solid solutions, give formulations for calculating f_{O2} in spinel lherzolites.

Application of the O'Neill and Wall (1987) thermobarometric method to mantle xenoliths from southern British Columbia shows that most of these samples have equilibrated over a range of f_{O2}'s from ~ 0.5 to 1.5 log f_{O2} units below FMQ at an assumed pressure of 15 kbar (Fig. 4.3a). Application of the Mattioli and Wood (1988) oxybarometer to the same samples gives a wider range of f_{O2}'s from ~ 1.0 log unit above, to 1.5 log units below FMQ at 15 kbar (Table 4.2). The average f_{O2} recorded by xenoliths from southern British Columbia using the O'Neill and Wall method is 1.05 log units below FMQ, compared with 0.61 log units below FMQ for the Mattioli and Wood method. The average f_{O2} calculated for all samples does not change appreciably if olivine-spinel rather than two-pyroxene equilibration temperatures are used in the O'Neill and Wall oxybarometer (Fig. 4.3b).

Errors in Ol-Opx-Sp Oxybarometers

Although both the O'Neill and Wall and Mattioli and Wood oxybarometers are based on the same principle (equation [4.1]), they give disparate results for many of the samples studied (Table 4.2). In all but one sample, the Mattioli and Wood oxybarometer produces higher calculated f_{O2}'s. Reasons for this disparity may be due to errors in mineral chemical data used as input, the inability to obtain accurate pressure estimates for the samples, the different parameters used in the activity-composition relations for olivine, orthopyroxene or spinel in either method, or combinations of all these factors.

Perhaps the most critical information used as input into either oxybarometer is Fe_{3+}/total Fe in spinel. The use of Fe^{3+} contents for spinel determined by electron microprobe results in shifts in the calculated f_{O2} of 1 to 2 log units for some samples. These shifts would obscure any trends in f_{O2} observed when the more precise Mossbauer Fe^{3+} contents are used in the calculations. The error quoted in the Mossbauer determinations for Fe^{3+}/total Fe in spinel of ±0.005 can produce shifts in calculated f_{O2} of ±0.05 log units.

Also important are X_{Fa} in olivine and X_{Fs} in orthopyroxene. If optimistic errors of 2% are assumed in microprobe analyses of olivines, errors of ±0.002 in X_{Fa} can be expected. Variations between grains of up to 0.003 in X_{Fa}, and 0.005 in X_{Fs}, were observed in some olivines and orthopyroxenes, respectively. If X_{Fa} and X_{Fs} are varied by ±0.003, f_{O2}'s calculated using the Mattioli and Woo method can change by ±0.2 log units. Most of the above shifts also apply to the O'Neill and Wall oxybarometer, although the observed variations in orthopyroxene compositions do not greatly affect calculated f_{O2}'s when using this method. It is evident that combined errors in mineral analysis alone can shift calculated f_{O2}'s using either the Mattioli and Wood or O'Neill and Wall method by ±0.2 to 0.3 log units, and explain the differences in calculated f_{O2}'s of less than 0.3 log units observed for many samples in this study (Table 4.2).

Another important parameter used in either thermobarometric method is the pressure of equilibration of each sample. Unfortunately, the lack of a satisfactory geobarometer for spinel lherzolites requires one to assume a pressure in the thermobarometric calculation. However, it is probable that many spinel lherzolite samples in this and other studies (e.g. O'Neill and Wall, 1987; Wood and Virgo, 1989) did not equilibrate at a common pressure in the mantle, but were derived over a range of pressures, which for natural Cr-bearing spinel lherzolites equilibrating between 900 and 1100°C could vary from 8 to 23 kbar (Herzberg, 1978; O'Neill, 1981). If one varies the assumed pressure in the thermobarometeric calculation (commonly 15 kbar) by ±8 kbar, shifts in f_{O2} of ±0.3 log units result. When errors in mineral analyses and pressure are considered together, an error of ±0.4 $\log f_{O2}$ units results using either the O'Neill and Wall or Mattioli and Wood method.

Differences in f_{O2} calculated using the two different oxybarometers can in some cases be greater than the expected error of ±0.4 log units determined above. Such large differences are, with one exception, observed for samples which contain spinels that are either high in Fe ($Mg/Mg+Fe^{2+} < 0.80$), high in Cr ($Cr/Cr+Al > 0.15$) or both (Table 4.2 - samples SL47, SL125, KLBR1, KR3003). In these samples, the large differences in calculated f_{O2} may be due to the different treatments of spinel solid solutions in both oxybarometers. For instance, Mattioli and Wood (1988) use magnetite activity-composition relations which are experimentally calibrated, albeit under oxidizing conditions (Hematite - Magnetite buffer), whereas O'Neill and Wall (1987) derive magnetite activities from a thermodynamic model based on cation distributions in binary spinel systems (c.f. O'Neill and Navrotsky, 1984). Comparison of the input parameters for the two different methods indicates that for a given set of spinels ranging in Fe and Cr content, the O'Neill and Wall (1987) method gives a smaller range of Mt activities than does the Mattioli and Wood (1988) method, perhaps explaining the more restricted range in calculated f_{O2} for the O'Neill and Wall (1987) results (Table 4.2).

For the sake of consistency, only the O'Neill and Wall results will be discussed further. It is emphasized, however, for the purpose of the following discussion, that the relative trends in f_{O2} between samples in this study are the same using either oxybarometer.

Geological Implications

The observed f_{O2}'s for spinel lherzolites and harzburgites from southern British Columbia fall close to the range of oxidation states preserved in fresh oceanic MORB glasses (Christie et al., 1986) and suggest that much of the upper mantle lithosphere beneath this region has a depleted, oceanic character. The bulk chemical and isotopic composition of many peridotite xenoliths from southern British Columbia support this interpretation (Sun, 1985; Xue, 1988; Xue et al., 1988). Most mantle peridotites sampled by alkaline magmas traversing the lithosphere in this region thus probably represent residua after extraction of melts, perhaps with MORB-like compositions. The more oxidized nature of alkaline lavas erupted in this province (Fig. 4.3c) indicates that they are either derived from a more oxidized source at greater depths, or originate in source regions with oxidation states similar to their entrained peridotite xenoliths, but are modified during ascent by degassing of H, C or S species (Mathez, 1984).

There appears to be little if any significant heterogeneity in the f_{O2} recorded by different peridotite xenoliths from different geographic regions within southern British Columbia. This is particularly evident for spinel samples separated from a composite xenolith comprised of both a 1 cm thick websterite vein (KR3020B) and host lherzolite (KR3020) which record similar f_{O2}'s (Table 4.2, Fig. 4.3ab). Moreover, xenoliths from eruptive centers located more than 100 km apart (Boss Mountain and Rayfield River - Table 4.1), record nearly identical f_{O2}'s (Table 4.2), and all samples from British Columbia generally plot above the magnetite-wustite (MW) buffer, and within 1 log unit of each other (Fig. 4.3ab). The similar f_{O2}'s recorded by different xenoliths from volcanic centers with varying eruption ages (26 Ma to 7550 B.P. - Table 1) indicate that the f_{O2} of the upper mantle beneath British Columbia was not affected by Cenozoic alkaline magmatism in the region.

The single sample studied (KLBR1) which shows evidence of modal metasomatism in the form of phlogopite (Canil and Scarfe, in press) consistently plots at the high f_{O2} end of all samples, regardless of whether the Mattioli and Wood or O'Neill and Wall thermobarometric method is used (Table 4.2, Fig. 4.3). Another sample (KR35) which records the vestiges of metasomatism in its O and Nd-Sr isotopic signature (Xue, 1988) also plots in the high f_{O2} range of the samples investigated (Fig. 4.3). Both these samples (KLBR1 and KR35) may indicate that metasomatism results in progressive oxidation of the upper mantle, and that C-O-H species involved in metasomatism of the mantle, either as free phases or as dissolved components in melts, occur in oxidized (CO_2 and H_2O) rather than reduced (CH_4 and H_2) forms. However, the lack of correlation between the f_{O2} and bulk Fe content of the xenoliths, as reflected by the $Mg/Mg+Fe^{2+}$ of their consistuent phases (Fig. 4.3d), suggests that the overall degree of major element depletion in the xenoliths is independent of the f_{O2} they record. This is further exemplified in the one harzburgite sample studied (KR37) which, although depleted in its mode (i.e. no clinopyroxene), records an f_{O2} similar to those of less-depleted lherzolite xenoliths from southern British Columbia (Table 4.2).

The f_{O2}'s calculated for mantle xenoliths from southern British Columbia are slightly more reducing than those reported for spinel lherzolite underlying parts of the southwestern United States (San Carlos and Kilbourne Hole) and Mongolia (Fig. 4.3c) although the differences approach the error in the oxybarometers (± 0.4 log units). Nonetheless, all samples in this study have calculated f_{O2}'s which are far more reducing than spinel lherzolites from Ichinomegata, Japan and the Massif Central (Fig. 4.3c). Mantle xenoliths from these latter localities represent lithosphere overlying subducted oceanic crust, and show petrographic evidence for interaction with fluid or fluid-rich melt (Takahashi, 1986). The more oxidized nature of the Ichinomegata and Massif Central samples is probably due to the influence of oxidized fluid/melt components liberated from downgoing slabs thrust beneath these regions (Wood and Virgo, in press). In contrast, subduction has occurred outboard of western Canada for over the last 200 Ma (Monger et al., 1982; Souther, 1978) yet samples of the upper mantle beneath this region record some of the most reduced f_{O2}'s reported to date using the thermobarometric method (Fig. 4.3c) and are anomalously "dry" in their modal composition (Nicholls et al., 1982; Canil and Scarfe, in press). These unique characteristics require that either the oxidation state and mineralogy of the upper mantle beneath British Columbia has remained isolated from, and unaffected by, the extensive history of subduction in this region, or that any oxidized fluid/melt component introduced by subduction over time has been removed by renewed late Cenozoic magmatism in this alkaline province (e.g. Souther, 1977; Gough, 1986).

4.5 SUMMARY

Determinations of Fe^{3+} in upper mantle spinels by electron microprobe can differ from that obtained by Mossbauer spectroscopy by up to 45% relative. These differences in Fe^{3+} contents for spinels can produce shifts in calculated f_{O2} of up to 2 log units when using either the Mattioli and Wood (1988) or the O'Neill and Wall (1987) thermobarometric method for estimating f_{O2}'s for mantle xenoliths from British Columbia.

The calculated f_{O2}'s for 17 mantle xenoliths from 6 eruptive centers in British Columbia range from 0.5 to 1.5 log units below FMQ. This range of f_{O2}'s is less than that of most Cenozoic alkaline lavas from this region, but overlaps those of MORB glasses. This observation lends support to the idea that most of the spinel lherzolite facies mantle underlying British Columbia has a depleted, oceanic character, in accord with geochemical and isotopic studies of many xenoliths from this region.

The calculated f_{O2} for the upper mantle beneath British Columbia shows no significant variation laterally between eruptive centers with ages ranging from 26 Ma to 7550 B.P. Thus, the f_{O2} of the upper mantle may have remained essentially constant during the generation of Cenozoic alkaline magmas in this geographic region.

Table 4.1 Sample Locations in British Columbia*

Sample #	Location	Estimated Age	Reference
KLBR1	Kostal Lake	< 7550 B.P.	Canil and Scarfe (in press)
KL39	"	"	"
KR1034	West Kettle River	2 - 3 Ma	Fujii and Scarfe (1982)
KR35		"	"
KR3020	"	"	"
KR3020B	"	"	"
KR37	"	"	"
KR3003	"	"	"
KR3008	"	"	"
KR1041	"	"	"
SL32	Summit Lake	26 Ma	Brearley *et al.* (1984)
SL47	"	"	"
SL125	"	"	"
JL8	Jaques Lake	< 1 Ma	Fujii *et al.* (1981)
JL1	"	"	"
TKN15	Boss Mountain	< 1 Ma	Fujii and Scarfe (1981)
RR222	Rayfield River	6 - 10 Ma	Canil *et al.* (1987)

Notes: * Geographic locations within British Columbia are given in Fig. 3.1.

Table 4.2 Compositional Data for Spinels and Olivines

Sample #	SL32	SI47	SL125	KLBR1	KL39	TKN15
SiO_2	0.09	0.09	0.08	0.07	0.09	0.04
Al_2O_3	54.64	51.97	50.29	46.83	37.05	59.16
TiO_2	0.26	0.30	0.13	0.27	0.66	0.11
Cr_2O_3	11.71	13.12	16.86	16.68	28.70	9.48
Fe_2O_3	4.02	4.28	3.41	6.01	4.37	2.03
FeO	9.79	4.28	10.88	12.62	11.79	8.93
MgO	20.13	19.35	19.25	17.59	18.13	21.31
MnO	0.12	0.14	0.15	0.17	0.20	0.12
CaO	nd	0.01	nd	0.02	nd	0.01
NiO	0.30	0.28	0.30	0.21	0.21	0.42
V_2O_3	0.12	0.14	0.10	0.16	0.19	0.07
ZnO	0.00	0.02	0.16	0.11	0.16	0.01
Total	101.18	100.68	101.62	100.74	101.56	101.70
O	4.000	4.000	4.000	4.000	4.000	4.000
Si	0.002	0.002	0.002	0.002	0.003	0.001
Al	1.671	1.617	1.564	1.499	1.216	1.763
Ti	0.005	0.006	0.003	0.006	0.014	0.002
Cr	0.240	0.274	0.352	0.358	0.632	0.190
Fe3+	0.079	0.085	0.068	0.123	0.092	0.039
Fe2+	0.212	0.242	0.240	0.287	0.275	0.189
Mg	0.779	0.761	0.757	0.712	0.753	0.803
Mn	0.003	0.003	0.003	0.004	0.005	0.003
Ca	nd	0.000	nd	0.001	nd	0.000
Ni	0.006	0.006	0.006	0.005	0.005	0.009
V	0.002	0.003	0.002	0.003	0.004	0.001
Zn	0.000	0.001	0.003	0.002	0.003	0.000
Mg#	78.6	75.9	75.9	71.3	73.3	80.9
Cr#	0.13	0.15	0.18	0.19	0.34	0.10
Fe3+/Fe*	0.25	0.28	0.24	0.31	0.32	0.18
Fe3+/Fe	0.27	0.26	0.22	0.30	0.25	0.17
Ol						
X_{Fa}	0.147	0.130	0.116	0.141	0.107	0.101
2Px	1078	1073	1067	1082	-	913
OlSp	1234	957	898	946	977	847
OWlogFMQ	-1.16	-0.97	-1.21	-0.63	-	-1.33
OWlogFMQ*	-1.29	-0.86	-1.07	-0.53	-1.04	-1.24
MWlogFMQ	-1.26	0.13	-0.04	0.85	-	-1.21

Notes: Fe3+/Fe* from microprobe analyses using Bence-Albee data reduction scheme. Fe3+/Fe from Mossbauer Spectroscopy. Two-pyroxene (2Px) and olivine-spinel (OlSp) temperatures (in °C) were calculated using the Wells (1977) and O'Neill and Wall (1987) geothermometers, respectively. Errors are ± 70°C and ±50°C, respectively.

Table 4.2 Continued...

Sample #	KR1034	KR35	KR37	KR3008	KR1041	KR3020
SiO_2	0.06	0.10	0.05	0.06	0.04	0.04
Al_2O_3	61.69	56.88	50.41	58.97	62.31	57.64
TiO_2	0.09	0.41	0.02	0.00	0.07	0.07
Cr_2O_3	6.64	9.77	18.78	9.11	6.33	7.95
Fe_2O_3	1.90	3.03	2.21	2.42	1.64	2.79
FeO	7.77	9.14	9.06	8.74	7.76	7.95
MgO	21.98	21.55	20.30	21.24	21.88	21.39
MnO	0.06	0.11	0.14	0.08	0.11	0.09
CaO	nd	nd	nd	0.02	0.02	0.01
NiO	0.36	0.39	0.24	0.35	0.38	0.34
V_2O_3	0.06	0.11	0.06	0.03	0.06	0.07
ZnO	0.18	0.07	0.05	0.05	0.05	0.08
Total	100.79	101.56	101.32	101.08	100.65	99.61
O	4.000	4.000	4.000	4.000	4.000	4.000
Si	0.002	0.003	0.001	0.002	0.001	0.001
Al	1.828	1.708	1.560	1.767	1.845	1.752
Ti	0.002	0.008	0.000	0.000	0.001	0.001
Cr	0.132	0.390	0.183	0.183	0.126	0.186
Fe3+	0.036	0.058	0.044	0.046	0.031	0.054
Fe2+	0.163	0.195	0.199	0.186	0.163	0.171
Mg	0.824	0.818	0.795	0.805	0.820	0.822
Mn	0.001	0.002	0.003	0.002	0.002	0.002
Ca	0.000	0.000	0.000	0.001	0.001	0.000
Ni	0.007	0.008	0.005	0.007	0.008	0.007
V	0.001	0.002	0.001	0.001	0.001	0.001
Zn	0.003	0.001	0.001	0.001	0.001	0.002
Mg#	83.4	80.8	80.0	81.2	83.4	82.7
Cr#	0.07	0.10	0.20	0.09	0.06	0.10
Fe3+/Fe*	0.16	0.29	0.19	0.20	0.12	0.25
Fe3+/Fe	0.18	0.23	0.18	0.20	0.16	0.24
OlX_{Fa}	0.105	0.103	0.092	0.107	0.104	0.108
2Px	937	953	-	-	-	898
OlSp	991	895	886	913	956	1046
OWlogFMQ	-1.45	-0.88	-	-	-	-1.05
OWlogFMQ*	-1.52	-0.81	-1.45	-1.19	-1.73	-1.08
MWlogFMQ	-1.57	-0.18	-	-	-	-0.82

Notes: Oxygen fugacities (in logFMQ format) calculated using the methods of O'Neill and Wall (1987) (OWlogFMQ) and Mattioli and Wood (1988) (MWlogFMQ) with Fe^{3+} from Mossbauer spectroscopy and 2Px temperatures. Uncertainties are ± 0.4 $\log f_{O2}$ units. OlSp temperatures were used to calculate OWlogFMQ*. Mg# = 100Mg/(Mg+Fe^{2+}) Cr# = Cr/(Cr+Al) nd = not detected. Compositional data for coexisting orthopyroxenes are given in Table 4.4.

Table 4.2 Continued....

Sample #	KR3020B	KR3003	RR222	JL8	JL1
SiO_2	0.04	0.05	0.09	0.04	0.04
Al_2O_3	59.50	50.51	56.86	54.55	58.97
TiO_2	0.11	0.09	0.12	0.01	0.09
Cr_2O_3	7.00	6.48	9.70	13.73	8.52
Fe_2O_3	2.92	2.35	2.11	2.19	2.19
FeO	7.48	11.12	8.11	9.01	8.42
MgO	21.89	18.50	20.96	20.82	21.23
MnO	0.08	0.15	0.14	0.14	0.09
CaO	0.01	0.02	0.00	0.00	0.00
NiO	0.37	0.30	0.37	0.35	0.40
V_2O_3	0.07	0.07	0.07	0.09	0.05
ZnO	0.05	0.15	0.09	0.09	0.14
Total	99.52	99.80	98.63	101.03	100.15
O	4.000	4.000	4.000	4.000	4.000
Si	0.001	0.001	0.002	0.001	0.001
Al	1.793	1.596	1.748	1.663	1.779
Ti	0.002	0.002	0.002	0.000	0.002
Cr	0.142	0.349	0.200	0.281	0.172
Fe3+	0.056	0.048	0.042	0.043	0.042
Fe2+	0.160	0.249	0.177	0.195	0.180
Mg	0.834	0.739	0.815	0.803	0.810
Mn	0.002	0.003	0.003	0.003	0.002
Ca	0.000	0.001	0.000	0.000	0.000
Ni	0.008	0.006	0.008	0.007	0.008
V	0.001	0.002	0.001	0.002	0.001
Zn	0.001	0.003	0.002	0.002	0.003
Mg#	83.9	74.8	82.2	80.5	81.8
Cr#	0.07	0.18	0.10	0.14	0.09
Fe3+/Fe*	0.27	0.16	0.19	0.18	0.19
Fe3+/Fe	0.26	0.16	0.19	0.18	0.19
[illegible] X_{Fa}	0.094	0.115	0.102	0.094	0.097
2Px	898	903	937	889	940
OlSp	937	824	939	839	847
OWlogFMQ	-0.47	-1.53	-1.29	-1.20	-1.09
OWlogFMQ*	-0.52	-1.45	-1.29	-1.14	-0.96
MWlogFMQ	-0.07	-0.99	-1.04	-0.89	-0.80

Table 4.3 Compositional Data for Orthopyroxenes*

Sample	SL32	SL47	SL125	KLBR1	TKN15	KR1034	KR35
O	6.000	6.000	6.000	6.000	6.000	6.000	6.000
Si	1.882	1.866	1.878	1.893	1.883	1.884	1.926
Al	0.189	0.205	0.185	0.153	0.197	0.179	0.163
Ti	0.005	0.004	0.002	0.004	0.003	0.003	0.002
Cr	0.010	0.014	0.016	0.010	0.010	0.007	0.008
Fe2+	0.179	0.229	0.211	0.258	0.184	0.186	0.225
Mn	0.005	0.005	0.005	0.006	0.003	0.004	0.004
Mg	1.697	1.648	1.676	1.660	1.700	1.731	1.627
Ca	0.041	0.043	0.041	0.034	0.027	0.022	0.024
Na	0.007	0.006	0.007	0.004	0.005	0.005	0.009
X_{Fs}	0.095	0.122	0.112	0.134	0.098	0.097	0.121

Sample	KR3020	KR3020B	KR3003	RR222	JL8	JL1
O	6.000	6.000	6.000	6.000	6.000	6.000
Si	1.895	1.895	1.910	1.886	1.895	1.885
Al	0.175	0.175	0.147	0.175	0.160	0.172
Ti	0.002	0.002	0.002	0.002	0.001	0.003
Cr	0.007	0.007	0.010	0.009	0.011	0.008
Fe2+	0.181	0.181	0.210	0.188	0.176	0.185
Mn	0.005	0.005	0.005	0.005	0.004	0.005
Mg	1.720	1.720	1.697	1.727	1.745	1.738
Ca	0.022	0.022	0.024	0.022	0.022	0.021
Na	0.008	0.008	0.007	0.006	0.003	0.003
X_{Fs}	0.095	0.095	0.110	0.091	0.092	0.096

Notes: * Based on six oxygen stoichiometry.

Table 4.4 Mossbauer Parameters for Spinels*

Sample #		JL1	TKN15	SL47	SL32	SL125	KLBR1	KL39
77 K								
Fe3+	FWHH	0.510	0.573	0.554	0.423	0.406	0.557	0.503
	QS	0.720	0.661	0.703	0.753	0.708	0.725	0.631
	IS	0.417	0.455	0.435	0.428	0.435	0.431	0.429
Fe2+ [I]	FWHH	0.581	0.602	0.609	0.611	0.609	0.583	0.595
	QS	2.464	2.530	2.526	2.408	2.474	2.516	2.562
	IS	1.083	1.065	1.083	1.080	1.077	1.080	1.071
Fe2+ [II]	FWHH	0.318	0.362	0.378	0.332	0.342	0.370	0.401
	QS	2.991	3.058	3.047	2.998	3.030	3.045	3.045
	IS	1.063	1.061	1.066	1.059	1.063	1.066	1.082
X^2		434	354	489	766	351	518	315
MISFIT%		0.417	0.256	0.200	0.328	0.264	0.250	0.212
MISFIT		0.069	0.059	0.028	0.03	0.063	0.033	0.066
Fe3+/Fe		0.19	0.17	0.26	0.27	0.22	0.30	0.25
298 K								
Fe3+	FWHH	0.314	0.302	0.331	0.338	0.319	0.367	0.352
	QS	0.697	0.712	0.753	0.784	0.762	0.737	0.649
	IS	0.303	0.306	0.291	0.295	0.283	0.323	0.312
Fe2+ [I]	FWHH	0.505	0.553	0.512	0.501	0.528	0.535	0.444
	QS	1.174	1.159	1.193	1.159	1.205	1.217	1.114
	IS	0.900	0.991	0.908	0.922	0.918	0.914	0.904
Fe2+ [II]	FWHH	0.403	0.408	0.422	0.474	0.457	0.429	0.576
	QS	1.890	1.894	1.903	1.867	1.893	1.933	1.861
	IS	0.901	0.908	0.938	0.942	0.944	0.928	0.912
X^2		280	300	360	909	262	478	326
MISFIT%		0.182	0.203	0.206	0.205	0.185	0.274	0.295
MISFIT		0.089	0.068	0.051	0.016	0.093	0.040	0.084
Fe3+/Fe		0.18	0.14	0.26	0.26	0.23	0.29	0.27

Notes: * All parameters given in mm/s relative to Fe metal at 298 K. Errors in Fe^{3+}/Fe ratios are estimated to be ± 0.005. Standard deviations for IS and QS are ± 0.01. Areas and widths for component peaks were constrained to be equal. Abbreviations are: FWHH = peak width at half height; IS= isomer shift; QS = quadrupole splitting.

Table 4.4 Continued....

77 K

Sample #		KR1034	KR3020B	KR37	KR3020	KR35
	FWHH	0.651	0.630	0.471	0.659	0.550
Fe3+	QS	0.734	0.712	0.714	0.682	0.632
	IS	0.453	0.388	0.426	0.377	0.484
	FWHH	0.555	0.610	0.618	0.611	0.576
Fe2+ [I]	QS	2.508	2.385	2.524	2.390	2.444
	IS	1.071	1.057	1.063	1.060	1.080
	FWHH	0.300	0.389	0.370	0.400	0.419
Fe2+ [II]	QS	3.000	2.907	3.028	2.922	3.012
	IS	1.061	1.043	1.069	1.047	1.070
X^2		319	373	374	339	330
MISFIT%		0.313	0.196	0.256	0.358	0.185
MISFIT		0.092	0.041	0.053	0.091	0.050
Fe3+/Fe		0.18	0.26	0.18	0.24	0.23

77 K

Sample #		KR3008	KR3003	KR1041	JL8	RR222
	FWHH	0.679	0.537	0.692	0.510	0.476
Fe3+	QS	0.667	0.635	0.746	0.720	0.714
	IS	0.436	0.452	0.422	0.417	0.422
	FWHH	0.598	0.578	0.654	0.581	0.578
Fe2+ [I]	QS	2.554	2.449	2.672	2.464	2.452
	IS	1.059	1.062	1.137	1.083	1.078
	FWHH	0.379	0.378	0.420	0.318	0.318
Fe2+ [II]	QS	3.073	2.965	3.239	2.991	2.997
	IS	1.061	1.046	1.140	1.063	1.063
X^2		423	433	522	384	342
MISFIT%		0.242	0.238	0.297	0.236	0.350
MISFIT		0.042	0.039	0.039	0.047	0.087
Fe3+/Fe		0.20	0.16	0.16	0.19	0.19

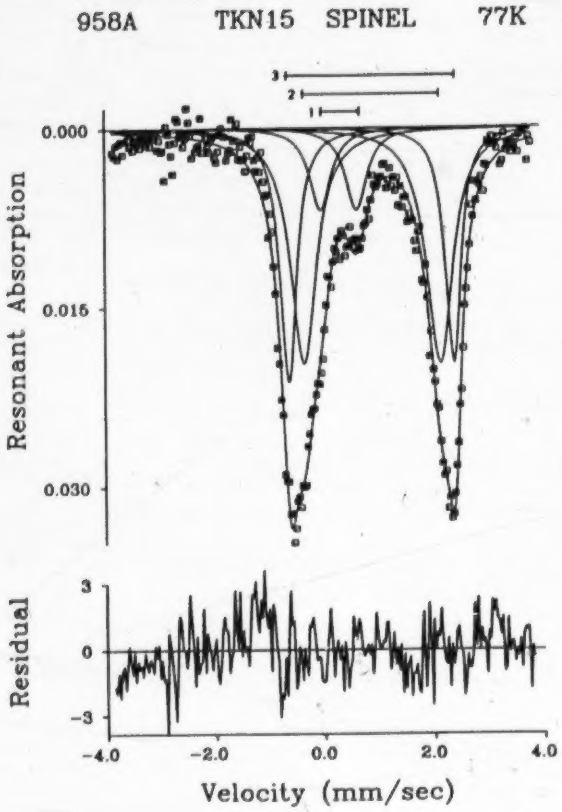

Figure 4.1. (a) Mossbauer spectrum of spinel measured at 77 K. The resonance envelope is fit with one Fe^{3+} doublet (1) and two Fe^{2+} doublets (2) and (3), with different quadrupole splittings.

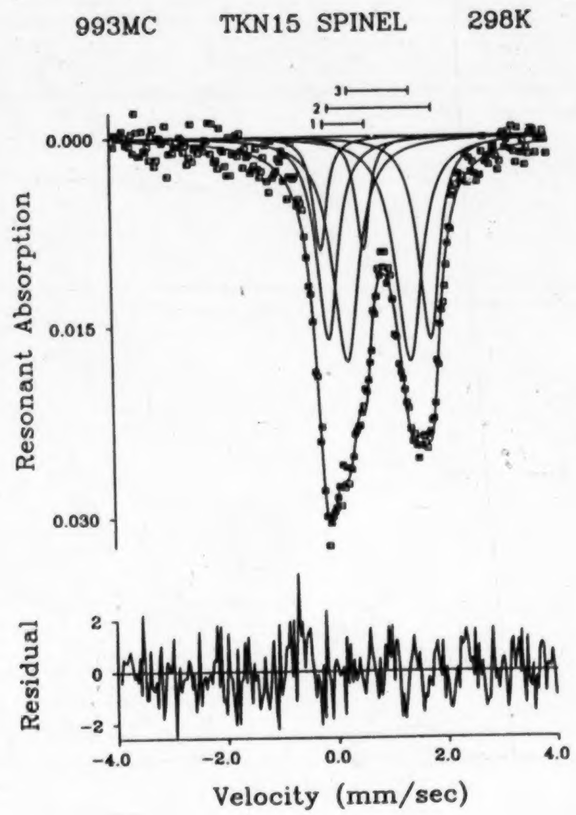

Figure 4.1. (b) Mossbauer spectrum at 298 K, same sample as 4.1a. Fit with three doublets labelled using same format as 4.1a.

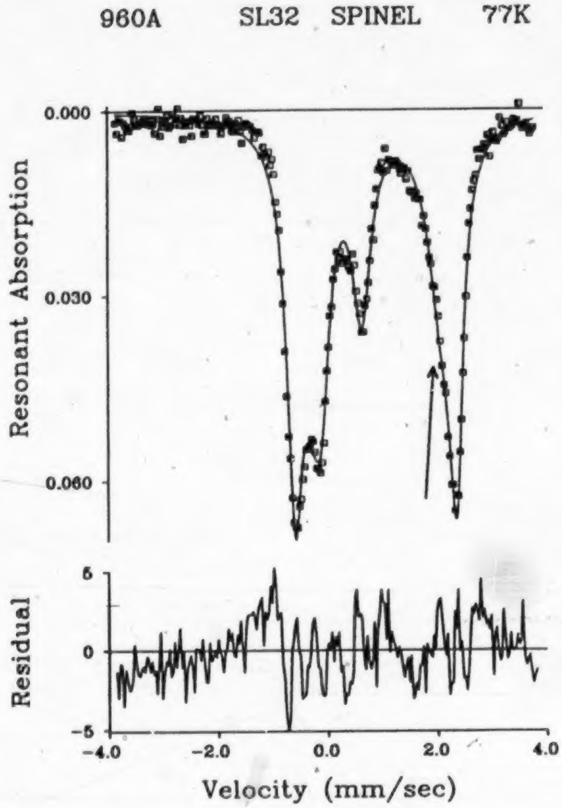

Figure 4.1. (c) Resonance envelope for spinel at 77 K. Note skew (arrow) on low velocity side of high velocity peak. Lorentzians omitted for clarity.

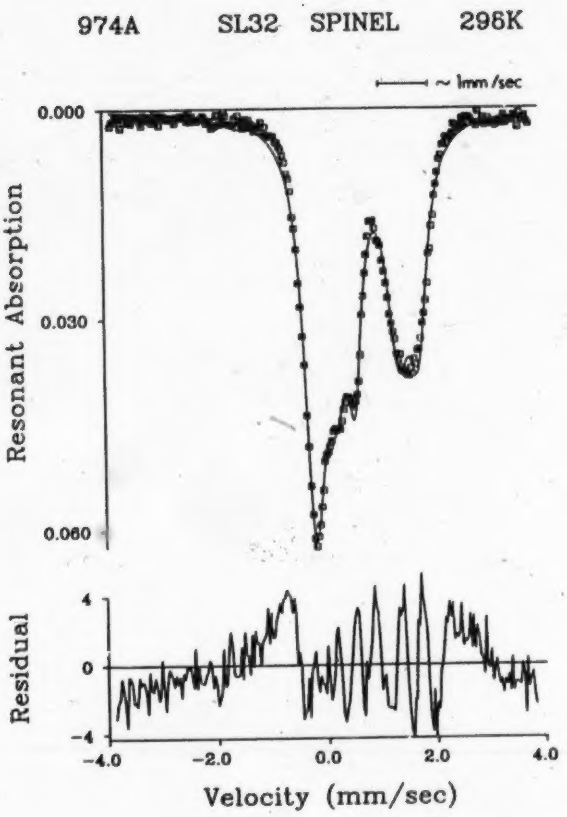

Figure 4.1. (d) Same sample as in 4.1c, at 298 K. Note large line width (horizontal bar = 1 mm/s) required to fit this high velocity peak to only one Fe^{2+} doublet. Lorentzians omitted from for clarity.

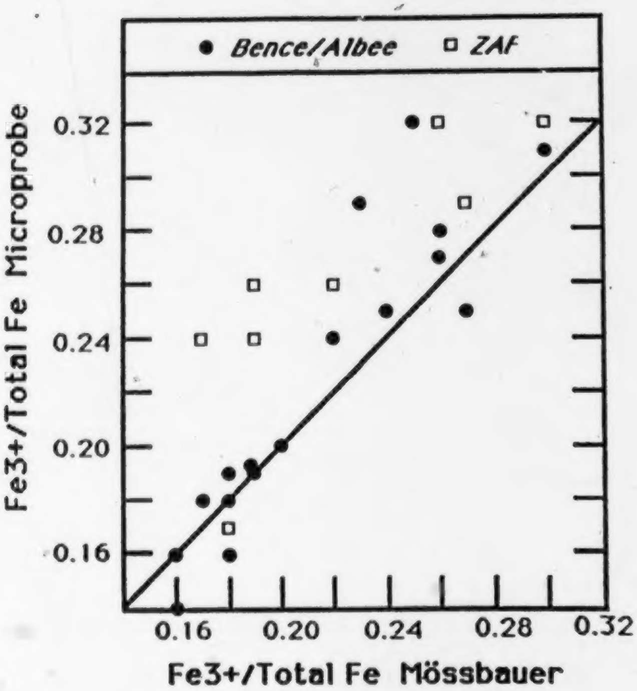

Figure 4.2. Comparison of Fe^{3+}/ total Fe determined for xenolith spinels using Mossbauer spectroscopy and electron microprobe (with two different data reduction schemes). Diagonal line is 1:1 correlation.

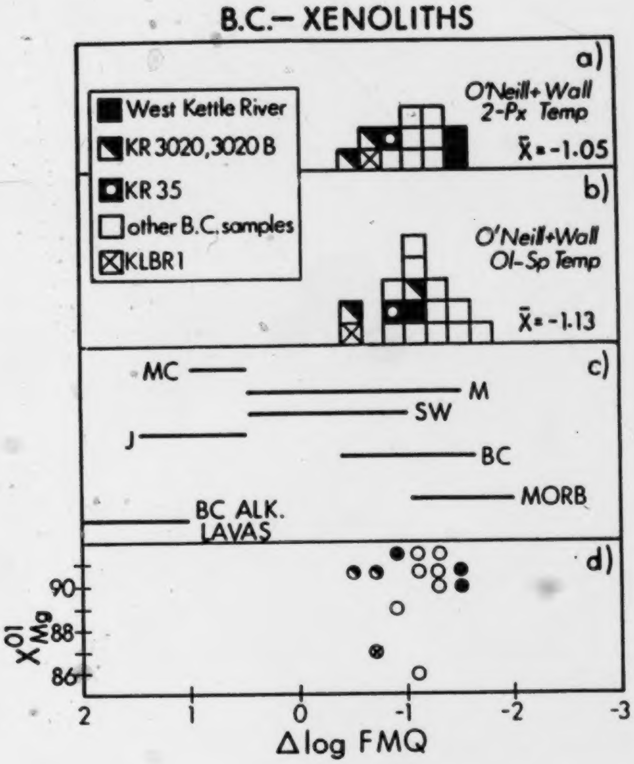

Figure 4.3. log FMQ histogram at 15 kbar for mantle xenoliths from British Columbia using (a) thermobarometric method of O'Neill and Wall (1987) with two-pyroxene temperatures. (b) Same as above using olivine-spinel temperatures. (c) Oxygen fugacities for mantle xenoliths from Mongolia (M), southwestern United States (San Carlos and Kilbourne Hole) (SW), the Massif Central, France (MC) and Ichinomegata, Japan (J) (adapted from Wood and Virgo, 1989) compared with the results from this study (BC) and with the range of f_{O_2}'s for MORB glasses (MORB) (adapted from Christie et al., 1986) (d) log FMQ of samples from British Columbia plotted against $(Mg/(Mg+Fe^{2+}))x100$ of their coexisting olivines.

4.6 REFERENCES

Albee AL, Ray L (1970) Correction factors for electron probe microanalysis of silicates, oxides, carbonates, phosphates and sulphates. Anal. Chem. 42:1408-1414.

Arculus RJ (1985) Oxidation status of the mantle: past and present. Ann. Rev. Earth Planet. Sci. 13:75-95.

Arculus RJ, Dawson JB, Mitchell RH, Gust DA, Holmes RD (1984) Oxidation states of the upper mantle recorded by megacryst ilmenite in kimberlite and Type A and B spinel lherzolites. Contrib. Mineral. Petrol. 85:85-94.

Bancroft GM (1973) Mossbauer Spectroscopy: an introduction for inorganic chemists and geochemists. McGraw-Hill, England, Wiley, New York.

Bence AE, Albee AL (1968) Empirical correction factors for the electron microanalysis of silicates and oxides. J. Geol. 76:382-403.

Brearley M, Scarfe CM, Fujii T (1984) Petrology of ultramafic xenoliths from Summit Lake, near Prince George, British Columbia. Contrib. Mineral. Petrol. 88:53-63.

Canil D, Brearley M, Scarfe CM (1987) Petrology of ultramafic xenoliths from Rayfield River, south-central British Columbia. Can. J. Earth Sci. 24:1679-1687.

Canil D, Scarfe CM (in press) Origin of phlogopite in mantle xenoliths from Kostal Lake, Wells Gray Park, British Columbia. J. Petrol.

Christie DM, Carmichael ISE, Langmuir CH (1986) Oxidation states of mid-ocean ridge basalt glasses. Earth Planet. Sci. Lett. 79:397-411.

Eggler DH (1983) Upper mantle oxidation state: evidence from olivine-orthopyroxene-ilmenite assemblages. Geophys. Res. Lett. 10:365-368.

Finger LW (1972) The uncertainty in the calculated ferric iron content of a microprobe analysis. Carnegie Inst. Washington Ybook. 71:600-604.

Fujii T, Scarfe CM (1981) Petrology of ultramafic nodules from Boss Mountain, central British Columbia. Geol. Assoc. Can./ Min. Assoc. Can. Abs. Prog. 6:A20.

Fujii T, Scarfe CM, Hamilton TS (1981) Geochemistry of ultramafic nodules from southern British Columbia: evidence for banding in the upper mantle. Geol. Assoc. Can./Min. Assoc. Can. Abs. Prog. 6:A20.

Fujii T, Scarfe CM (1982) Petrology of ultramafic nodules from West Kettle River, near Kelowna, British Columbia. Contrib. Mineral. Petrol. 80:297-306.

Gough DI (1986) Mantle uplow tectonics in the Canadian Cordillera. J. Geophys. Res. 91:1909-1919.

Herzberg CT (1978) The bearing of phase equilibria in simple and complex systems on the origin and evolution of some well documented garnet websterite. Contrib. Mineral. Petrol. 66:375-382.

Kilinc A, Carmichael ISE, Rivers ML, Sack RO (1983) The ferric-ferrous ratio of natural silicate liquids equilibrated in air. Contrib. Mineral. Petrol. 83:136-140.

Marshall L, Dollase W (1984) Cation arrangement in Fe-Zn-Cr spinel oxides. Am. Miner. 69:928-936.

Mathez EA (1984) Influence of degassing on the oxidation states of basaltic magmas. Nature 310:371-375.

Mattioli GS, Wood BJ (1986) Upper mantle oxygen fugacity recorded by spinel lherzolites. Nature 322:626-628.

Mattioli GS, Wood BJ (1988) Magnetite activities across the $MgAl_2O_4$ - Fe_3O_4 spinel join, with application to thermobarometric estimates of upper mantle oxygen fugacity. Contrib. Mineral. Petrol. 98:148-162.

Monger JWH, Price RA, Tempelman-Kluit DJ (1982) Tectonic accretion and the origin of the two major metamorphic and plutonic welts in the Canadian Cordillera. Geology 10:70-75.

Nicholls J, Stout MZ, Fiesinger, DW (1982) Petrologic variations in Quaternary volcanic rocks, British Columbia and the nature of the underlying upper mantle. Contrib. Mineral. Petrol. 79:201-218.

O'Neill HStC (1981) The transition between spinel lherzolite and garnet lherzolite, and its use as a geobarometer. Contrib. Mineral. Petrol. 77:185-195.

O'Neill HStC, Ortez N, Arculus RJ, Wall VJ, Green DH (1982) Oxygen fugacities from the assemblage olivine-orthopyroxene-spinel. Terra Cognita 2:228.

O'Neill HStC, Navrotsky A (1984) Cation distributions and thermodynamic properties of binary spinel solid solutions. Am. Miner. 69:733-753.

O'Neill HStC, Wall VJ (1987) The olivine-orthopyroxene-spinel oxygen barometer, the nickel precipitation curve, and the oxygen fugacity of the Earth's upper mantle. J. Petrol. 28:1169-1191.

Osborne MD, Fleet ME, Bancroft GM (1981) Fe^{2+} - Fe^{3+} ordering in chromite and Cr-bearing spinels. Contrib. Mineral. Petrol. 77:251-255.

Osborne MD, Fleet ME, Bancroft GM (1984) Next-nearest neighbor effects in the Mossbauer spectra of (Cr, Al) spinels. J. Solid State Chem. 53:174-183.

Smith DGW, Gold C (1979) EDATA2: a FORTRAN IV computer program for processing wavelength and/or energy dispersive electron microprobe analyses. In: Newbury D.E. (ed.) Microbeam Anal. Soc. Proc. 14th Ann. Conf. 273-278.

Souther JG (1977) Volcanism and tectonic environments in the Canadian Cordillera - a second look. In: Baragar WRA, Coleman LC, Hall JM (eds) Volcanic regimes in Canada. Geol. Assoc. Canada Spec. Pap. 16:3-24.

Souther JG, Hickson CJ (1984) Crystal fractionation of the basalt comendite series of the Mount Edziza Volcanic Complex, British Columbia: major and trace elements. J. Volc. Geotherm. Res. 21:79-106.

Sun M (1985) Sr isotopic study of ultramafic nodules from Neogene alkaline lavas of British Columbia, Canada and Josephine Peridotite, southwestern Oregon, U.S.A. Unpubl MSc Thesis, Univ. British Columbia, 132 pp.

Takahashi E (1986) Genesis of calc-alkali andesite magma in a hydrous mantle - crust boundary: petrology of lherzolite xenoliths from the Ichinomegata crater, Oga Peninsula, northeast Japan, Part II. J. Volc. Geotherm. Res. 29:355-395.

Ulmer GC, Grandstaff DE, Weiss D, Moats M, Buntin TJ, Gold DP, Hatton CJ, Kadik A, Koseluk RA, Rosenhauer M (1987) The mantle redox story; an unfinished story? Geol. Soc. Am. Spec. Pap. 215:5-23.

Virgo D, Luth RW, Moats M, Ulmer GC (1988) Constraints on the oxidation state of the mantle: an electrochemical and ^{57}Fe Mossbauer study of mantle-derived ilmenites. Geochim. Cosmochim. Acta 52:1781-1795.

Wells PRA (1977) Pyroxene thermometry in simple and complex systems. Contrib. Mineral. Petrol. 62:129-139.

Woermann E, Rosenhauer M (1985) Fluid phases and the redox state of the Earth's mantle. Extrapolations based on experimental, phase theoretical and petrological data. Fortschr. Miner. 63:263-349.

Wood BJ, Virgo D (1989) Upper mantle oxidation state: ferric iron contents of lherzolite spinels by ^{57}Fe Mossbauer spectroscopy and resultant oxygen fugacities. Geochim. Cosmochim. Acta 53:1277-1292.

Xue X (1988) Isotopic and geochemical study of ultramafic xenoliths from West Kettle River, British Columbia. Unpubl. M.Sc. Thesis, Univ. of Alberta 206 pp.

Xue X, Baadsgaard H, Scarfe CM (1988) Sr and Nd isotopic systematics of ultramafic xenoliths from West Kettle River, British Columbia: implications for an oceanic lithospheric mantle beneath southern British Columbia. EOS Trans. Amer. Geophys. Union 69:1517.

5. PHASE RELATIONS IN PERIDOTITE + CO_2 SYSTEMS TO 12 GPa: IMPLICATIONS FOR THE ORIGIN OF KIMBERLITE AND CARBONATE STABILITY IN THE UPPER MANTLE

5.1 INTRODUCTION

The occurrence of hydrous minerals, fluid inclusions, carbon and/or carbonates in mantle-derived xenoliths and xenocrysts entrained in alkaline magmas attests to the presence of C-O-H volatiles in the Earth's upper mantle (Roedder, 1965; McGetchin and Besancon, 1973; Arai, 1986; Berg, 1986). These volatiles also occur in gases produced during the eruption of mantle-derived basalts (Anderson, 1975; Gerlach, 1980), providing more indirect evidence for a volatile component in their mantle source region. Several recent studies indicate that the oxidation state of both the spinel and garnet lherzolite facies of the upper mantle are within ±2 log units of the fayalite-magnetite-quartz (FMQ) oxygen buffer (Eggler, 1983; Virgo _et al._, 1988; Wood and Virgo, 1989; Luth _et al._, in press; Canil _et al._, submitted). Under these conditions, C-O-H volatiles in the upper mantle will be dominantly CO_2 and H_2O (Eggler and Baker, 1982). Some relatively reduced regions may exist, however, where C-O-H species would be mainly CH_4 and H_2O (Haggerty and Tompkins, 1983).

The most abundant volatile species in mid-ocean ridge basalts (MORB's) are CO_2 and H_2O (Anderson, 1975; Delaney _et_ al., 1978). Because MORB's represent the most volumetrically abundant lava on Earth, and are derived from partial melting of mantle peridotite, it follows that CO_2 and H_2O should be the most important volatiles in the source regions of mantle-derived magmas.

With this in mind, the effect of CO_2 and H_2O on partial melting in the upper mantle has long been appreciated. Numerous experimental investigations have shown that the presence of CO_2 enhances the degree of silica - undersaturation in melts derived by partial melting of peridotite (Mysen and Boettcher, 1975; Wyllie and Huang, 1976; Brey and Green, 1977; Eggler, 1978). The presence of CO_2 in the mantle source regions of many alkaline, Si-poor magmas, such as kimberlites, melilitites and nephelinites, can thus explain their silica undersaturated nature.

Some kimberlites contain diamond, and therefore, originated at pressures greater than 5 GPa in the upper mantle, within the stability field of diamond. The origin of kimberlite magma deep in the upper mantle is poorly understood, however, due to the fact that few experimental studies have been undertaken on systems pertinent to the petrogenesis of kimberlite at pressures greater than 5 GPa. The ambiguity in obtaining a true primary kimberlite composition (Mitchell, 1986) on which to perform relevant phase equilibrium experiments has also compounded the problem of kimberlite genesis.

Perhaps the most definitive experimental studies bearing on this problem are those of Eggler and Wendlandt (1979) and Wendlandt and Eggler (1980). Eggler and Wendlandt (1979) determined the phase relations of a natural Lesotho kimberlite analogue in an effort to define the source mineralogy and depth of origin of this kimberlite, assuming it is primary. To avoid Fe loss to Pt capsules, Eggler and Wendlandt (1979) substituted Co for Fe in the starting material. Extrapolation of their results demonstrate that this kimberlite could have been derived by partial melting of CO_2-bearing garnet peridotite at 5.5 to 6 GPa in the upper mantle. This conclusion is fortified by phase equilibrium work in the $KAlSiO_4 - MgO - SiO_2 - CO_2 - H_2O$ system at 3 to 5 GPa (Wendlandt and Eggler, 1980). That some kimberlites originate at even higher pressures in the upper mantle (> 6 GPa) is evidenced by the presence of a significant component of pyroxene solid solution in garnets included in diamonds from the Monastery kimberlite (Moore and Gurney, 1985). Pressures of 5 to 18 GPa are required to stabilize these solid solutions (Akaogi and Akimoto, 1977; Kanzaki, 1987).

Wyllie (1980) provided a more hypothetical model for kimberlite genesis, based on phase relations in peridotite + CO_2 systems deduced in a large part from theory. His model requires volatile emanations from depth in the Earth to lower the solidus of mantle peridotite, cause ascent of mantle diapirs containing H_2O and CO_2, and episodic emplacement of kimberlite in the crust. A drawback of Wyllie's model is that it is critically dependent on his version of the peridotite - CO_2

- H_2O solidus, which has not been verified experimentally (Olafsson and Eggler, 1983; Wallace and Green, 1988). Moreover, it relies on extrapolation of the peridotite - CO_2 - H_2O solidus to pressures above 3 GPa, where the P - T topology is not defined by experiment (Mitchell, 1986). In this respect, Wyllie's (1980) and other models for kimberlite generation in the upper mantle remain unconstrained by the necessary experimental data at pressures above 4 GPa.

In this study, the phase relations in simplified peridotite + CO_2 systems from 4.5 to 12 GPa have been determined, and provide an essential foundation for understanding the genesis of deep-seated, diamond-bearing kimberlites and allied magmas which are thought to contain a significant CO_2 component in their mantle source regions. Some reconnaissance experiments in the simplified peridotite - CO_2 - H_2O system are also presented to elucidate the effect of H_2O on the carbonate buffered solidus. The results of this investigation define the effect of CO_2 on the topology of the mantle solidus at depth in the Earth, provide constraints on the P - T regime for kimberlite generation, and have implications for the storage of CO_2 in the deeper parts of the Earth's upper mantle.

5.2 EXPERIMENTAL METHODS

Starting Compositions

The compositions chosen for study were synthetic peridotites in the CaO - MgO - SiO_2 - CO_2 (CMS-CO_2), CaO - MgO - Al_2O_3 - SiO_2 - CO_2 (CMAS-CO_2) and CaO - MgO - SiO_2 - CO_2 - H_2O (CMS-CO_2-H_2O) systems. These systems were chosen due to their compositional simplicity, yet ability to adequately model melting in natural peridotites, as noted by Wendlandt and Mysen (1980). Because sealed capsules are required for experimentation with volatiles at high temperature and pressure, Fe-free systems were deemed more experimentally tractable, and circumvented problems of Fe loss to Pt capsules during the experiments.

Starting compositions were combined mineral mixes of pure, synthetic, end member diopside (Di), forsterite (Fo), enstatite (En), and pyrope (Py) (Table 5.1) which were stored at 110°C prior to use. To avoid errors in weighing small amounts of volatiles into each individual run charge, CO_2 and H_2O were added to the starting materials as pure calcite (Iceland Spar) and brucite (Br), respectively (Table 5.1, Fig. 5.1). The resultant mineral mixes were ground in alcohol to less than 10 um grain size, dried, and stored under dessicant.

High Pressure Experiments

Samples were loaded into 2 mm diameter Pt capsules sealed at one end, and then dried overnight at 400°C to remove any adsorbed water. Capsules were sealed immediately after drying by arc welding, and pressed into thin wafers less than 1 mm thick and 2 to 3 mm wide.

The use of a thin wafer, rather than a long capsule, helps to minimize thermal gradients across the sample, which can be substantial in straight walled furnaces of small dimension (Takahashi et al., 1982). The thermal gradient across the sample in assemblies used in this study was estimated using a method similar to Takahashi et al. (1982). The results show that the thermal gradient across the sample is about 25°C (Fig. 5.2).

The charges and other assembly parts were then loaded into an 18 mm edged (18M) MgO octahedron which served as the pressure medium. All parts of the sample assembly were fired at 1000°C prior to loading to remove H_2O, and then stored at 110°C.

Experiments were performed at pressures of 4 to 12 GPa in a multi-anvil apparatus (USSA 2000). Pressure generation in the 18M assembly was calibrated at 5.3 and 9.2 GPa at 1000°C using the fayalite -   - spinel (Yagi et al., 1987) and coesite - stishovite (Yagi and Akimoto, 1976) transitions, respectively. These transitions were bracketed to within ± 0.3 GPa, and this value serves as an estimate of the error in pressure for experiments below 12 GPa.

Heating was accomplished by graphite or $LaCrO_3$ furnaces, depending on the temperature and pressure of the experiment. Graphite heaters were stable within the stability field of diamond at temperatures less than 1500°C. Temperature was monitored using either $Pt-PtRh_{13}$ or $WRe_3 - WRe_{25}$

thermocouples inserted through the center of the 18M assembly (Fig. 5.3). The EMF of these thermocouples were uncorrected for pressure. Temperature was controlled to within ± 10°C of the set point. In some runs, thermocouples were lost during heating, and run temperature was estimated using furnace power (Table 5.2).

For almost all experiments, the sample was pressurized at room temperature and then heated at a rate of 100°C/min to the run temperature. In a few experiments, the sample was pressurized at 500°C and then heated to the run temperature. Experiments using either of these procedures produced identical results. Runs were quenched at a rate of 1000°C/s by terminating the power to the furnace. Run durations varied from 20 minutes to 4.5 hours (Table 5.2).

Analytical Methods

Phases in the run products were identified by petrographic examination in oil mounts, powder X-ray diffraction and back scattered electron (BSE) imaging of polished sections. The proportions of phases in selected run products along the solidus for the CCMS2 composition were determined by point counting (1500 points) BSE images of the experimental charges. Compositions of phases in selected run products were determined using wavelength dispersive analysis on a JEOL JXA 8600 electron microprobe at the University of Saskatchewan. A 15 kV operating voltage and 10 nA probe current were employed in all analyses. Standards used were pyrope (Al), olivine (Mg) and diopside (Ca, Si). Data were reduced with a ZAF procedure.

The proportions and compositions of phases determined by point counting and electron microprobe, respectively, allowed calculation of liquid compositions in selected runs above the CCMS2 solidus by mass balance (Table 5.3). In three out of five cases, these calculations produced residuals within 2 % of the bulk composition. The two exceptions were Runs 120A and 124A, which gave residuals within 4 %. Errors in these liquid compositions at the 95 % confidence level, considering standard deviations in the point counting and errors in microprobe analyses, are ± 3 wt.% of each oxide. It should also be noted that partial melts from experiments 175A and 133A do not contain CO_2 (Table 5.3). This result is most likely due to the errors stated above.

Equilibrium and Experimental Conditions

The solidi for both the CCMS2 and CCMAS1 starting compositions were reversed at 5 GPa. No further reversals were attempted due to the difficulty in unambiguously identifying the onset of melting in mostly crystalline run products. To obtain these reversals, the solidus temperature had to be understepped 50°C to recrystallize all incipient liquid generated at a temperature above the solidus (Table 5.2). It was discovered that the temperature of the reversed solidus at 5 GPa coincided with the loss of magnesite in the XRD patterns (but not in the mode) of run products at this pressure. This criteria was then used to delineate the onset of melting (i.e. the solidus) in higher pressure experiments and confirmed by petrographic and back scatterred electron imaging of run products.

No time studies were undertaken to evaluate whether liquid coexisting with restite crystals changed composition with varying run duration (e.g. Fujii and Scarfe, 1985). However, the fast rate of cation exchange in carbonate-bearing and Al-free CMS systems in the temperature range investigated here (Irving and Wyllie, 1975; Eggler, 1978) and absence of zoning in any stable phases in the CCMS2 run products, suggests that equilibrium was approached in the experiments. Zoning was observed in stable crystals in the CCMAS1 run products, indicating that true equilibrium between liquid and crystals was not achieved in this composition, perhaps due to sluggish kinetics in Al-bearing systems at these temperatures and run durations. Experiments with different run durations produced identical results with respect to the stable phases present in both the CCMS2 and CCMAS1 starting compositions.

Although the f_{O2} of the charges was not externally buffered, the presence of coexisting orthopyroxene (Opx), magnesite (Cm), carbon (G,D) and olivine (Ol) in several runs on the CCMAS1 composition indicates that the f_{O2} during the experiments was at or near the EMOG or EMOD (enstatite -

magnesite - olivine - graphite/diamond) buffer (Eggler and Baker, 1982). The EMOG or EMOD buffer lies between the FMQ and magnetite - wustite (MW) oxygen buffers in temperature - f_{O2} space. Both CO_2 and H_2O are the dominant C-O-H species under these conditions (Eggler and Baker, 1982).

Hydrogen Diffusion

In initial experiments, anomalously low melting temperatures were encountered for the peridotite + CO_2 starting compositions. It was immediately suspected that H_2 was migrating into the charge during a run and combining with O to form H_2O, which greatly effects the stability of the subsolidus carbonates (Goldsmith and Newton, 1969). To test this hypothesis, a few "dummy" experiments were performed in which MgO powder, dried at 1200°C, was loaded in one of the Pt capsules and sealed by arc welding. After a typical experiment (e.g. 5 GPa, 1250°C) the MgO was examined by X-ray diffraction. Peaks for Br appeared in the X-ray pattern, suggesting that H_2 diffusion was indeed occurring. Pyrophyllite sleeves used for thermal insulation in the original 18M assembly design (Fig. 5.3) were the most probable source for the H_2. Similar test experiments with ZrO_2 replacing the pyrophyllite sleeve showed much smaller peaks for Br in XRD patterns of the MgO "dummy" run products, indicating that H_2 diffusion had been minimized, but not eliminated. ZrO_2 sleeves were then adopted for all the experiments reported in this study.

Decomposition of pyrophyllite gaskets surrounding the MgO octahedrons during a run is also a potential source of H_2, as shown by lines for Br in XRD patterns of both MgO octahedrons and Pt capsules containing a MgO "dummy", after an experiment. The effect of this source of H_2 on the resultant phase relations is not known. Because Br does not appear in any of the CCMS2 or CCMAS1 run products, the amount of H_2O actually formed by H_2 diffusion through Pt capsules during an experiment is expected to be small, but may slightly affect the melting temperature of these compositions. It is apparent that in spite of all precautions used to rid sample assemblies of H_2O before experiments (i.e. assembly dryout at 1000°C) truly anhydrous experiments cannot be achieved in the multi-anvil apparatus if pyrophyllite is employed as a gaket material.

5.3 EXPERIMENTAL RESULTS

All run products below the solidus of each composition contained a mixture of subhedral grains 5 to 20 um in diameter. Stable equilibrium phases formed grains with compositions different from the minerals used in the starting material. Metastable restite phases were recognized by their zoned rims and ragged edges (Fig. 5.4a), and had compositions identical to the minerals used in the starting material.

In runs above the solidus, liquid was distributed evenly amongst the restite crystals in the charge, and always quenched to feathery and acicular Ol and Cpx (Fig. 5.4b). Quench carbonate was not identified in runs above the solidus. Any CO_2 partitioned into the melt may have quenched to glass or carbonate which was unrecognizable in BSE images or oil mounts. Stable Cm was identified in BSE images of several run products below and above the solidus (Fig. 5.4a).

The Peridotite + CO_2 Solidus

The solidus for the CCMS2 composition (in the CMS - CO_2 system) at pressures greater than 5 GPa (Fig. 5.5a) is consistent with lower pressure data for the CMS - CO_2 system (Eggler, 1978). The solidus for CCMS2 changes slope near 10 GPa. Reasons for this inflection in the solidus are not obvious. The change in slope probably reflects a gradual change in the structure of melts generated along the CCMS2 solidus.

Subsolidus phases for CCMS2 at pressures above 5 GPa are Ol + Cpx + Cm. Opx does not appear in the subsolidus of CCMS2 at these pressures due to its increased solubility in clinopyroxene with increasing pressure in ultramafic bulk compositions (Table 5.3, Fig. 5.6, see also Takahashi, 1986; Takahashi and Ito, 1987) combined with its reaction with calcite in the starting materials to form Cpx and Cm at pressures above the reaction:

$$\underset{\text{En}}{2\,MgSiO_3} + \underset{\text{Cd}}{CaMg(CO_3)_2} = \underset{\text{Di}}{CaMgSi_2O_6} + \underset{\text{Cm}}{2\,MgCO_3} \quad [1]$$

(Brey et al., 1983). Opx does appear in both sub- and hyper-solidus runs below reaction [1] (Fig. 5.5a). Ol + Cpx + Cm coexist with liquid up to about 100°C above the solidus, upon which Cm is consumed by further partial melting (Fig. 5.5a).

The addition of Al to the CMS - CO_2 system does not greatly affect the topology of the peridotite + CO_2 solidus (Fig. 5.5b) as was realized in phase equilibrium work at lower pressures (e.g. Maaloe and Wyllie, 1975; Eggler, 1978). Solidus temperatures for the CCMAS1 starting composition are slightly lower than for CCMS2 at pressures below 6 GPa, but are higher above 6 GPa (Fig. 5.5b). Unlike in the CCMS2 composition, a change in slope of the solidus is not observed near 10 GPa in CCMAS1.

Ol + Opx + Cpx + Gt + Cm are subsolidus phases in CCMAS1 to pressures as high as 11 GPa. The appearance of Opx in the subsolidus of the CCMAS1 composition is due to the high normative En content of the starting material (Table 5.1). Unlike in the CCMS2 starting material, not all Opx in the CCMAS1 composition is consumed by solid solution with coexisting clinopyroxene and garnet (Fig. 5.5) or by reaction with calcite in the starting materials at pressures above reaction [1]. That reaction [1] is operative is evidenced by the appearance of Cpx (not present in the starting materials, Table 5.1) in the CCMAS1 composition at pressures above 5 GPa.

The Peridotite + CO_2 + H_2O Solidus

The results presented here for the peridotite + CO_2 + H_2O solidus in the CMS - CO_2 - H_2O system (CCMSH2 composition) can at best be considered preliminary, due to the fact that only six reconnaissance experiments were performed in this system. Nonetheless, the five experiments do provide a fairly tight bracket on the solidus at pressures above 5 GPa (Fig. 5.5c) and are consistent with lower pressure data for CMS - CO_2 - H_2O data presented by Eggler (1977). Subsolidus phases for this composition are Ol + Cpx + Cm + Br ± V. The absence of Opx is again attributed to its solution into coexisting Cpx (see above discussion) and reaction with Br at pressures below the reaction (Ellis and Wyllie, 1979):

$$\underset{\text{En}}{MgSiO_3} + \underset{\text{Br}}{Mg(OH)_2} = \underset{\text{Fo}}{Mg_2SiO_4} + \underset{\text{Vap}}{H_2O} \qquad [2]$$

Vapor was not recognized in the run products, but may be present at pressures below reaction [2]. At pressures above reaction [2] all H_2O can be contained in Br. Metastable, quench Br coexists with Ol + Cpx + Liq outside of its stability field (Fig. 5.5c) in hypersolidus runs. Cm is probably consumed at the solidus.

Clinopyroxene Compositions

Clinopyroxenes in equilibrium with melt along the CCMS2 solidus become more sub-calcic with increasing pressure (Fig. 5.6). This trend was also observed in experiments on anhydrous peridotites at pressures above 5 GPa (Takahashi, 1986; Takahashi and Ito, 1987). The data from this study support the proposal that sub-calcic pyroxenes occurring as discrete nodules in kimberlites (e.g. Boyd and Nixon, 1978) represent phenocrysts which crystallized at high pressure in kimberlite magmas (Eggler and Wendlandt, 1979).

5.4 PARTIAL MELTS ALONG THE PERIDOTITE + CO_2 SOLIDUS AND THE ORIGIN OF KIMBERLITES

At 5 and 7 GPa, partial melts within 100°C of the solidus have compositions very close to that of the starting material (Fig. 5.7) and confirm the eutectic-like melting at carbonate-buffered solidi predicted in previous studies (Eggler, 1977, 1978; Eggler and Wendlandt, 1979). Near-solidus partial melts at 5 to 7 GPa are not unlike those of presumed primary, uncontaminated, natural kimberlites (Fig. 5.7) when projected using their CMS components. In contrast, the partial melt calculated at 9 GPa lies very close to Fo in CMS projection (Fig. 5.7) and is more Mg-rich than any kimberlite or other natural melt.

Higher degree partial melts at 5 to 7 GPa tend to plot towards the Cm (M) apex when projected in the CMS ternary (Fig.

5.7). This trend reflects the progressive melting out of Cm in the source, observed in hyper-solidus runs on the CCMS2 starting composition (Fig. 5.5a). These partial melts are shifted away from the spectrum of natural kimberlites (dashed arrows in Fig. 5.7) and suggest that kimberlite and other silica undersaturated magmas represent partial melts generated within a small temperature range above the solidus. These results support the contention that high degrees of partial melting (> 20%) are probably not realized in kimberlite petrogenesis (Mitchell, 1986). This conclusion is further corroborated by studies on the wetting properties of near-solidus, carbonate-rich melts (Hunter and McKenzie, 1989) which indicate they are efficiently removed from their source region soon after melting occurs.

The above data indicates that most kimberlites erupted on the Earth's surface, if represented by the field of compositions in Fig. 5.7, are generated by partial melting of CO_2-bearing peridotite at pressures of 5 to 7 GPa in the upper mantle. Kimberlite cannot be derived at pressures below 3 GPa (Eggler and Wendlandt, 1979). The proposed 5 to 7 GPa "window" for kimberlite generation may represent a restricted region in the Earth from which these magmas can ascend essentially unmodified. A likely "window" at the appropriate depth interval (150 to 250 km) beneath the continents may be the transition between the lithosphere and asthenosphere (Boyd and Gurney, 1986; Finnerty and Boyd, 1987), where diapirs of CO_2-bearing peridotite rising from the asthenosphere become trapped (Eggler and Wendlandt, 1979).

That other "proto-kimberlite" magmas originate at pressures above 7 GPa in the upper mantle is not precluded. Such magmas may exist in the upper mantle, but for tectonic reasons are not represented on the Earth's surface (Eggler and Wendlandt, 1979). Alternatively, kimberlite magmas derived at pressures above 7 GPa may fractionate olivine before emplacement into the crust as the "primary" kimberlites represented Fig. 5.7. "Proto-kimberlites" generated at pressures greater than 7 GPa could also become contaminated, or mix with other magmas, during their ascent through shallower depths in the mantle. Evidence for mixing in kimberlites is recorded in their megacryst and whole rock major, trace and isotopic chemistry (Hunter and Taylor, 1984; Shervais _et al._, 1987). A possible product of such mixing could be the enigmatic Si-poor kimberlites studied by Edgar _et al._ (1988). Those rocks may represent mixtures between near-solidus kimberlite derived above 5 GPa and carbonatitic melts generated at less than 3 GPa (Fig. 5.7).

The effect of other important components such as Fe, Ti and K on the phase relations of simplified peridotites used in this study need to be evaluated in the future before a truly complete experimental interpretation of kimberlite genesis can be advanced. The effect of Fe would be to lower solidus temperatures. The addition of Ti and K may stabilize high pressure titanates, phlogopite and K-richterite, all of which occur in mantle lithosphere sampled by kimberlites (Haggerty, 1987; Erlank et al., 1987) and are stable at the pressures predicted for kimberlite generation (Liu and Bassett, 1986, p.140; Tronnes et al., 1989). Notwithstanding these complications, it is comforting that the interpretation described above, based on phase relations in the simple CMS - CO_2 system, is in accord with previous phase equilibrium work on natural kimberlite (Eggler and Wendlandt, 1979).

5.5 CONCERNING KIMBERLITE AND MELILITITE

The spatial association of kimberlite with melilitites in some alkaline provinces could indicate that these two rock types are somehow related. However, Brey (1978) proposed that kimberlites and melilitites are derived at different depths in the upper mantle, and are therefore unrelated. Kimberlites have low Ca/Mg, and are probably generated from Cm-peridotite, whereas melilitites have high Ca/Mg, and are derived from Cd-peridotite (Brey, 1978). The melting of carbonated peridotite at higher pressures, where Cm is stable, should produce melts with lower Ca/Mg ratios (kimberlites) than those produced by melting of Cd-peridotite (melilitites) at lower pressures.

Differences between melilitites and kimberlites outlined by Brey (1978) are well illustrated in CMS projections of these rock types (Fig. 5.7) when contrasted with experimental data on peridotite + CO_2 systems. Kimberlites, and near solidus partial melts in equilibrium with Cm at 5 and 7 GPa have lower Ca/Mg than do melilitites and partial melts of Cd-peridotite at 3 GPa (Fig. 5.7). The fact that melilitites are always diamond-free, whereas kimberlites can be diamond-bearing, is consistent with the derivation of these two magmas from carbonated peridotite at lower and higher pressures, respectively.

5.6 THE STORAGE OF CARBON IN THE EARTH'S UPPER MANTLE

Where and how carbon is stored in the upper mantle is important in order to understand the distribution and geochemical cycle of this element in the Earth. Carbon may reside in the upper mantle in a free vapor (Roedder, 1965), in diamonds or graphite, as tetrahedral carbon in silicates (Fyfe, 1970) or as carbonate (Berg, 1986).

Whether carbon is contained in upper mantle carbonates is critically dependent on the f_{O2} of this region of the Earth. The f_{O2} in the spinel and garnet lherzolite facies of the upper mantle to pressures of 6 GPa is near the FMQ buffer (Wood and Virgo, 1989; Luth _et al._, in press; Canil _et al._, submitted) and therefore high enough to stabilize carbonates. The f_{O2} of the upper mantle at depths from which we have no representative samples (> 180 km), is unknown and can only be inferred at present. However, the occurrence of magnesite inclusions in some diamonds (Bulanova, 1986) is evidence that the f_{O2} of the mantle at pressures greater than 5 GPa is near the EMOD oxygen buffer (Eggler and Baker, 1982) and may be suitable for carbonate stability.

If the upper mantle is relatively oxidizing at pressures above 5 GPa, then Cm is a potential host for C to depths of at least 350 km in the Earth. This possibility does not eliminate the existence of elemental C at these depths; diamonds and carbonates can coexist under suitably oxidizing conditions (Eggler and Baker, 1982).

5.7 SUMMARY

Near-solidus partial melts of peridotite + CO_2 in the CMS - CO_2 system at 5 to 7 GPa are similar in composition to uncontaminated kimberlites observed in nature. In contrast, partial melts generated at higher temperatures above the solidus, or at pressures above 8 or 9 GPa, are unlike natural kimberlite, and have Mg-rich compositions which are not represented by any magma on the Earth's surface. These magmas may have, however, fractionated olivine in transit to the surface.

The inferred depth of generation for diamond-bearing kimberlite is 150 to 250 km in the upper mantle. This restricted depth interval or "window" could represent the interface between cold, elastic lithosphere and hotter, anelastic asthenosphere beneath the cratons of continental regions. Diamond-free or "off-craton" kimberlites probably originate beneath continental regions where the lithosphere is thinner, and "window" at a lower pressure (3 to 5 GPa).

The contrasting compositional variation between kimberlites and melilitites, when compared with partial melts of peridotite + CO_2 deduced from experiment, confirm that kimberlites are derived by partial melting of magnesite peridotite whereas melilitites are derived from dolomite peridotite at lower pressures. The spatial association of these two rock types in some alkaline provinces does not reflect a common source region in the upper mantle.

Under appropriate, but not unrealistic, f_{O2}'s carbonates are potential hosts for carbon in a peridotitic upper mantle to depths of at least 350 km.

Table 5.1 Compositions of Starting Materials* (wt%)

	CCMS2	CCMAS1	CCMSH2	Fo	En	Di	Py
SiO_2	43.18	48.31	39.22	42.55	59.85	54.40	44.80
Al_2O_3	-	3.06	-	-	-	-	25.73
MgO	44.27	43.93	46.54	57.87	40.00	20.89	29.73
CaO	8.08	2.86	7.45	-	-	24.11	-
CO_2	4.40	2.24	4.00	-	-	-	-
H_2O	-	-	2.80	-	-	-	-
Total	99.93	100.40	100.01	100.42	99.85	99.40	100.26
Ca/Al	-	0.93	-				
Mg/Si	1.03	0.91	1.19				
Ca/Mg	0.19	0.07	0.16				
mode wt%							
Fo	60.0	40.0	54.5				
En	20.0	43.0	18.2				
Di	10.0	-	9.1				
Py	-	12.0	-				
Cc	10.0	5.0	9.1				
Br	-	-	9.1				
norm wt%							
Fo	73.7	52.56	86.4				
En	-	34.31	-				
Di	22.1	4.63	2.1				
Ln	4.2	-	11.43				
An	-	8.51	-				

Notes: * Synthetic Fo and En were purchased by CMS from a Japanese ceramic materials company. Diopside was crystallized from a melt at 1360°C and 1 atm for 24 h. Pyrope was synthesized from an oxide mix + 10 wt% H_2O + 2 wt% natural garnet seeds at 1050°C and 2.8 Gpa for 24 h. The purity of all synthetic starting materials was verified by electron microprobe analysis. The synthetic diopside is slightly Mg-rich compared to stoichiometric diopside.

Table 5.2 Experimental Run Conditions

Run#	P(GPa)	T(°C)	t(min)	Assembly	Run Products
			CCMS2		
511	4.0	1200r	210	18MGS	Ol+Opx+Cpx+Cm
222A**	5.0	1200r	60	18MGL	Ol+Cpx+Cm
92A	5.0	1250d	60	18MGL	Ol+Cpx+Cm
274A**	5.0	1260r	50	18MGS	Ol+Cpx+Cm
110A	5.0	1310d	60	18MGL	Ol+Cpx+Cd+Opx+L
175A	5.0	1320d	75	18MGL	Ol+Cpx+Cd+Opx+L
101A	5.0	1410p	30	18MGL	Ol+Cpx+Opx+L
231A**	5.3	1300r	70	18MGS	Ol+Cpx+Cm+L
253A	5.5	1210r	60	18MGS	Ol+Cpx+Cm
201A*	5.5	1290r	70	18MGS	Ol+Cpx+Cm+L
216A*	5.5	1300r	110	18MGS	Ol+Cpx+Cm+L
191B	5.5	1340d	95	18ML	Ol+Cpx+Cm+L
49A	6.0	1200d	60	18MGL	Ol+Cpx+Cm
268B	6.0	1250r	230	18MGS	Ol+Cpx+Cm
143B	6.0	1340d	60	18MGL	Ol+Cpx+Cm+L
195A	6.0	1355d	90	18MGS	Ol+Cpx+Cm+L
128B	7.0	1250p	40	18MGS	Ol+Cpx+Cm
150A	7.0	1300p	95	18MGS	Ol+Cpx+Cm
133A	7.0	1360d	30	18MGL	Ol+Cpx+Cm+L
327B	7.0	1370r	150	18MGS	Ol+Cpx+Cm+L
117A	7.0	1380d	20	18MGS	Ol+Cpx+Cm+L
124A	7.0	1450d	35	18MGL	Ol+Cpx+L
282A	9.0	1350r	45	18MGS	Ol+Cpx+Cm
154B	9.0	1400p	70	18MGS	Ol+Cpx+Cm+L
120A	9.0	1420p	30	18MGL	Ol+Cpx+L
344B	11.0	1490r	50	18ML	Ol+Cpx+Cm
347A	11.0	1590r	20	18ML	Ol+Cpx+Cm+L
31	12.0	1000d	240	18MGL	Ol+Cpx+Cm
34	12.0	1200d	120	18MGL	Ol+CPx+Cm
			CCMSH2		
518	5.0	1150r	100	18MGS	Ol+Cpx+Cm+Br
49B	6.0	1200d	60	18MGL	Ol+Cpx+Br+L
355B	7.0	1150r	60	18MGS	Ol+Cpx+Br+Cm
358A	8.0	1250r	60	18MGS	Ol+Cpx+Br+L
120B	9.0	1420p	30	18MGL	Ol+Cpx+L
43	10.0	1200d	95	18MGL	Ol+Cpx+Cm+Br
			Brucite		
355A	7.0	1150r	60	18MGS	Br
358A	8.0	1250r	60	18MGS	Per+V±Br

Notes: 18M=18M assembly; 18MGS=3 mm i.d. graphite heater; 18MGL=3.5 mm i.d. graphite heater; 18ML=3.2 mm i.d. $LaCrO_3$ heater; p=estimated using power; r=Pt-$PtRh_{13}$ thermocouple; d=WRe_3-WRe_{25} thermocouple; **=successful reversal; *=unsuccessful reversal; Ol=olivine, Cpx=clinopyroxene, Opx=orthopyroxene, Cm=magnesite, Cd=dolomite, Br=brucite, Gt=garnet, L=liquid, LHZ=Ol+Cpx+Opx+Gt, Per=periclase, V=vapor

Table 5.2 continued...

CCMAS1

Run#	P(GPa)	T(^{o}C)	t(min)	Assembly	Run Products
241A*	4.5	1200r	125	18MGS	LHZ+L
222B**	5.0	1200r	60	18MGS	LHZ+Cm
274B*	5.0	1250r	50	18MGS	LHZ+Cm+L
175B	5.0	1320d	75	18ML	LHZ+Cm+L
238B	5.3	1300r	60	18MGS	LHZ+Cm+L
253B	5.5	1210r	60	18GS	LHZ+Cm
201B*	5.5	1290r	70	18MGS	LHZ+Cm+L
216B*	5.5	1300r	110	18MGS	LHZ+Cm+L
191A	5.5	1340d	95	18ML	LHZ+Cm+L
268A	6.0	1250r	230	18MGS	LHZ+Cm
143A	6.0	1340d	60	18MGL	LHZ+Cm+L
195B	6.0	1355d	90	18MGS	LHZ+Cm+L
150B	7.0	1300d	95	18MGS	LHZ+Cm
327A	7.0	1370r	150	18MGS	LHZ+Cm+L
282B	9.0	1350r	45	18MGS	LHZ+Cm
154B	9.0	1400d	70	18MGS	LHZ+Cm
335A	9.0	1475r	270	18MGS	LHZ+Cm+L
344A	11.0	1490r	50	18ML	LHZ+Cm
347B	11.0	1590r	20	18ML	LHZ+Cm+L

Table 5.3 - Compositions of Phases in Selected Run Products*

Clinopyroxenes

Run#	175A	101A	133A	117A	124A	120A	347A
P(GPa)	5.0	5.0	7.0	7.0	7.0	9.0	11.0
T(^{o}C)	1320	1410	1360	1380	1450	1420	1590
mode%	24	25	21	27	28	29	n.d.
SiO$_2$	55.53	55.53	55.18	55.94	57.56	55.86	55.09
MgO	23.00	23.23	22.80	23.88	26.10	27.43	29.40
CaO	21.00	21.07	21.51	20.12	17.49	17.31	15.02
Total	99.53	99.83	99.49	99.94	101.15	100.60	99.51
Ca/(Ca+Mg)	0.39	0.39	0.40	0.38	0.33	0.31	0.27

Orthopyroxenes

Run#	175A	101A
P(GPa)	5.0	5.0
T(^{o}C)	1320	1410
mode%	6	8
SiO$_2$	58.39	59.54
MgO	39.49	38.68
CaO	1.51	1.88
Total	99.39	100.10
Ca/(Ca+Mg)	0.03	0.03

Carbonates

Run#	175A	133A	117A
P(GPa)	5.0	7.0	7.0
T(^{o}C)	1320	1360	1380
mode%	10	10	8
SiO$_2$	-	-	-
MgO	46.31	46.23	45.09
CaO	5.47	6.39	6.42
Total	51.78	52.62	51.51

Partial Melts

Run#	175A	101A	133A	117A	124A	120A
P(GPa)	5.0	5.0	7.0	7.0	7.0	9.0
T(^{o}C)	1320	1410	1360	1380	1450	1420
mode%	23	39	36	32	36	37
Ol mode%	37	28	33	33	36	34
SiO$_2$	45.87	33.06	48.61	43.70	30.88	37.14
MgO	46.27	49.10	44.72	48.30	45.06	50.81
CaO	10.37	7.26	8.12	8.67	8.36	7.93
CO$_2$	-	11.00	-	1.70	12.22	1.43
Total	102.51	100.42	101.45	100.37	96.52	97.31

Notes: * Compositions represent average of at least 3 analyses of each phase in each run product. Partial melt compositions were calculated using mass balance, with olivine compositions assumed to be nearly pure Fo (as verified by microprobe analyses not presented here).

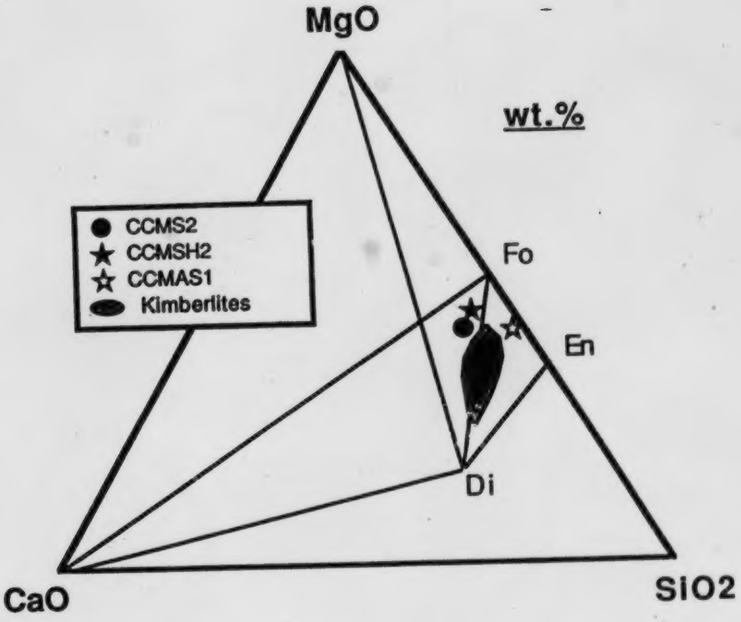
MgO
wt.%
● CCMS2
★ CCMSH2
☆ CCMAS1
Kimberlites
Fo
En
Di
CaO
SiO2

Figure 5.1. Starting compositions projected in the CaO - MgO - SiO_2 ternary. Field for average uncontaminated kimberlites adapted from Mitchell (1986).

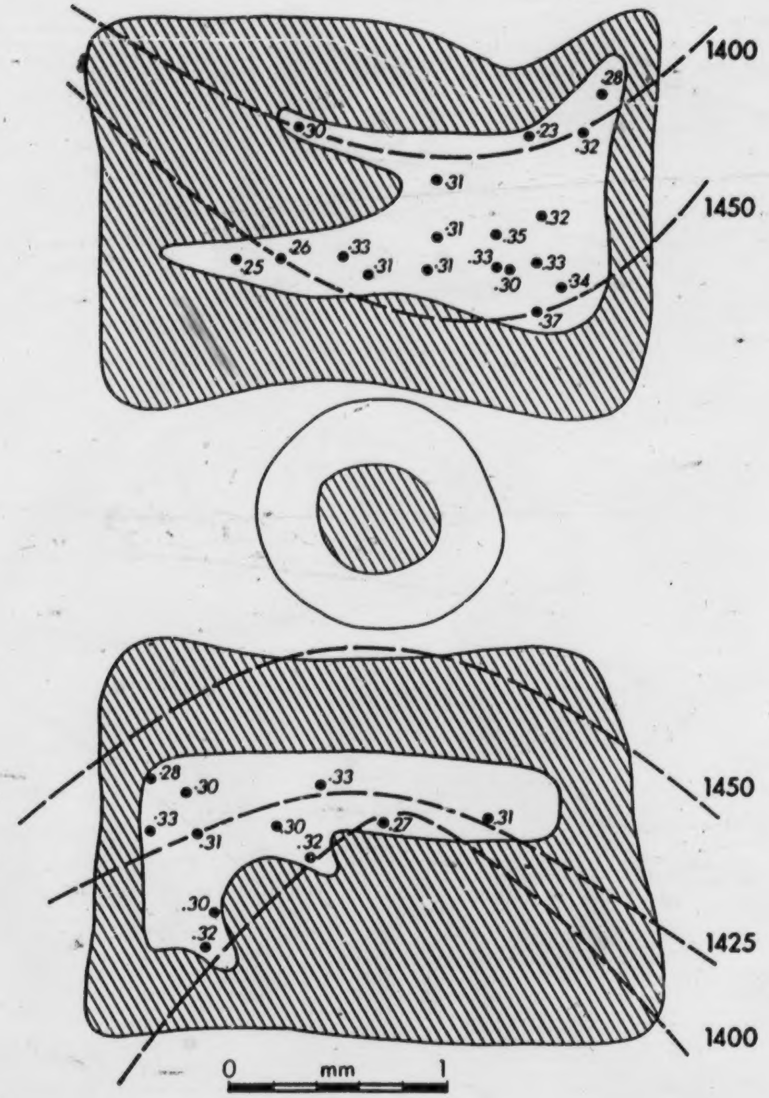
1400
.28
.30
.23
.32
.31
1450
.32
.31
.35
.26
.33
.25
.31
.31
.33
.33
.30
.34
.37
.28
.30
.33
1450
.33
.31
.30
.32
.27
.31
.30
.32
1425
1400
0
mm
1

Figure 5.2. Thermal gradient in 18M assembly used for experiments in this study determined using a method similar to that of Takahashi et al. (1982). Pure end member diopside and enstatite were equilibrated at 5 GPa and 1450°C for 3 h. Their resultant compositions were determined by electron microprobe analysis after the run, and the equilibrium temperature they record throughout the charge (plotted as K_D values) was determined using the two pyroxene thermometer of Nickel et al. (1985).

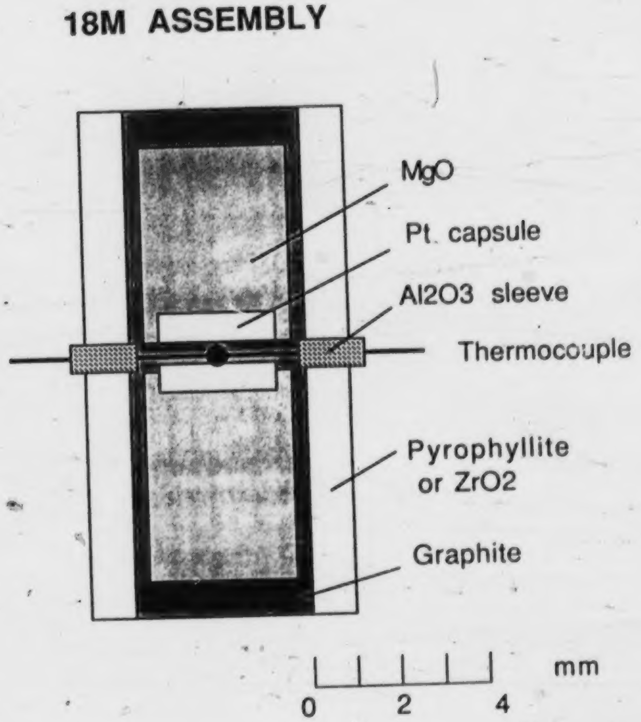
18M ASSEMBLY
MgO
Pt. capsule
Al2O3 sleeve
Thermocouple
Pyrophyllite
or ZrO2
Graphite
mm
0
2
4

Figure 5.3. Cross-section of assembly used in this study.

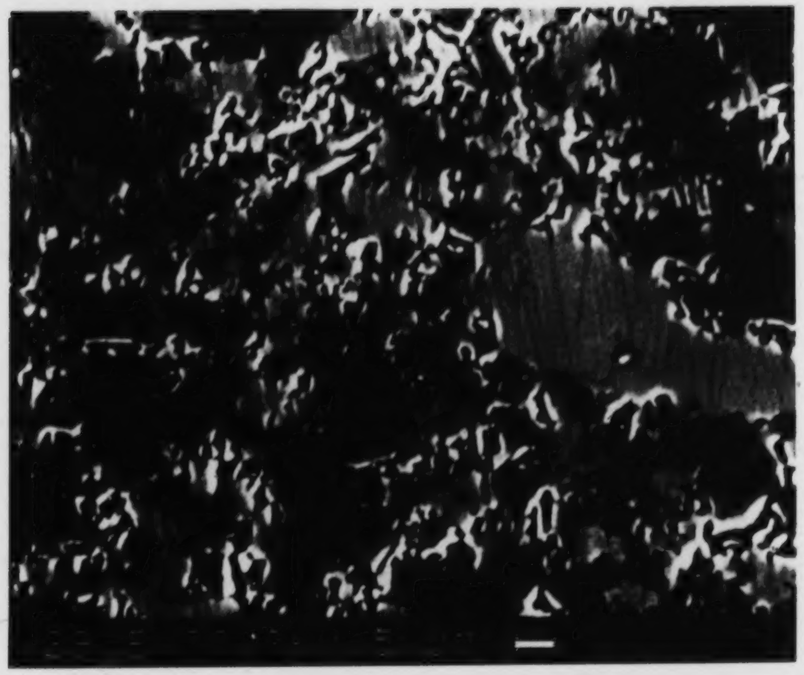

Figure 5.4. (a) Back-scattered electron (BSE) image of run product 274A (5 GPa, 1260°C). Clinopyroxenes are bright white, olivines are dark grey, carbonates are dark black. Note metastable restite minerals (ragged, large grains) and stable equilibrium grains (subhedral, 5-15um).

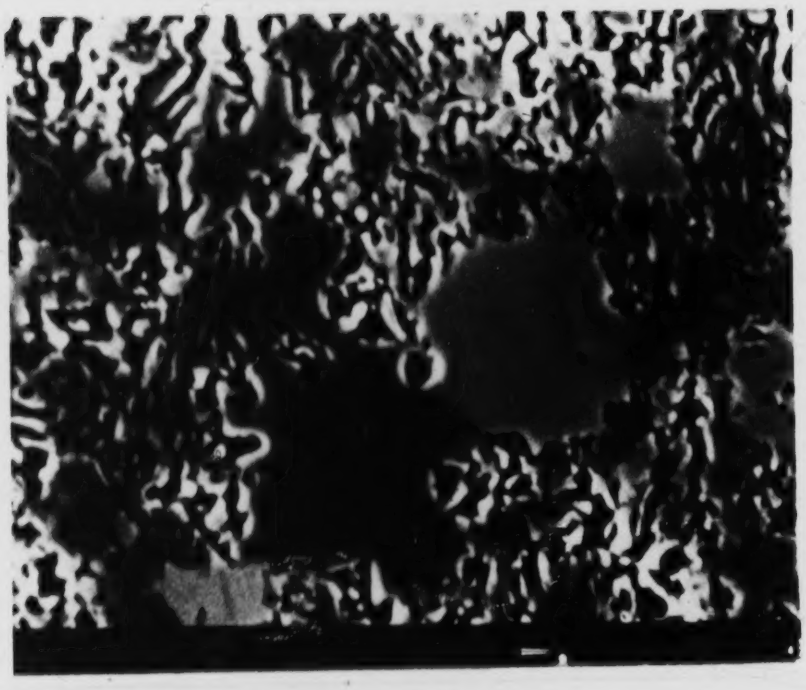

Fig. 5.4. (b) BSE image of run product 101A (5 GPa, 1410°C). Note bladed, acicular olivine and clinopyroxene (quenched from liquid) amongst larger stable restite grains. Image contrasts same as in 5.4.(a).

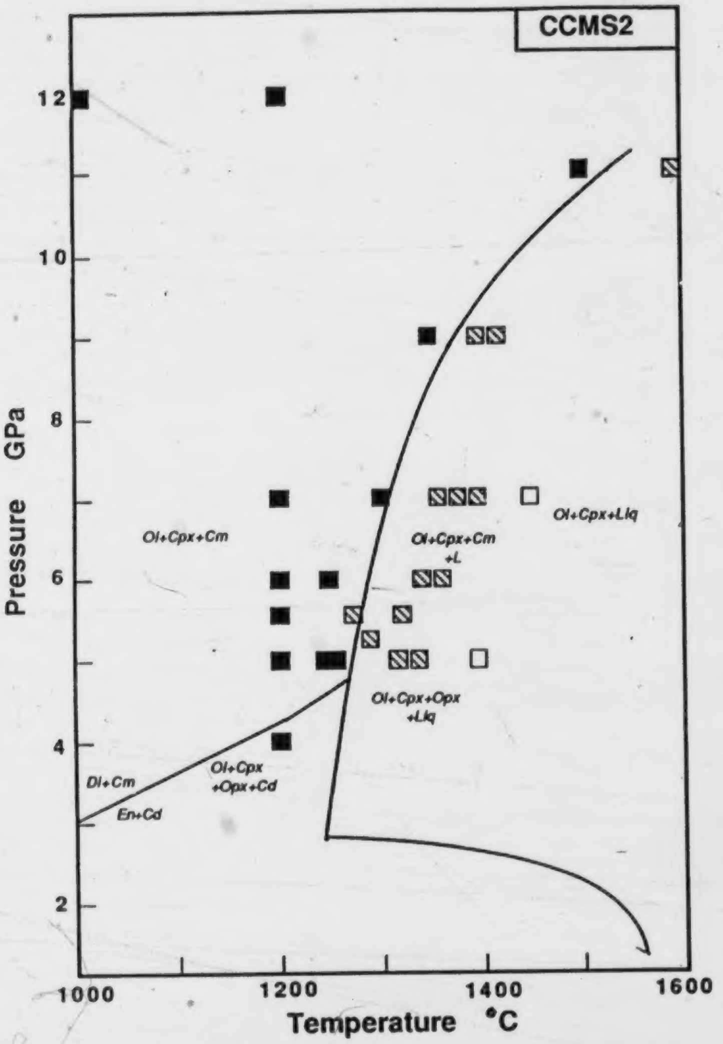

Figure 5.5. (a) Phase relations for the simplified peridotite CCMS2 in the CMS - CO_2 system. Solidus below 5 GPa adapted from Eggler (1978). Filled squares are subsolidus runs, hatchured squares are hyper-solidus runs which contain a carbonate phase, and open squares are carbonate-free hyper-solidus runs. In principle, a cusp must be present at the invariant point where the subsolidus reaction En + Dol = Di + Mag intersects the solidus, but was omitted for clarity.

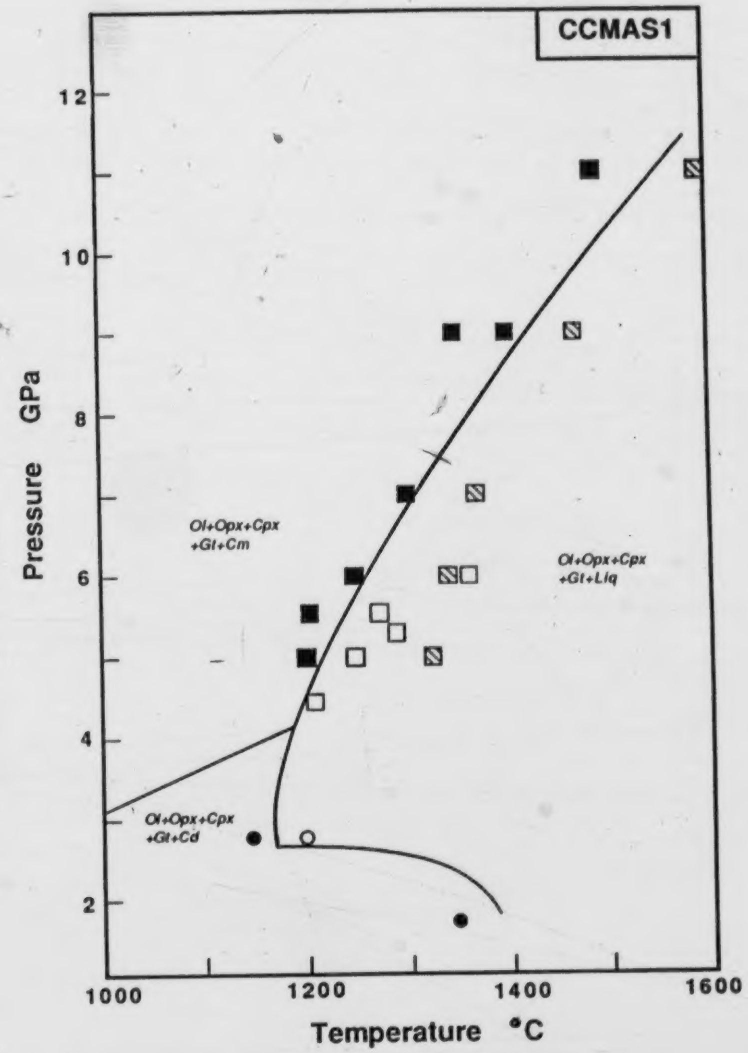

Figure 5.5. (b) Phase relations for the synthetic peridotite CCMAS1 in the CMAS - CO_2 system. Symbols as in (a) except that open symbols above the solidus are runs for which no BSE examination of charges was performed. Circles at 2.8 GPa represent the solidus bracket for peridotite in the CMAS - CO_2 system (adapted from Adam, 1988). Circle at 1.5 GPa is the solidus for peridotite PHN 1611 (adapted from Wendlandt and Mysen, 1980).

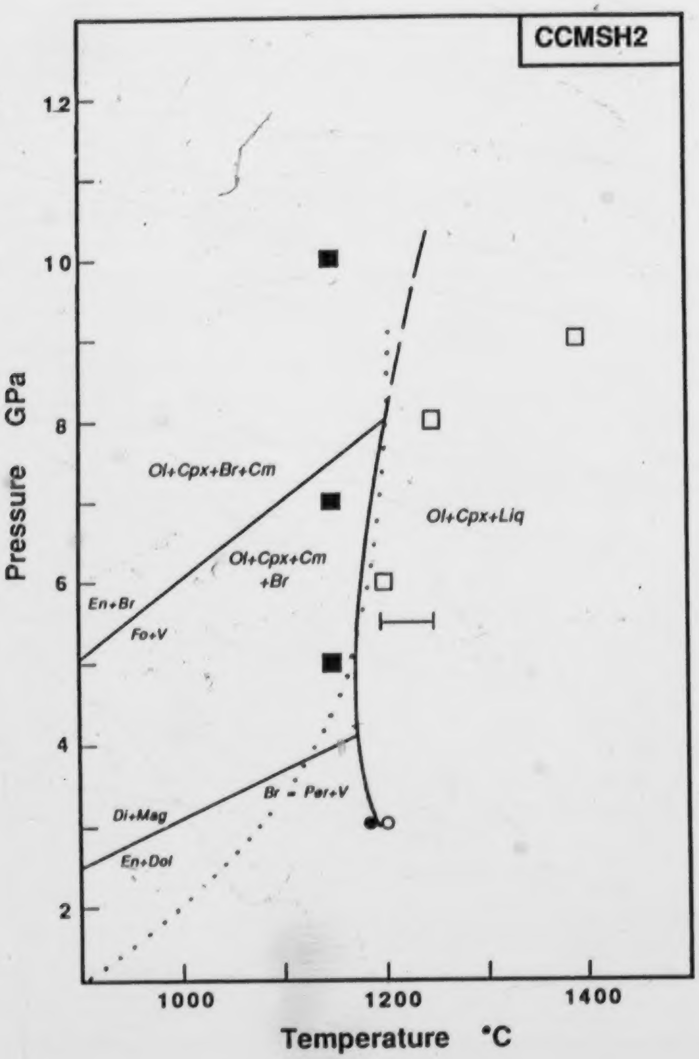

Figure 5.5. (c) Preliminary phase relations for synthetic peridotite CCMSH2 in the CMS - CO_2 - H_2O system. Solid squares are subsolidus, open squares are hyper-solidus. Circles at 3.1 GPa represent brackets for the peridotite solidus in the CMS - CO_2 - H_2O system (adapted from Eggler, 1977). The reaction En + Br == Fo + V is adapted from Ellis and Wyllie (1979). Dotted line is the brucite decomposition curve to 3.3 GPa adapted from Irving et al. (1977) and by two recconnaissance runs from this study at 7 and 8 GPa (Table 5.2). Bracket at 5.5 GPa is solidus for a natural kimberlite analogue (adapted from Eggler and Wendlandt, 1979).

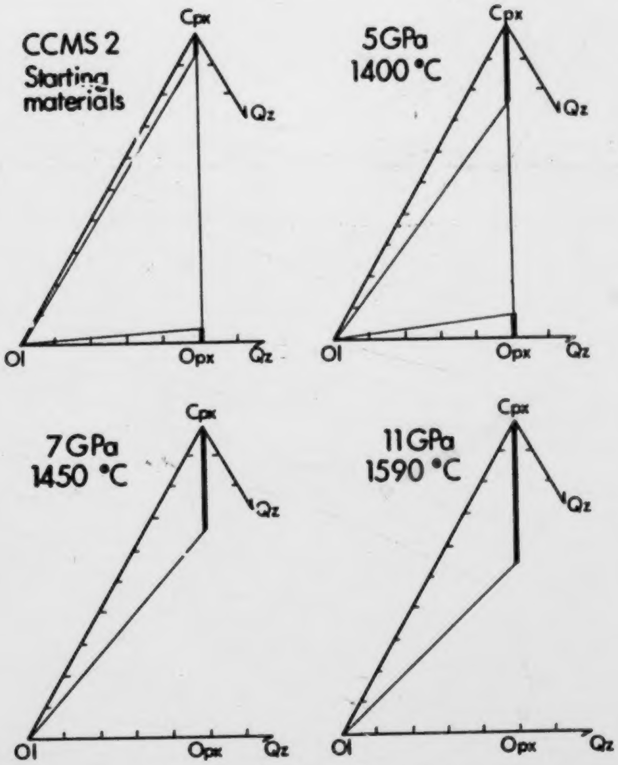
CCMS 2
Starting materials
Cpx
Qz
Ol
Opx
Qz
5GPa
1400 °C
Cpx
Qz
Ol
Opx
Qz
7GPa
1450 °C
Cpx
Qz
Ol
Opx
Qz
11GPa
1590 °C
Cpx
Qz
Ol
Opx
Qz

Figure 5.6. Clinopyroxene compositions (in mol.%) from various runs in the CMS - CO_2 system from this study plotted in the Fo - Di - Si ternary. Note that Opx does not crystallize in runs above 5 GPa in the CCMS2 starting composition.

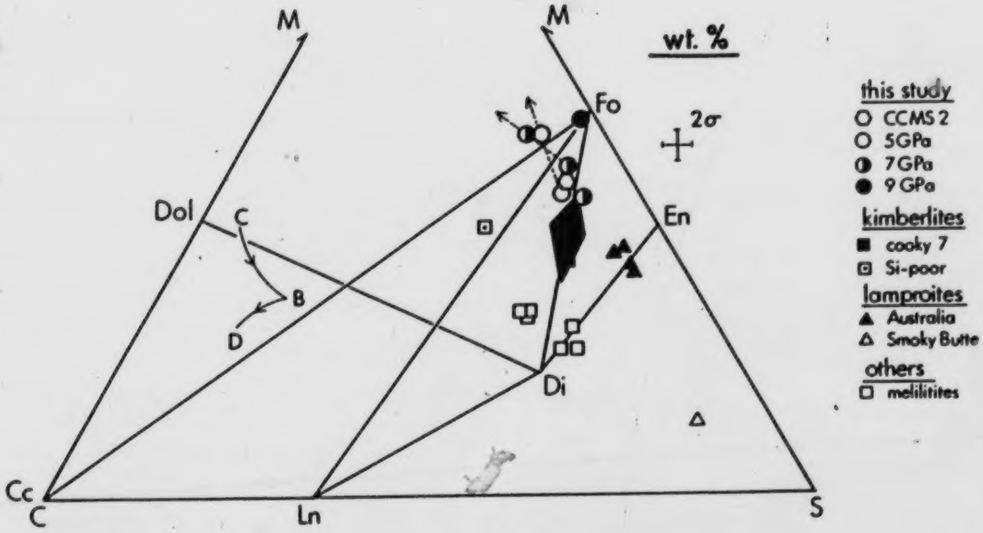

Figure 5.7. Compositions of partial melts of the CCMS2 composition from this study projected (in wt%) in the CMS ternary. Representative compositions of natural kimberlites, lamproites and melilitites are projected onto the CMS plane from Al_2O_3 using a method modified after O'Hara (1968). Cross-hatchured field reperesents analyses of "uncontaminated" natural kimberlite (adapted from Mitchell (1986)). Data for melilitites are adapted from Brey (1978). Data for W. Australian and Smoky Butte lamproites are adapted from Jaques et al. (1984) and Bergman (1988), respectively. Data for Lesotho (cooky 7) and Wesselton Si-poor kimberlite are adapted from Eggler and Wendlandt (1979) and Edgar et al. (1988), respectively. The arrows for partial melts from this study represent the shift in composition for melts further above the solidus (i.e. higher degree partial melts). Error bars represent error in partial melt compositions from this study estimated at the 95% confidence level. Also shown is the liquidus trace in the system CMS - CO_2 at 3 GPa (adapted from Eggler (1978)).

5.9 REFERENCES

Akaogi M, Akimoto S (1977) Pyroxene-garnet solid solution equilibria in the system $Mg_4Si_4O_{12}$ - $Mg_3Al_2Si_3O_{12}$ and $Fe_4Si_4O_{12}$ - $Fe_3Al_2Si_3O_{12}$ at high pressures and temperatures. Phys. Earth Planet. Int. 15:90-106.

Adam J (1988) Dry, hydrous, and CO_2-bearing liquidus phase relationships in the CMAS system at 28 kb, and their bearing on the origin of alkali basalts. J. Geol. 96:709-719.

Anderson AT (1975) Some basaltic and andesitic gases. Rev. Geophys. 13:37-56.

Arai S (1986) K/Na variation in phlogopite and amphibole of upper mantle peridotites due to fractionation of the metasomatising fluids. J. Geol. 94:436-44.

Berg GW (1986) Evidence for carbonate in the mantle. Nature, 324,50-51,

Brey G (1978) Origin of olivine melilitites - chemical and experimental constraints. J. Volc. Geotherm. Res. 3:61-73.

Brey G, Green DH (1977) Systematic study of liquidus phase relations in olivine melilitite + H_2O + CO_2 at high pressures and petrogenesis of an olivine melilitite magma. Contrib. Mineral. Petrol. 61:141-153.

Brey G, Brice WR, Ellis DD, Green DH, Harris KL, Ryabchikov ID (1983) Pyroxene-carbonate reactions in the upper mantle. Earth Planet. Sci. Lett. 62:63-74.

Boyd FR, Nixon PH (1978) Ultramafic nodules from the Kimberley pipes, South Africa. Geochim. Cosmo. Acta 42: 1367-1382.

Boyd FR, Gurney JJ (1986) Diamonds and the African lithosphere. Science 232:472-477.

Bulanova GP (1986) Compositional evolution of syngenetic inclusions of ultrabasic association in Yukation diamond. Geol. Soc. Australia Abs. Series 1G:371-373.

Bergman S (1988) Lamproites and other potassium-rich igneous rocks: a review of their occurrence, mineralogy and geochemistry. In: Alkaline Igneous Rocks, J.G. Fitton and B.G.J. Upton, eds., Geol. Soc. Special Publication

Canil D, Virgo D, Scarfe CM Oxidation state of mantle xenoliths from British Columbia, Canada. Contrib. Mineral. Petrol., submitted.

Delaney JR, Muenow DJ, Graham DG (1978) Abundance and distribution of water, carbon, and sulfur in the glassy rims of submarine pillow basalts. Geochim. Cosmochim. Acta 42:581-594.

Edgar AD, Arima M, Baldwin DK, Bell DR, Shee SR, Skinner EMW, Walker EC (1988) High-pressure - high-temperature melting experiments on a SiO_2-poor aphanitic kimberlite from the Wesselton mine, Kimberley, South Africa. Am. Miner. 73:524-533.

Eggler DH (1977) The principle of the zone of invariant vapor composition. Carnegie Inst. Wash. Ybook. 76:428-435.

Eggler DH (1978) The effect of CO_2 on partial melting of peridotite in the system Na_2O - CaO - Al_2O_3 - MgO - SiO_2 - CO_2 to 35 kb, with an analysis of melting in a peridotite - H_2O - CO_2 system. Am. J. Sci. 278:305-343.

Eggler DH (1983) Upper mantle oxidation state: evidence from olivine - orthopyroxene - ilmenite assemblages. Geophys. Res. Lett. 10:365-368.

Eggler DH (1987) Discussion of recent papers on carbonated peridotite, bearing on mantle metasomatism and magmatism: an alternative. Earth Planet. Sci. Lett. 82:398-400.

Eggler DH, Wendlandt RF (1979) Experimental studies on the relationship between kimberlite magmas and partial melting of peridotite. In: Kimberlites, Diatremes and Diamonds: Their Geology, Petrology, and Geochemistry, F.R. Boyd and H.O.A. Meyer, eds., American Geophysical Union, pp. 330-338.

Eggler DH, Baker DR (1982) Reduced volatiles in the system C-O-H: Implications to mantle melting, fluid formation, and diamond genesis. In: High Pressure Research in Geophysics, S. Akimoto and M.H. Manghnani, eds., Reidel Publishing, pp. 237-250.

Ellis DJ, Wyllie PJ (1979) Hydration and melting reactions in the system MgO - SiO_2 - H_2O at pressures up to 100 kbar. Am. Miner. 64:41-48.

Erlank AJ, Waters AG, Hawkesworth CJ, Haggerty SE, Alsopp HL, Rickard RS, Menzies MA (1987) Evidence for mantle metasomatism in peridotite nodules from the Kimberley Pipes, South Africa. In: Mantle Metasomatism, M.A. Menzies and C.J. Hawkesworth, eds., pp. 221-309.

Finnerty AA, Boyd FR (1987) Thermobarometry for garnet peridotites: basis for the determination of thermal and compositional structure of the upper mantle. In: Mantle Xenoliths, P.H. Nixon, ed., pp. 381-402.

Fujii T, Scarfe CM (1985) Composition of liquids coexisting with spinel lherzolite at 10 kbar and the genesis of MORBs. Contrib. Mineral. Petrol. 90:18-28.

Fyfe WS (1970) Lattice energies, phase transformations and volatiles in the mantle. Phys. Earth Planet. Int. 3:196-200.

Gerlach TM (1980) Evaluation of volcanic gases from Kilauea volcano. J.Volc. Geotherm. Res. 7:295-317.

Goldsmith JR, Newton RC (1969) P-T-X relations in the system $CaCO_3$ - $MgCO_3$ at high temperatures and pressures. Am. J. Sci. 267A:160-190.

Haggerty SE (1987) Metasomatic mineral titanates in upper mantle xenoliths. In: Mantle Xenoliths, P.H. Nixon, ed., pp. 671-690.

Haggerty SE, Tompkins IA (1983) Redox state of the Earth's upper mantle from kimberlitic ilmenites. Nature 303:295-300.

Hunter RH, Taylor LA (1984) Magma mixing in the low velocity zone: kimberlitic megacrysts from Fayette County, Pennsylvania. Am. Miner. 69:16-29.

Hunter RH, McKenzie D (1989) The equilibrium geometry of carbonate melts in rocks of mantle composition. Earth Planet. Sci. Lett. 92:347-356.

Irving AJ, Wyllie PJ (1975) Subsolidus and melting relationships for calcite, magnesite and the join $CaCO_3$ - $MgCO_3$ to 36 kb. Geochim. Cosmochim. Acta 39:35-53.

Irving AJ, Huang WL, Wyllie PJ (1977) Phase relations of portlandite, $Ca(OH)_2$, and brucite, $Mg(OH)_2$, to 33 kb. Am. J. Sci. 277:313-321.

Jaques AL, Lewis JD, Smith CB, Gregory GP, Ferguson J, Chappell BW, McCulloch MT (1984) The diamond-bearing ultrapotassic (lamproitic) rocks of the West Kimberley region, Western Australia. In: Kimberlites 1: Kimberlites and related rocks, J. Kornprobst, ed., pp. 225-254.

Kanzaki M (1987) Ultrahigh pressure phase relations in the system $MgSiO_3$ - $Mg_3Al_2Si_3O_{12}$. Phys. Earth Planet. Int. 49:168-175.

Liu L, Bassett WA (1986) Elements, Oxides, Silicates High Pressure Phases with Implications for the Earth's Interior. Oxford University Press, New York, 250 p.

Luth RW, Virgo D, Boyd FR, Wood BJ Ferric and ferrous iron in mantle-derived garnets: coordination state and implications for the oxidation state of the mantle. Contrib. Mineral. Petrol., in press.

Maaloe S, Wyllie PJ (1975) The join grossularite - calcite through the system CaO - Al_2O_3 - SiO_2 - CO_2 at 30 kb: crystallization range of silicates and carbonates on the liquidus. Earth Planet. Sci. Lett. 28:205-208.

McGetchin TR, Besancon JR (1973) Carbonate inclusions in mantle derived pyropes. Earth Planet. Sci. Lett. 18:408-410

Mitchell RH (1986) Kimberlites, Plenum Press, 442 p.

Moore RO, Gurney JJ (1985) Pyroxene solid solution in garnets included in diamond. Nature 318:553-555.

Mysen BO, Boettcher AL (1975) Melting of a hydrous mantle. J. Petrol. 16:520-548.

O'Hara MJ (1968) The bearing of phase equilibria studies in synthetic and natural systems on the origin and evolution of basic and ultrabasic rocks. Earth Sci. Rev. 4:69-133.

Olafsson M, Eggler DH (1983) Phase relations of amphibole, amphibole - carbonate, and phlogopite - carbonate peridotite: petrologic constraints on the asthenosphere. Earth Planet. Sci. Lett. 64:305-315.

Roedder E (1965) Liquid CO_2 inclusions in olivine-bearing nodules and phenocrysts from basalts. Am. Miner. 50:1746-1782.

Shervais JW, Taylor LA, Laul JC (1987) Magma mixing and kimberlite genesis: mineralogic, petrologic and trace element evidence from eastern U.S.A. kimberlites. In: Mantle Metasomatism and Alkaline Magmatism, E.M. Morris and J.D. Pasteris, eds., Geol. Soc. America Spec. Pap. 215:101-114.

Takahashi E (1986) Melting of a dry peridotite KLB-1 up to 14 GPa: implications on the origin of peridotitic upper mantle. J. Geophys. Res. 91:9367-9382.

Takahashi E, Yamada H, Ito E (1982) An ultrahigh-pressure furnace assembly to 100 kbar and 1500°C with minimum temperature uncertainty. Geophys. Res. Lett. 9:805-807.

Takahashi E, Ito E (1987) Mineralogy of mantle peridotite along a model geotherm up to 700 km depth. In: High Pressure Research in Mineral Physics, M.H. Manghnani and Y. Syono, eds., pp. 427-437.

Tronnes RG, Takahashi E, Scarfe CM (1989) Stability and phase relations of phlogopite and K-richterite to 15 GPa. *Geol. Assoc. Can./Min. Assoc. Can. Abs. Prog.* 14:A93.

Virgo D, Luth RW, Moats M, Ulmer GC (1988) Constraints on the oxidation state of the mantle: an electrochemical and ^{57}Fe Mossbauer study of mantle-derived ilmenites. *Geochim. Cosmochim. Acta* 52:1781-1795.

Wallace ME, Green DH (1988) An experimental determination of primary carbonatite magma composition. *Nature* 335:343-346.

Wendlandt RF, Mysen BO (1980) Melting phase relations of natural peridotite + CO_2 as a function of degree of partial melting at 15 and 30 kbar. *Am. Miner.* 65:37-44.

Wendlandt RF, Eggler DH (1980) The origins of potassic magmas: 2. Stability of phlogopite in natural spinel lherzolite and in the system $KAlSiO_4$ - MgO - SiO_2 - H_2O - CO_2 at high pressures and high temperatures. *Am. J. Sci.* 280:421-453.

Wood BJ, Virgo D (1989) Upper mantle oxidation state: ferric iron contents of lherzolite spinels by ^{57}Fe Mossbauer spectroscopy and resultant oxygen fugacities. *Geochim. Cosmochim. Acta* 53:1277-1292.

Wyllie PJ (1979) Magmas and volatile components. *Am. Miner.* 64:469-500.

Wyllie PJ (1980) The origin of kimberlite. *J. Geophys. Res.* 85:6902-6910.

Wyllie PJ, Huang WL (1975) Carbonation and melting reactions in the system CaO - MgO - SiO_2 - CO_2 at mantle pressures with geophysical and petrological applications. *Contrib. Mineral. Petrol.* 54:79-107.

Yagi T, Akimoto S (1976) Direct determination of coesite - stishovite transition by in-situ X-ray measurements. *Tectonophys.* 35:259-270.

Yagi T, Akaogi M, Shimomura O, Suzuki T, Akimoto S (1987) In situ observation of the olivine spinel transformation in Fe_2SiO_4 using synchrotron radiation. *J. Geophys. Res.* 92:6207-6213.

6. THESIS SUMMARY AND CONCLUSIONS

A series of petrological and experimental studies of mantle-derived peridotites has been undertaken in this thesis. The three petrological studies contained herein have addressed different, yet interelated, aspects of the upper mantle beneath the Canadian Cordillera, including its geothermal characteristics, metasomatic history and oxidation state. An experimental study investigating the melting relations of CO_2-bearing peridotites in compositionally simple systems, has attempted to provide some constraints on the origin of deep-seated, alkaline magmas in the mantle, such as kimberlite.

The mantle-derived xenolith population hosted in hawaiite at Rayfield River, south-central British Columbia confirms the dominance of spinel lherzolite in the upper mantle beneath the Canadian Cordillera noted in previous studies (Brearley et al., 1984). Harzburgite, dunite, wehrlite, and mineralogically banded peridotite, also occur as xenoliths at Rayfield River and other localities in British Columbia, and indicate that the upper mantle beneath this region is heterogeneous on a cm to meter scale. A geotherm constructed for the upper mantle beneath Rayfield River based on the geothermometry of xenoliths (23°C/km) is similar to those determined for other xenolith suites from the Cordillera (Fujii and Scarfe, 1982; Brearley et al., 1984). The consistency of these xenolith-derived geotherms with a geotherm calculated from present day heat flow measurements, suggests that geothermal conditions were probably uniform during Cenozoic alkaline magmatism in this province, and have not changed significantly over time.

The first occurrence of phlogopite in mantle xenoliths from the Canadian Cordillera has been documented in wehrlite and peridotite xenoliths from a volcano near Kostal Lake, eastern British Columbia. The phlogopites provide evidence for the infiltration of a fluid phase or fluid-rich melt in the upper mantle beneath a recently active alkaline volcano. The fluid phase is shown to have contained alkalies, Cl, P , S and probably H_2O, and to have oxidized the upper mantle beneath Kostal Lake. Fluid or fluid-rich melt infiltration and the formation of phlogopite in the upper mantle underlying eastern British Columbia may have occurred less than 3.5 Ma ago. The relationship between metasomatism and magmatism in the upper mantle is well demonstrated in this petrological study.

The redox equilibria recorded by coexisting olivine, orthopyroxene and spinel in seventeen mantle-derived xenoliths from six localities throughout British Columbia were used to estimate the oxidation state of the upper mantle beneath this region. The precise determination of Fe^{3+} concentrations in spinels by Mossbauer spectroscopy, was found to be essential in order to detect any real differences in the f_{O2} calculated for the xenoliths. The results indicate that the f_{O2} of the upper mantle beneath the Canadian Cordillera is similar to that of mid-ocean ridge basalt glasses (slightly below the FMQ buffer at 15 kbar) and was unaffected by Late Cenozoic magmatism in this region. Subtle variations in the oxidation state between samples could not be detected due to errors and assumptions inherent in the thermobarometric calculations. However, metasomatized samples appear to have slightly higher f_{O2}'s than anhydrous xenoliths, suggesting that metasomatism is a potential process for oxidation of the upper mantle. The overall oxidized nature of the samples investigated requires that C-O-H volatile species contained in fluids or melts in the sub-Cordilleran mantle occur in their oxidized forms (i.e. H_2O and CO_2).

Recent studies on the oxidation state of the upper mantle, including that described above, indicate that fluid species in the upper mantle are dominantly CO_2 and H_2O (Eggler, 1983; Virgo et al., 1988; Wood and Virgo, 1989; Luth et al., in press). With this in mind, the role of CO_2 in the generation of deep-seated, diamond-bearing kimberlites was investigated by melting synthetic peridotite + CO_2 compositions at pressures of 4.5 to 12 GPa. The spectrum of melt compositions determined over a range of pressures in the experiments indicate that diamond-bearing kimberlite may be formed by partial melting of CO_2-bearing peridotite at pressures of 5 to 7 GPa beneath the stable cratons of continental regions. This 5 to 7 GPa "window" for diamond-bearing kimberlite formation may correspond to the lithosphere-asthenosphere boundary beneath stable cratons. It is proposed that the interface between cold, elastic lithosphere and hot, anelastic asthenosphere may prevent the passage of magmas formed at higher pressures in the mantle. Thus, melts derived from CO_2-bearing peridotite at higher pressures in the mantle ("proto kimberlites ?") are not represented on the Earth's surface. The subsolidus stability of magnesite to pressures of 12 GPa in these experiments suggests that this phase is a potential reservoir for carbon in the Earth to depths of at least 350 km.

6.1 REFERENCES

Brearley M, Scarfe CM, Fujii T (1984) The petrology of ultramafic xenoliths from Summit Lake, near Prince George, British Columbia. Contrib. Mineral. Petrol. 88:53-63.

Eggler DH (1983) Upper mantle oxidation state: evidence from olivine - orthopyroxene - ilmenite assemblages. Geophys. Res. Lett. 10:365-368.

Fujii T, Scarfe CM (1982) Petrology of ultramafic nodules from West Kettle River, near Kelowna, southern British Columbia. Contrib. Mineral. Petrol. 80:297-306.

Luth RW, Virgo D, Boyd FR, Wood BJ Ferric and ferrous iron in mantle-derived garnets: coordination state and implications for the oxidation state of the mantle. Contrib. Mineral. Petrol. in press

Virgo D, Luth RW, Moats M, Ulmer GC (1988) Constraints on the oxidation state of the mantle: an electrochemical and ^{57}Fe Mossbauer study of mantle-derived ilmenites. Geochim. Cosmochim. Acta 52:1781-1795.

Wood BJ, Virgo D (1989) Upper mantle oxidation state: ferric iron contents of lherzolite spinels by ^{57}Fe Mossbauer spectroscopy and resultant oxygen fugacities. Geochim. Cosmochim. Acta 53:1277-1292.